INNOVATION IN SCIENCE AND TECHNOLOGY

ISSN 2788-7030

SEP. 2025 VOL. 4, NO. 8

CONTENTS

Failure Analysis of Heat-Exchanger Sheets at Coke Oven	1-9
J. N. Mohapatra, Arun Kumar Panda, D. Satish Kumar	
Research on the Dynamic Control Path of Procurement Costs Driven by	10-15
Information Technology Tools: A Case Study of the QG Project	
Kai Zhang	
Enhancing the Production Efficiency of Textile Dyeing Auxiliaries Through	16-21
Intelligent Retrofitting of Storage Systems: A Case Study of Leveling Agent	
Storage	
Dongmei Shi	
Development and Die-Cutting Process Optimization of High-Temperature- Resistant and Anti-Aging Barcode Substrate for Photovoltaic Modules	22-28
Quanzhen Ding	
A Carbon Reduction-Oriented Synergistic Optimization Model for	29-37
Manufacturing SAP Systems and Production Planning: Architectural	
Innovation, Algorithmic Advancement, and Global Industrial Validation	
Qiang Fu	
Construction and Practice of Digital Twin Operation and Maintenance	38-46
Platform for Water Supply and Drainage Systems in New Energy Power	
Stations	
Liqin Liu	
Liver Transplantation: A Treatment Option for Survival in End-Stage Liver	47-54
Disease	
Haradhan Kumar Mohaian	

INNOVATION IN SCIENCE AND TECHNOLOGY

ISSN 2788-7030

SEP. 2025 VOL. 4, NO. 8

CONTENTS

Design and Engineering Practice of a Visual-Voice Multimodal Collaborative 55-65

Perception System for Community Security

Yang Zhong

Paradigm Academic Press Innovation in Science and Technology ISSN 2788-7030 SEP. 2025 VOL.4, NO.8



Failure Analysis of Heat-Exchanger Sheets at Coke Oven

J. N. Mohapatra¹, Arun Kumar Panda¹ & D. Satish Kumar¹

¹ JSW Steel Ltd. Vijaynagar Works, Bellari-583275, Karnataka, India

Correspondence: J. N. Mohapatra, JSW Steel Ltd. Vijaynagar Works, Bellari-583275, Karnataka, India.

doi:10.63593/IST.2788-7030.2025.09.001

Abstract

The heat exchanger sheets at JSW Steel coke oven is 316L used in ammonia stripping / distillation waste water plate heat exchanger (PHE) with the waste water inlet temperature 110°C and outlet temperature 40°C, with water temperature between 35-43°C. The solution include 250mg/liter Ammonical Nitrogen open to atmosphere. The sheets of two heat exchangers, showed pitting/pin holes all over the plates in just 14 days of use after commissioning. Chemical composition of the sheets showed lower Ni (9.3-9.6% against 10%) than the specification. Varying hardness (189-249 Hv0.5 kgf) on the sheets indicating different phases present on the sheets. The analysis revealed the pits are from the top surface (extrusion side) of the plates. SEM-EDS revealed presence of chlorine on the plate, leading to pitting corrosion of the plates. The sheets were checked for their magnetic properties by a permanent magnet showed attracting nature and with a NDE magnetic device the sheets showed magnetic hysteresis loop, indicating presence of magnetic phase (deformation induced martensite) in the sheets. It is inferred that, martensitic transformation from the austenite due to severe plastic deformation has occurred at the manufacturing stage. Hence, galvanic effect caused by the presence of two distinct phases, austenite and martensite, which exhibit different corrosion potentials lead to formation of pitting corrosion due to presence of higher level of chlorides in the water.

Keywords: sheet type heat exchanger, failure analysis, pitting corrosion, magnetic properties

1. Introduction

A heat exchanger is a device that transfers heat between two or more fluids that are typically at different temperatures, but remain physically separated. This process allows one fluid to gain heat while the other loses it, enabling applications such as heating, cooling, and recovering waste heat from industrial processes or mechanical systems (https://www.sciencedirect.com/topics/chemistry/heat-exchanger). A plate heat exchanger is a type of heat exchanger that uses a series of thin, parallel metal plates to facilitate heat transfer between two fluids (Willem Faes, Steven Lecompte, Zaaquib Yunus Ahmed, Johan Van Bael, Robbe Salenbien, Kim Verbeken & Michel De Paepe, 2019). The design maximizes the surface area for heat exchange, making it efficient and compact. These plates are typically corrugated or have pressed patterns to encourage turbulence and improve heat transfer. For plate heat exchangers stainless steel is a common material, however for the high efficiency low thickness of the plates makes them extremely vulnerable to local corrosion attacks in chloride containing water (Georgii Vasyliev, Ihor Pylypenko, Oleg Kuzmenko & Yuriy Gerasymenko, 2022). The austenitic stainless steels under plastic deformation transformed to martensite as given below:

Austenite γ (FCC) \rightarrow martensite ϵ (HCP) \rightarrow martensite α' (BCC).....(1)

The amount of deformation induced martensite depends upon several factors such as: temperature, plastic strain, strain rate, stress state, deformation mode, grain size, and grain orientation. The increase of α' martensite by martensitic transformation induced by plastic deformation causes a change in physical properties of austenitic stainless steels. The martensitic transformation causes the rupture of the passive film due to higher density of flaws and generates residual stress or a galvanic effect caused by the presence of two distinct phases, austenite

and martensite, which exhibit different corrosion potentials. The results show that corrosion rate is function of stress level and amount of dissolved chloride ions in water. SCC resistance of tested samples depends on the magnitude of cold work at surface layers; high level of cold work decreases corrosion resistance. The design and production of plate heat exchangers, which are cyclically loaded parts, made of AISI 316 austenitic stainless steel demands a substantial understanding of the correlation between fatigue life, martensitic transformation and damage mechanisms (Nicolae Solomon & Iulia Solomon, 2017).

The chloride/chlorine contents in the cooling tower system have caused pitting corrosion (perforation) of PHE's 316L stainless steel plates on the open circuit side (CT water side). The 316L plate samples also registered very low pitting corrosion resistance in CT feed and CT bleed water during electrochemical testing. The electrochemical results proved the chloride level as a damaging entity. There was complete non-compliance of sound scientific knowledge and practice of the cooling water treatment especially chloride concentration, which cannot be ignored even at ppm level. Hence, water of reverse osmosis (R/O) quality should be used in the CT feed and qualification of feed water system must focus on chloride contents rather than TDS values (K.M. Deen, M.A. Virk, C.I. Haque, R. Ahmad & I.H. Khan, 2010).

The principal causes of corrosion failure in the plate heat exchanger (PHE) of Jam Petrochemical Complex (JPC), Asalouyeh, Iran, showed chloride ions build-up in crevices formed between plates and gaskets (at high temperatures), is the main reason for the occurrence of SCC. The suspended soil of the service water settled in the crevices between gasket and plate and provides a favorable position (dead zone) for building-up of the chloride ions. When the level of chloride ions in the water is low, the evaporation of water in the crevices leads to chloride ions build-up. Moreover, the high temperature of the transport water outlet and cooling water inlet results in the acceleration of this building-up. By chloride ions concentration in the crevices, the pitting corrosion under gasket seat occurs. In addition, the simultaneous presence of chloride and sulfide ions intensifies the SCC failure in the heat exchanger plates. Since the appearance of the cracks in the heat exchangers occurs after cooling the TW outlet by the service water (SW), the use of higher number of the plates in the heat exchangers together with the higher flow rate of cooling water is strongly recommended; in this way, at a constant flow rate of transport water, not only the temperature of transport water is decreased but also the SCC cracks resulted from the direct contact of the service water (which usually contains some levels of Cl⁻) can be effectively avoided (S.H. Khodamorad, N. Alinezhad, D. Haghshenas Fatmehsari & K. Ghahtan, 2016).

2. Materials and Methods

Sheets of 316 L were received from the JSW Steel coke oven for characterization to sort out the root cause of leakage. The sheets were visually tested for the presence of defects and measured the thickness. The steels were evaluated for their chemical composition through a SPECTRO make optical emission spectroscopy. The sheets were evaluated for their micro hardness through a micro Vicker's hardness tested at a load of 0.5kg. The optical microscopy through a opto-digital Olympus make microscope and scanning electron microscopy (SEM) through a Hitachi make SEM were conducted for the microstructure and defect analysis. SEM-EDS was conducted for the presence of inclusion and corrosion product identification. A permanent magnet and a portable NDE magnetic device (*MagStar*) were used for the magnetic property and magnetic hysteresis loop measurement of the sheets (http://www.nmlindia.org/download/Tech_HB/files/assets/downloads/page0026.pdf.; ftp://ftp.technofour.com/pub/catalogs/MagStar.pdf.). The MHL measurement was carried out at a magnetizing field of 1000Oe and magnetizing frequency of 50 mHz.

3. Results and Discussion

3.1 Visual Examination, Chemical Composition and Hardness

The sheets with the top (extrusion side) and bottom (intrusion side) shown in Figure 1. Pitting marks can be seen on the sheets surface responsible for the leakages.





Figure 1. Heat exchanger plates received from JSW coke oven with pitting marks on it

Chemical composition of the sheets is shown in Table 1. The chemical composition shows a small deviation in Ni content in the sheets (lower-9.3-9.6 wt. % Ni) compared to the specification (10-13%). Thickness of the sheets measured through SEM is shown in Figure 2. The thickness of the sheets were found to be in the range of 0.592-0.601mm. Micro hardness of the sheets are shown in Table 2. As per the specification the hardness has to be 217 BHN which is 222Hv0.5kgf. It can be seen that the hardness is different at different regions varying in the range of 189-249 Hv0.5kgf, indicating presence of hard and soft phases in the sheet leading to different level of hardness.

Table 1. Chemical composition of the heat exchanger sheets comparison with 316L

Sample ID	С	Si	Mn	Р	S	Cr	Ni	Мо	Al	Cu	Ti	V	N	w	Fe
316L	0.03	1	2	0.045	0.015	16.50- 18.50	10.0- 13.0	2.0- 2.5					0.1		
Sample-1	0.014	0.397	1.416	0.037	0.008	17.421	9.642	2.499	0.000	0.108	0.000	0.089	-	0.025	68.344
Sample-2	0.014	0.397	1.415	0.034	0.007	17.484	9.270	2.445	0.000	0.109	0.000	0.091	-	0.026	68.708
Sample-3	0.014	0.399	1.423	0.035	0.007	17.485	9.313	2.431	0.000	0.109	0.000	0.091	-	0.027	68.666

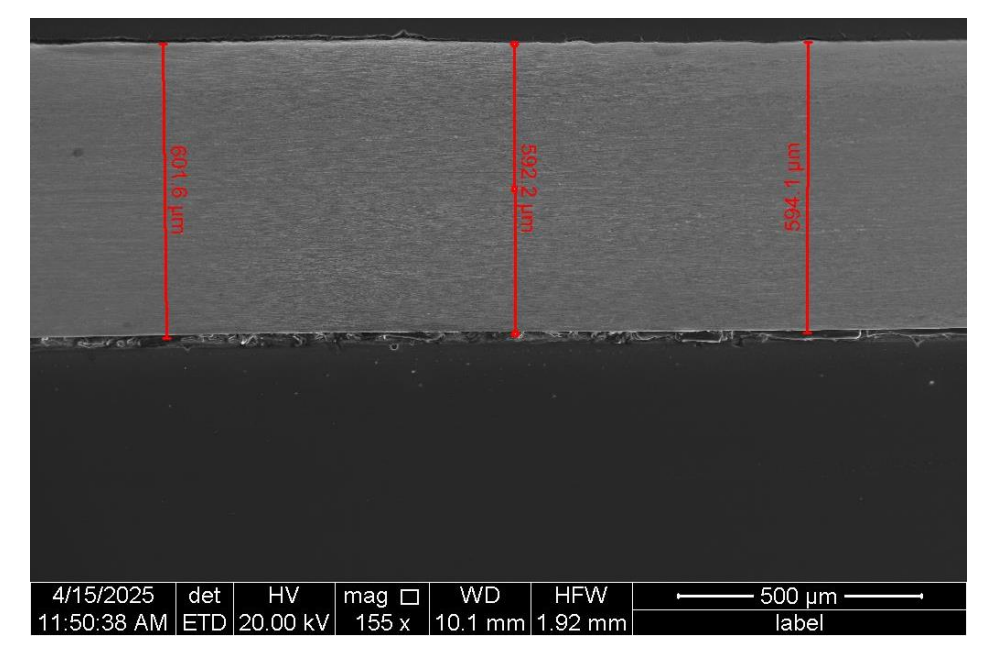


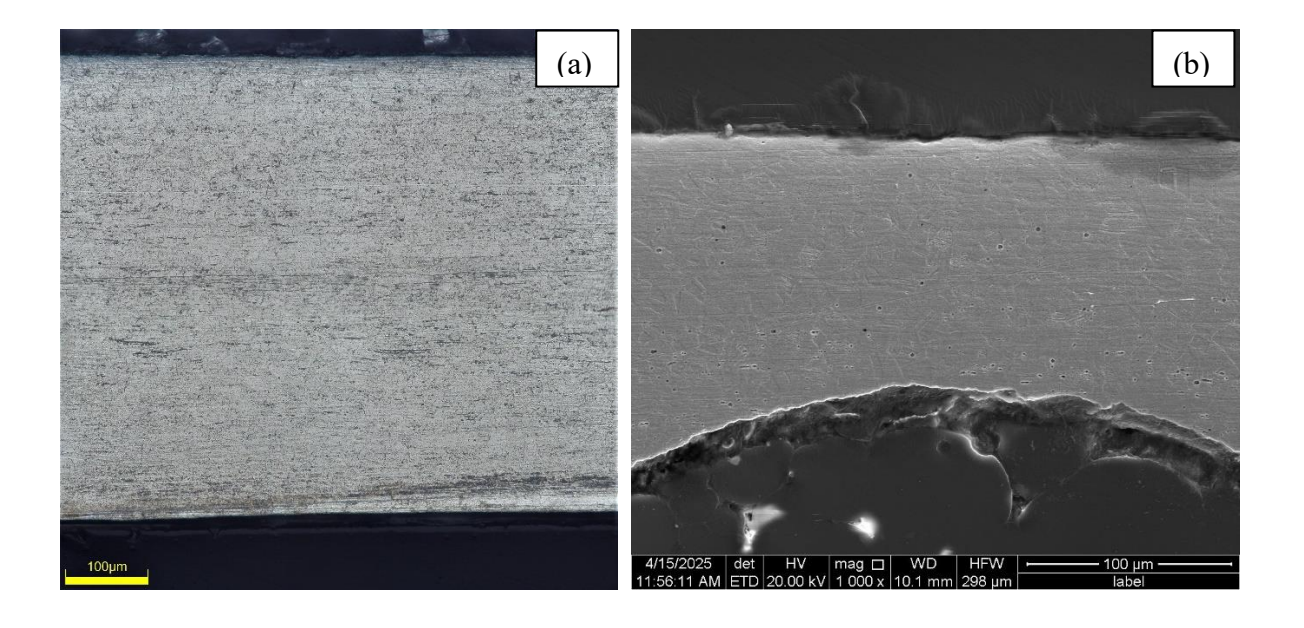
Figure 2. Thickness of the heat exchanger sheets measured through SEM

Table 2. Micro hardness of the sheet

SL NO	Weight - 0.5kg
1	189 Hv
2	211Hv
3	249Hv

3.2 Microstructure

Microstructure of the sheet is shown in Figure 3 (a) with the SEM micrographs in (b) and (c) respectively. Small pits can be seen on the sheets at high magnification SEM micrograph (Figure 3(c)). Corrosion pits can be seen in un-etched and etched condition as shown in Figure 4 (a) and (b) respectively. SEM micrograph of the sheets with the corrosion pits are shown in Figure 5. It can be seen that some of the pits are not having through hole whereas some are having through holes.



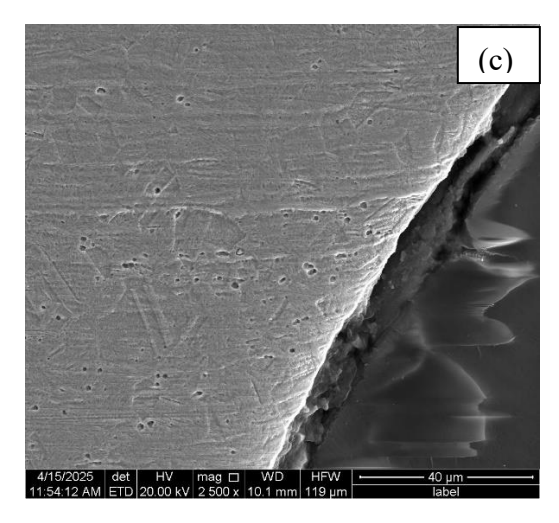


Figure 3. (a) Optical microstructure, (b) SEM micrograph and (c) high magnification SEM micrograph of the heat exchanger sheets

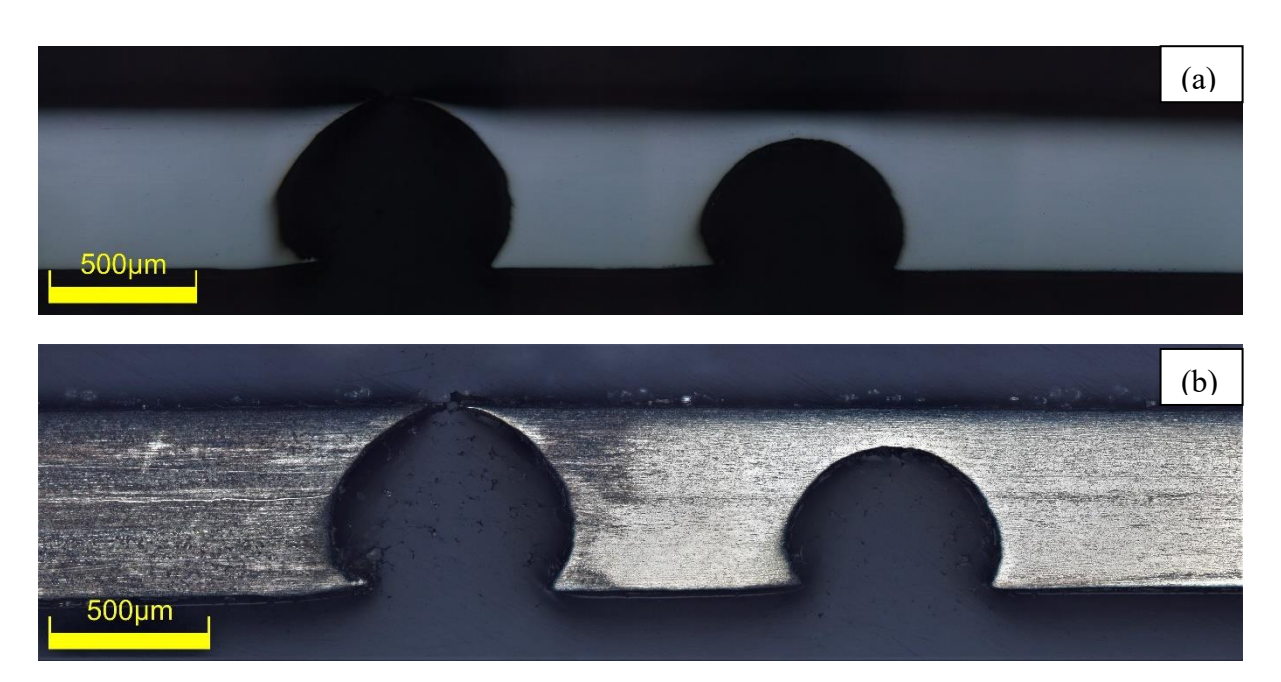


Figure 4. Corrosion pits on the sheet (a) un-etched and (b) etched condition

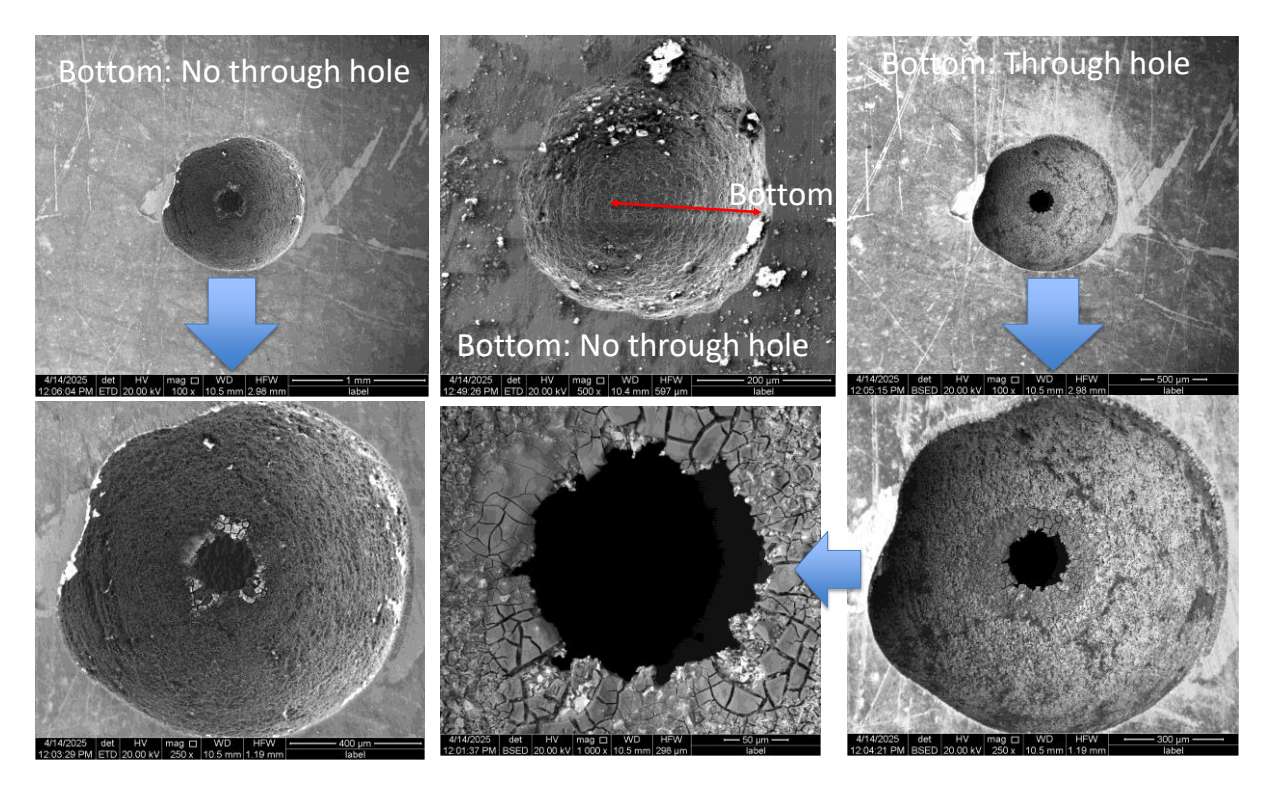


Figure 5. SEM micrograph of the pits with through hole on the sheet and partial pits

SEM EDS of the on the sheets near to the pits and away from the pits are shown in Figure 6 and 7 respectively. It shows presence of chloride near to the pits and such chlorides are in very high in level found away from the pits. It indicates that the high level of chloride responsible for the pitting corrosion of the sheets. The source of the chloride was found to be the water. The higher level of chloride in the water leading to pitting corrosion of the sheets.

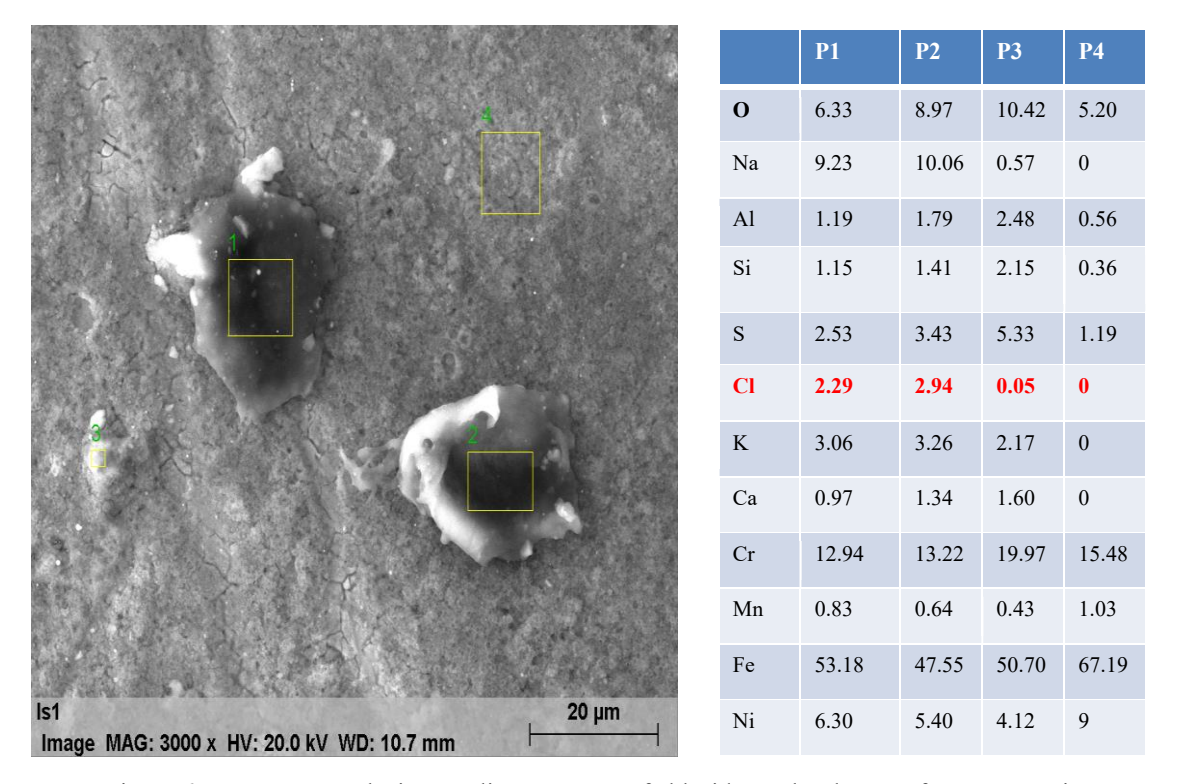
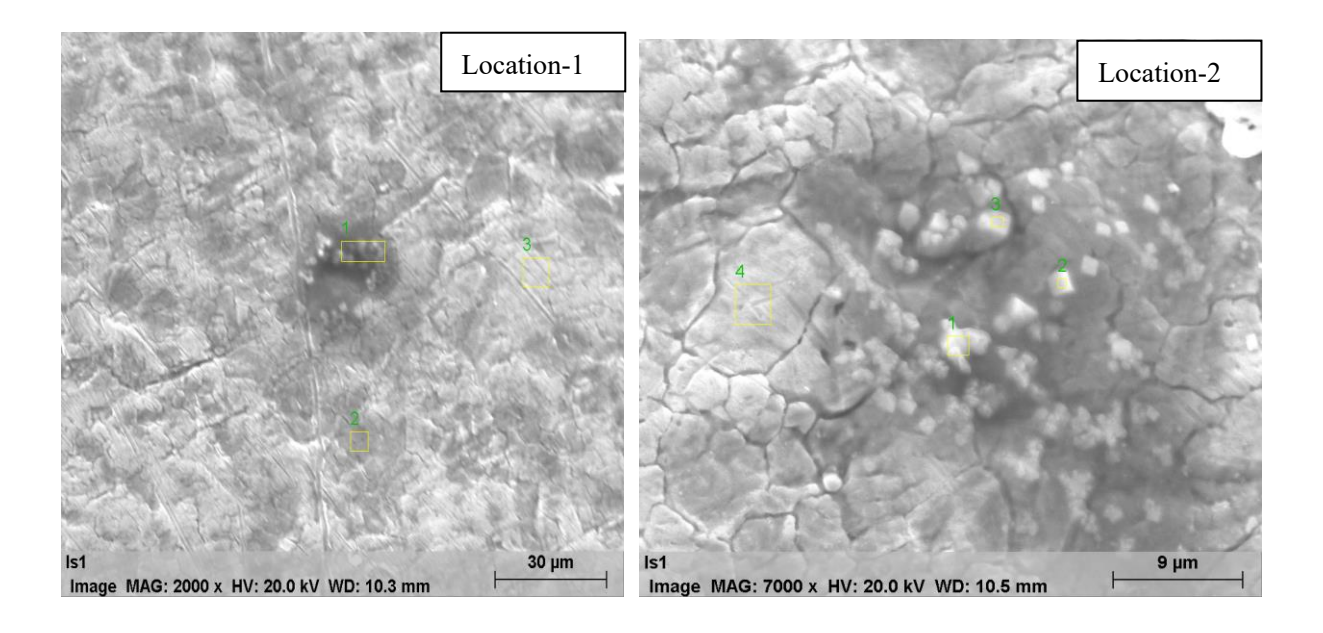


Figure 6. SEM-EDS analysis revealing presence of chloride on the sheet surface near to pit



Mass percent (%)

Spectrum	0	Na	Al	Si	s	C1	K	Ca	Cr	Mn	Fe	Ni
1 2 3	11.46 2.36 0.00	-	0.50	0.46	0.85	13.32 0.00 0.00	-	-	8.08 14.83 15.35	1.04	69.72	10.24

Mass percent (%)

Spectrum	0	Na	Al	Si	s	Cl	K	Ca	Cr	Mn	Fe	Ni
1	10.14	14.55	0.94	0.77	0.93	17.01	14.99	0.47	8.07	0.41	28.20	3.52
2	4.18	5.76	0.00	-	0.75	11.34	11.41	-	10.99	0.54	48.43	6.59
3	6.53	7.51	0.03	_	0.67	14.09	14.73	-	9.53	0.49	40.98	5.44
4	0.53	_	-	-	0.77	0.00	-	-	15.89	1.23	71.18	10.40

Figure 7. SEM EDS revealing presence of high level of chloride on the sheet surfaces away from the corrosion pit

3.3 Magnetic Properties

A permanent was used to check the magnetic properties of the sheets. Figure 8 shows that the sheets are getting attracted by a permanent magnet. Generally 316L steel is non-magnetic in nature due to the fully austenitic phase. As it is getting attracted by a magnet, it indicates presence of ferromagnetic phase such as martensite in the steel. Figure 9 Shows formation of hysteresis loop on the sheet with the application of cyclic magnetic field through a magnetic NDE device (*MagStar*) indicating presence of ferromagnetic phase on the sheets. Such martensites are generated due to transformation of austenite to martensite due to severe plastic deformation during the manufacturing stage. However, after deformation the sheets need to be annealed above the A₃ temperature to remove the martensites, which has not been done in the present case.

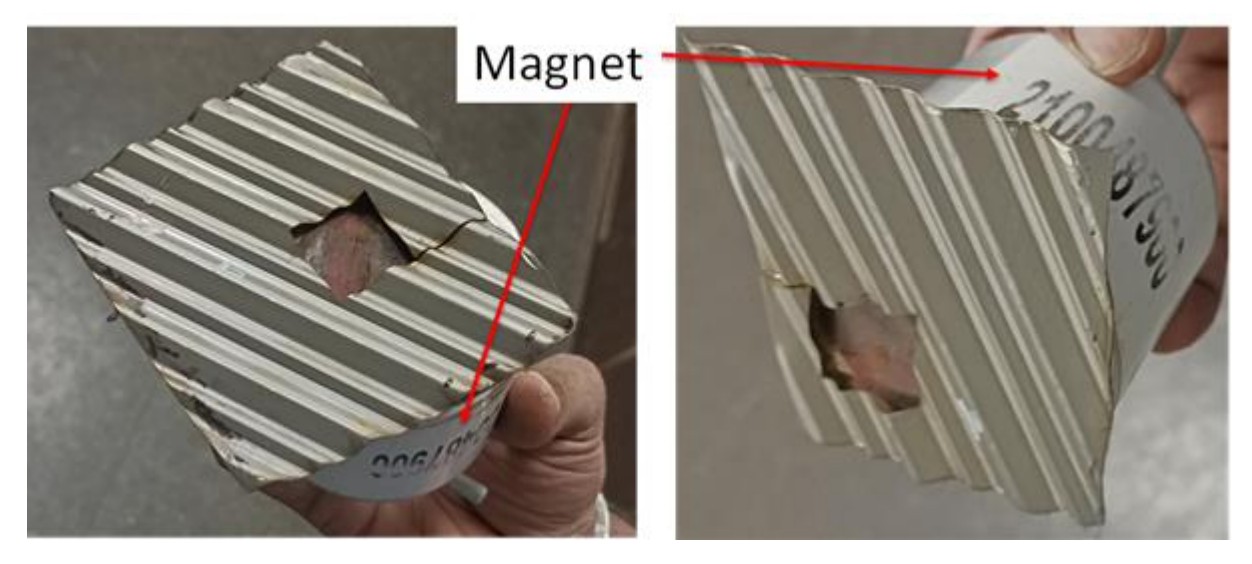


Figure 8. Permanent magnet shows attraction of the sheets indicating presence of magnetic phase (Martensite)

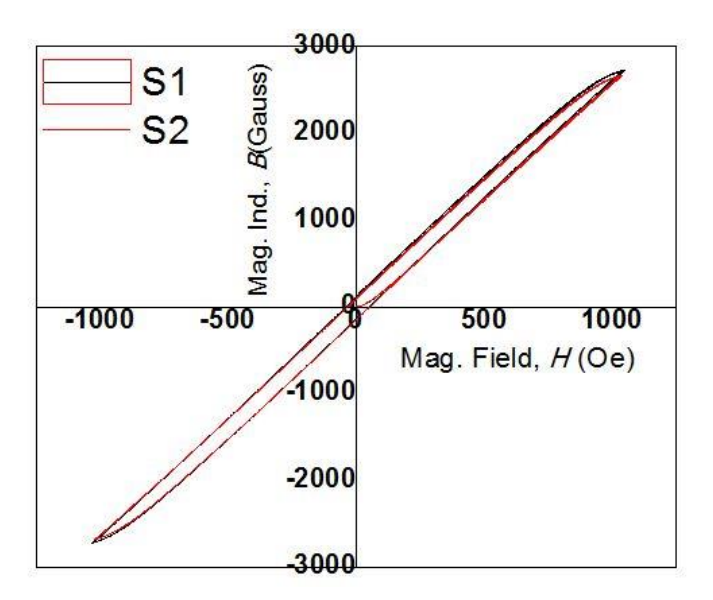


Figure 9. Hysteresis loop formed on the sheets with a portable magnetic NDE device indicating presence of ferromagnetic phase (Martensite) in the sheets

4. Conclusions

Leakage of the plate/sheet type exchanger tube were analyzed in the present study to sort out the root cause of failure in service in a very short period. It was found that pitting corrosion on the sheets responsible for the leakage/failure. Such pitting corrosion occurred due to the presence of high level of chlorides in the water. The pitting corrosion are sever due to the presence of martensitic phase which were generated at the manufacturing stage due to severe plastic deformation and acts as galvanic effect for the presence of two phases such as austenite and martensite. The presence of martensitic phase was conformed through the attraction of such heat exchanger sheets to a permanent magnet and further conformed by the formation of hysteresis loop through a magnetic NDE device by the application of cyclic magnetic field.

References

Georgii Vasyliev, Ihor Pylypenko, Oleg Kuzmenko, Yuriy Gerasymenko, (2022). Fouling influence on pitting corrosion of stainless steel heat exchanging surface, Thermal Science and Engineering Progress. https://doi.org/10.1016/j.tsep.2022.101278.

K.M. Deen, M.A. Virk, C.I. Haque, R. Ahmad, I.H. Khan, (2010). Failure investigation of heat exchanger plates due to pitting corrosion. *Engineering Failure Analysis*, 17, 886-893.

Nicolae Solomon, Iulia Solomon, (2017). Effect of deformation-induced phase transformation on AISI 316 stainless steel corrosion resistance. *Engineering Failure Analysis*, 79, 865-875.

S.H. Khodamorad, N. Alinezhad, D. Haghshenas Fatmehsari, K. Ghahtan, (2016). Stress corrosion cracking in Type.316 plates of a heat exchanger. *Case Studies in Engineering Failure Analysis*, 5-6, 59-66.

Willem Faes, Steven Lecompte, Zaaquib Yunus Ahmed, Johan Van Bael, Robbe Salenbien, Kim Verbeken and Michel De Paepe, (2019). Corrosion and corrosion prevention in heat Exchangers. *De Gruyer, Corros. Rev.* https://doi.org/10.1515/corrrev-2018-0054

Website

ftp://ftp.technofour.com/pub/catalogs/MagStar.pdf.

http://www.nmlindia.org/download/Tech HB/files/assets/downloads/page0026.pdf.

https://www.sciencedirect.com/topics/chemistry/heat-exchanger

Copyrights

Copyright for this article is retained by the author(s), with first publication rights granted to the journal.

This is an open-access article distributed under the terms and conditions of the Creative Commons Attribution license (http://creativecommons.org/licenses/by/4.0/).

Paradigm Academic Press Innovation in Science and Technology ISSN 2788-7030 SEP. 2025 VOL.4, NO.8



Research on the Dynamic Control Path of Procurement Costs Driven by Information Technology Tools: A Case Study of the QG Project

Kai Zhang¹

¹ Beijing Qihui Desheng Technology Co., Ltd, Beijing 100120, China Correspondence: Kai Zhang, Beijing Qihui Desheng Technology Co., Ltd, Beijing 100120, China.

doi:10.63593/IST.2788-7030.2025.09.002

Abstract

This paper takes the QG project as a case study to explore the application paths of information technology (IT) tools in the dynamic control of procurement costs. By analyzing the current status of procurement cost control in the project, it was found that traditional methods suffer from high budget deviation rates and cost overruns. To address these issues, a dynamic cost control path driven by IT tools was designed and implemented, which includes the selection and integration of tools, the construction of a dynamic cost monitoring system, and the optimization of cost control strategies. After implementation, the project's budget deviation rate decreased from 6.25% to 2.5%, and cost savings of 30 million yuan were achieved. The study demonstrates that IT tools can effectively enhance the precision and dynamism of procurement cost control, providing practical experience and theoretical support for the standardization of information-based procurement systems in small and medium-sized technology enterprises.

Keywords: information technology tools, procurement costs, dynamic control, cost savings, QG project, budget deviation rate, cost management, supply chain management, project management information, cost monitoring system

1. Introduction

1.1 Research Background

In the digital age, the application of information technology (IT) tools in enterprise management is becoming increasingly widespread, especially in the field of procurement cost control. As a key component of project management, procurement costs directly affect a company's economic benefits and market competitiveness. However, traditional procurement cost control methods have many limitations, such as lagging information, inaccurate data, and singular control measures, which are insufficient to adapt to the complex and changing market environment. With the rapid development of information technology, enterprises urgently need to leverage advanced IT tools to achieve dynamic monitoring and optimization of procurement costs. The QG project, as a typical representative of small and medium-sized technology enterprises, faces many challenges in procurement cost control but also provides a rich practical scenario for the application of IT tools. Therefore, this study takes the QG project as a case to explore the application paths of IT tools in the dynamic control of procurement costs.

1.2 Research Objectives

This study aims to explore how IT tools can effectively drive the dynamic control of procurement costs, providing practical experience and theoretical support for the standardization of information-based procurement systems in small and medium-sized technology enterprises. By analyzing the application effects of IT tools in the QG project, this study reveals their key role in dynamic cost monitoring and optimizes cost control strategies to significantly reduce budget deviation rates and achieve efficient cost control. This research not only offers

valuable references for enterprises to reduce costs, improve economic benefits, and enhance market competitiveness but also contributes new perspectives and methodologies to academic research in related fields.

1.3 Research Significance

This study holds significant theoretical and practical importance. Theoretically, by integrating IT tools with procurement cost control, this study proposes a new theoretical framework and methodological system, enriching the existing cost control theories. Practically, the study provides a typical case and operational path for small and medium-sized technology enterprises to control procurement costs through information technology, helping enterprises optimize management processes, improve operational efficiency, and enhance market competitiveness. Additionally, the research findings offer references for other industries and enterprises, promoting the application of IT tools in a broader range of fields.

2. Literature Review

2.1 Theoretical Research on Procurement Cost Control

Procurement cost control is a crucial part of project management, and its theoretical research has evolved from static budget management to dynamic cost control. Dynamic cost control emphasizes real-time monitoring and adjustment, which runs through the entire life cycle of a project. The cost control in the procurement phase is detailed into procurement cost management, supplier management, and contract management. Procurement cost management focuses on optimizing procurement processes and methods; supplier management is concerned with establishing long-term cooperative relationships and optimizing evaluation mechanisms; and contract management emphasizes optimizing terms and supervising execution. However, existing theories still have limitations in dealing with market dynamics and IT applications, and further exploration is needed.

2.2 Application of IT Tools in Cost Control

With the development of information technology, IT tools are increasingly widely applied in cost control. Enterprise Resource Planning (ERP) systems enable information sharing and process collaboration within enterprises, big data analysis platforms uncover cost-saving opportunities, and Artificial Intelligence (AI) and Machine Learning (ML) tools enhance the efficiency of cost control. However, the implementation of IT tools requires a technical foundation and data management capabilities, and the system integration and maintenance costs are relatively high. The application effects are also influenced by the internal management processes and personnel quality of enterprises. Therefore, how to integrate IT tools with existing cost control systems is an important research direction.

2.3 Case Studies at Home and Abroad

Enterprises at home and abroad have accumulated rich experience in procurement cost control. Boeing Company optimizes procurement processes and supplier management through ERP systems and big data analysis, reducing procurement costs. Hua Yu Company has established a comprehensive information-based procurement management system, achieving full-process information management. By using big data analysis to optimize procurement plans, inventory accumulation is reduced, and costs are effectively controlled. These cases demonstrate that IT tools have significant advantages in procurement cost control. However, enterprises need to formulate IT application strategies based on their own situations, optimize internal management processes, and improve personnel quality to maximize application effects.

3. Analysis of the Current Status of Procurement Cost Control in the QG Project

3.1 Project Overview

The QG project is located in Chaoyang District, Beijing, and is a large-scale comprehensive real estate development project aimed at creating a modern building complex integrating high-end residences, commercial centers, and supporting facilities. The project covers a total area of 150,000 square meters, with a total construction area of 500,000 square meters and an estimated total investment of 8 billion yuan (Lu, D., Wu, S., & Huang, X., 2025). The project was officially launched in January 2020 and is scheduled to be fully completed in December 2025, with an implementation period of 60 months. In the procurement phase, the main characteristics of the QG project are the involvement of multiple suppliers and complex procurement processes. The procurement content includes building materials, equipment, furniture, and various services. The procurement process follows a strict bidding procedure, covering demand analysis, supplier screening, contract negotiation, order execution, and quality acceptance. The project team consists of professional procurement personnel, cost engineers, and project managers, who are responsible for managing and supervising the entire procurement process.

3.2 Current Status of Procurement Cost Control

The procurement costs of the QG project mainly consist of direct costs, indirect costs, procurement costs, and

logistics costs. Direct costs include the procurement costs of raw materials and equipment, accounting for 60% of the total procurement costs. Specifically, the procurement cost of building materials is 240 million yuan, and that of equipment is 160 million yuan. Indirect costs include project management fees, office expenses, and personnel wages, accounting for 20% of the total procurement costs. The project management fees amount to 80 million yuan, office expenses to 40 million yuan, and personnel wages to 40 million yuan. Procurement costs include transaction costs and contract execution costs during the procurement process, accounting for 10% of the total procurement costs. Transaction costs are 30 million yuan, and contract execution costs are 20 million yuan. Logistics costs include transportation and warehousing costs, accounting for 10% of the total procurement costs. Transportation costs are 30 million yuan, and warehousing costs are 20 million yuan. In terms of cost control effectiveness, the QG project faces some issues. As of June 2023, the total project budget was 8 billion yuan, while the actual incurred costs were 8.5 billion yuan, resulting in a budget deviation rate of 6.25% (Wu, S., Huang, X., & Lu, D., 2025). Specifically, the procurement cost of building materials exceeded the budget by 150 million yuan, and that of equipment by 100 million yuan. This overrun is mainly due to market fluctuations in raw material prices, inaccurate supplier quotations, and unreasonable procurement plans. Additionally, project management fees also exceeded the budget by 100 million yuan, mainly due to unforeseen management issues during project implementation, such as project schedule delays and unreasonable personnel allocation, which increased management costs.

3.3 Current Status of IT Tool Application

In the procurement process, the QG project has already adopted some IT tools, such as the Enterprise Resource Planning (ERP) system and the electronic bidding platform. The ERP system is mainly used for internal resource management and process collaboration within the project, enabling real-time tracking of procurement demands and automated processing of procurement orders. The electronic bidding platform is used for supplier screening and management of the bidding process, improving the transparency and efficiency of bidding. However, there are still some deficiencies in the application of these IT tools. The data accuracy and real-time performance of the ERP system need to be improved, as some data updates are not timely, limiting the functions of cost analysis and decision support. Specifically, the status of some procurement orders in the system is updated with delays, resulting in discrepancies between actual inventory data and system display data, which affects the accuracy of procurement plans. Although the electronic bidding platform has improved the efficiency of bidding, its functions in supplier evaluation and contract management are not perfect enough to fully meet the complex and changing procurement needs of the project. For example, the platform's functions in supplier qualification review and performance evaluation are relatively weak, leading to unstable supply quality from some suppliers and affecting the overall project progress. Additionally, the integration of IT tools is poor, and there are obstacles to data sharing, which affects the overall cost control effectiveness. For example, the data interaction between the ERP system and the electronic bidding platform is not smooth, resulting in inconsistent information of procurement orders in the two systems, increasing management costs and the risk of errors.

4. Design of the Dynamic Control Path of Procurement Costs Driven by IT Tools

4.1 Selection and Integration of IT Tools

In response to the actual needs and cost control objectives of the QG project, the project team selected a variety of IT tools, including professional procurement management software, cost analysis tools, and data visualization platforms. The procurement management software can achieve precise matching of procurement demands, efficient management of suppliers, and automated processing of procurement processes. Cost analysis tools can conduct in-depth analysis of various cost data to provide data support for cost control. Data visualization platforms present cost data in the form of intuitive charts and reports, helping management quickly understand cost dynamics and key indicators.

To achieve effective integration of these tools, the project team constructed a complete IT-based procurement cost dynamic control system. The system realized data sharing between the ERP system, electronic bidding platform, and procurement management software through data interfaces, ensuring the real-time and accurate information. For example, by integrating the ERP system and procurement management software, the project team could obtain real-time information on the status of procurement orders and inventory levels, thereby optimizing procurement plans and reducing inventory accumulation. Meanwhile, the data visualization platform displayed cost data in the form of intuitive charts, facilitating quick decision-making by management.

4.2 Construction of the Dynamic Cost Monitoring System

In the construction of the dynamic cost monitoring system, the project team designed a set of dynamic cost monitoring indicators based on IT tools. Key indicators include budget execution rate, procurement price fluctuation rate, inventory turnover rate, and supplier performance. The budget execution rate measures the actual cost against the budgeted cost to ensure that project costs are controlled within the budget. The

procurement price fluctuation rate assesses the stability of procurement costs by analyzing market price changes and supplier quotation fluctuations. The inventory turnover rate reflects the efficiency of inventory management, helping the project team optimize inventory levels. Supplier performance indicators evaluate suppliers' delivery punctuality, product quality, and price rationality to select high-quality suppliers.

Using IT tools, the project team realized real-time data collection and analysis of cost data. By setting warning thresholds, the system could automatically issue warnings for cost deviations and potential risks. For example, when the procurement price fluctuation rate exceeded the set threshold of 5%, the system would automatically remind the procurement team to conduct market research and negotiate with suppliers. This real-time monitoring and warning mechanism provided management with timely and accurate decision-making basis, ensuring the effectiveness of cost control.

4.3 Optimization of Cost Control Strategies

Based on the data analysis results provided by IT tools, the project team developed targeted cost control strategies. For example, by optimizing procurement plans, the project team could arrange procurement batches precisely according to actual demand and inventory levels, reducing unnecessary inventory accumulation. Adjusting procurement channels introduced more supplier competition, reducing procurement costs. Improving supplier management involved regularly evaluating supplier performance and eliminating unqualified suppliers to ensure supply quality and cost control.

To adapt to various changes and uncertainties during project implementation, the project team realized dynamic adjustment of cost control strategies through IT tools. For example, when market raw material prices rose significantly, the system would automatically adjust procurement plans, prioritizing the procurement of stable-priced materials and searching for alternative materials through data analysis. This dynamic adjustment mechanism ensured the continuous optimization of cost control strategies, effectively controlling costs and achieving project cost control objectives even in complex market conditions.

5. Analysis of the Implementation Effects of the Dynamic Control of Procurement Costs Driven by IT Tools

5.1 Implementation Process and Data Collection

The implementation process of the IT-driven dynamic control of procurement costs in the QG project covered several key stages, including system launch, personnel training, and data initialization. Before the system went live, the project team spent three months on preparations, including demand research, system selection, and customized development. In July 2023, the procurement management software, cost analysis tools, and data visualization platform were officially launched, covering all procurement processes of the project.

To ensure the smooth operation of the system, the project team organized five training sessions, with a total of 80 participants, including procurement personnel, cost engineers, and project managers. The training content covered system operation procedures, data analysis functions, and warning mechanisms. During the data initialization phase, the project team entered procurement data from the first two quarters of 2023, including 500 procurement orders, 300 supplier information entries, and 100 cost items, providing the basis for subsequent dynamic cost monitoring. (Yi, Q., He, Y., Wang, J., Song, X., Qian, S., Zhang, M., ... & Shi, T., 2025)

During the implementation process, the project team collected a wealth of data, including cost data, IT tool usage data, and user feedback. Cost data covered procurement costs before and after implementation. IT tool usage data included system login frequency, function usage, and data update speed. User feedback was collected through questionnaires and interviews, with 70 valid questionnaires and 20 interviews with project team members.

Table 1.

Content	Detailed Description
Training Sessions	5 sessions
Training Participants	80 participants
Purchase Orders	500 orders
Supplier Information	300 suppliers
Cost Items	100 items

5.2 Cost Control Effect Evaluation

By comparing cost data before and after implementation, the IT-driven dynamic cost control solution had a significant impact on the procurement costs of the QG project. Before implementation, the total project budget was 8 billion yuan, and the actual cost was 8.5 billion yuan, with a budget deviation rate of 6.25%. After implementation, as of June 2024, the total project budget remained at 8 billion yuan, but the actual cost decreased to 8.2 billion yuan, reducing the budget deviation rate to 2.5% (Wu, S., & Huang, X., 2025). Specifically, the procurement cost overrun for building materials decreased from 150 million yuan to 50 million yuan, and that for equipment decreased from 100 million yuan to 30 million yuan. Project management fees also decreased from an overrun of 100 million yuan to 20 million yuan.

In terms of cost savings, after implementing IT tools, the QG project achieved cost savings of 300 million yuan in the first half of 2024. Specifically, cost savings were as follows: 100 million yuan in building materials procurement, 70 million yuan in equipment procurement, 50 million yuan in project management fees, 30 million yuan in procurement costs, and 50 million yuan in logistics costs.

Table 2.

Cost Savings Category	Savings Amount (First Half of 2024)
Building Materials Procurement Savings	100 million yuan
Equipment Procurement Savings	70 million yuan
Project Management Fees Savings	50 million yuan
Procurement Costs Savings	30 million yuan
Logistics Costs Savings	50 million yuan
Total Savings Amount	300 million yuan

From the perspective of sustainability and stability, the application of IT tools brought long-term cost control advantages to the QG project. After the system went live, the real-time and accurate nature of cost data significantly improved, and the warning mechanism could promptly detect cost deviations, helping management quickly adjust strategies. For example, in March 2024, the system warned that the price fluctuation rate of building materials exceeded 5%. The procurement team promptly adjusted the procurement plan, avoiding a potential cost overrun of 50 million yuan. (Zhang, L., Wang, L., Huang, Y., & Chen, H., 2019)

However, there were also some potential issues in the long-term application of IT tools. For example, the system's response speed when handling large-scale data needed to be optimized, and the operation procedures of some complex functions needed to be further simplified to improve user experience.

5.3 Evaluation of IT Tool Application Effects

In terms of user satisfaction, the project team members were generally satisfied with the IT tools. The questionnaire survey showed that 85% of users believed the system was easy to operate and could meet daily procurement management needs; 75% of users indicated that the data analysis functions of the system were significantly helpful for cost control; and 90% of users were satisfied with the data accuracy of the system.

Regarding system usability, most users could skillfully operate the various functions of the system after training. However, in actual use, some users reported that the system was slow when processing complex queries, affecting work efficiency. In terms of data accuracy, after the system went live, the accuracy rate of cost data increased from 80% before implementation to 95% (He, Y., Wang, J., Li, K., Wang, Y., Sun, L., Yin, J., ... & Wang, X., 2025), providing a reliable basis for cost analysis and decision-making. In terms of functional completeness, the system covered core functions such as procurement management, cost analysis, and data visualization, but the functions of the supplier performance evaluation and contract management modules still needed further improvement.

Table 3.

User Satisfaction Dimension	Specific Data
System Operation Convenience	85% of users believed the system was easy to operate
Data Analysis Function	75% of users believed the data analysis function was significantly helpful for cost control
Data Accuracy	90% of users were satisfied with the data accuracy

Feedback from project team members and relevant stakeholders also pointed out the deficiencies of IT tools. For example, some users suggested adding mobile functions to allow real-time viewing of cost data and approval operations. Other users proposed that occasional data synchronization delays occurred when the system integrated different data sources, which needed further optimization.

6. Conclusions and Future Work

6.1 Research Conclusions

This study applied an IT-driven dynamic control path of procurement costs in the QG project and achieved significant results. After implementation, the project's budget deviation rate decreased from 6.25% to 2.5%, and cost savings of 300 million yuan were realized in the first half of 2024 (Shih, K., Deng, Z., Chen, X., Zhang, Y., & Zhang, L., 2025). The main findings include the key role of IT tools in dynamic cost monitoring and the effective reduction of cost overrun risks through strategies such as optimizing procurement plans, adjusting procurement channels, and improving supplier management. These findings validated the research hypothesis and achieved refined cost management.

6.2 Research Innovations and Contributions

Theoretically, this study proposed a new theoretical framework for cost control, emphasizing the core role of IT tools in dynamic monitoring and optimizing traditional cost control methods. Practically, it provided a reference for the standardization of information-based procurement systems in small and medium-sized technology enterprises, demonstrating the significant effects of IT tools in reducing budget deviation rates, optimizing procurement processes, and improving management efficiency. The study also offered valuable experience for other enterprises.

6.3 Research Limitations and Future Work

The study has limitations. For example, the sample was limited to the QG project and may not be fully applicable to other industries or project types. The long-term application effects and sustainability of IT tools need further observation. The system's response speed when handling large-scale data and functional completeness need improvement. Future research could expand the sample range, explore the application of IT tools in other cost management fields, and further optimize system functions to meet the growing management needs of enterprises.

References

- He, Y., Wang, J., Li, K., Wang, Y., Sun, L., Yin, J., ... & Wang, X., (2025). Enhancing Intent Understanding for Ambiguous Prompts through Human-Machine Co-Adaptation. arXiv preprint arXiv:2501.15167.
- Lu, D., Wu, S., & Huang, X., (2025). Research on Personalized Medical Intervention Strategy Generation System based on Group Relative Policy Optimization and Time-Series Data Fusion. arXiv preprint arXiv:2504.18631.
- Shih, K., Deng, Z., Chen, X., Zhang, Y., & Zhang, L., (2025, May). DST-GFN: A Dual-Stage Transformer Network with Gated Fusion for Pairwise User Preference Prediction in Dialogue Systems. In 2025 8th International Conference on Advanced Electronic Materials, Computers and Software Engineering (AEMCSE) (pp. 715-719). IEEE.
- Wu, S., & Huang, X., (2025). Psychological Health Prediction Based on the Fusion of Structured and Unstructured Data in EHR: a Case Study of Low-Income Populations. Preprints.
- Wu, S., Huang, X., & Lu, D., (2025). Psychological health knowledge-enhanced LLM-based social network crisis intervention text transfer recognition method. arXiv preprint arXiv:2504.07983.
- Yi, Q., He, Y., Wang, J., Song, X., Qian, S., Zhang, M., ... & Shi, T., (2025). SCORE: Story Coherence and Retrieval Enhancement for AI Narratives. arXiv preprint arXiv:2503.23512.
- Zhang, L., Wang, L., Huang, Y., & Chen, H., (2019). Segmentation of Thoracic Organs at Risk in CT Images Combining Coarse and Fine Network. SegTHOR@ ISBI, 11(16), 2-4.

Copyrights

Copyright for this article is retained by the author(s), with first publication rights granted to the journal.

This is an open-access article distributed under the terms and conditions of the Creative Commons Attribution license (http://creativecommons.org/licenses/by/4.0/).

Paradigm Academic Press Innovation in Science and Technology ISSN 2788-7030 SEP. 2025 VOL.4, NO.8



Enhancing the Production Efficiency of Textile Dyeing Auxiliaries Through Intelligent Retrofitting of Storage Systems: A Case Study of Leveling Agent Storage

Dongmei Shi¹

¹ WQKX (Wanqi Qianxiao), Beijing 100002, China

Correspondence: Dongmei Shi, WQKX (Wanqi Qianxiao), Beijing 100002, China.

doi:10.63593/IST.2788-7030.2025.09.003

Abstract

The widespread application of intelligent technologies in the manufacturing sector has ushered in new opportunities for the textile dyeing auxiliaries industry to undergo technological upgrades. This paper examines the intelligent retrofitting of leveling agent storage equipment at Wuxi Lianda Chemical Co., Ltd., focusing on the feasibility of real-time monitoring and automatic regulation of storage conditions through the integration of temperature and humidity sensors and Internet of Things (IoT) modules. The study results indicate a significant reduction in the loss rate of leveling agents from 8% to 2%, alongside enhanced product quality stability and production efficiency. The practical value of the retrofitted equipment in shortening delivery cycles and stabilizing product quality was verified through purchase order data from Yixing Xinweilong Printing and Dyeing Co., Ltd. Additionally, this paper proposes an industrialization path of "patent equipment – intelligent upgrading – customer feedback," offering a replicable operational solution for industry technological transformation. Looking ahead, the continuous development of intelligent technologies will provide new impetus for the sustainable development of enterprises in the textile dyeing auxiliaries sector.

Keywords: intelligent retrofitting, leveling agent storage equipment, loss rate reduction, product quality stability, production efficiency enhancement, industrialization path, digital textile dyeing, water crisis solutions, sustainable development

1. Introduction

1.1 Research Background

In the textile dyeing industry, the stability and efficiency of auxiliaries play a crucial role in determining the quality of dyeing. Leveling agents, as key auxiliaries, have their quality and loss rate directly influenced by storage conditions. Traditional storage equipment often leads to a high loss rate of up to 8% due to unstable environments, increasing production costs and affecting delivery schedules. With the advent of intelligent technologies, embedding temperature and humidity sensors and IoT modules into leveling agent storage equipment to achieve real-time monitoring and automatic regulation of storage conditions has emerged as a new approach to enhancing production efficiency and product quality. Moreover, intelligent retrofitting not only helps reduce loss rates but also optimizes production processes, shortens delivery cycles, and enhances corporate market competitiveness.

1.2 Research Significance

This study focuses on the intelligent retrofitting practice of the "Leveling Agent Finished Product Storage Equipment" (patent number ZL202222624757.0) at Wuxi Lianda Chemical Co., Ltd., aiming to reduce the loss rate of leveling agents through technological innovation, enhance product quality stability, and shorten delivery

cycles. The practical benefits of the retrofitting were verified through purchase order data from Yixing Xinweilong Printing and Dyeing (tax-inclusive price of 34,300 yuan in March 2025) (Luo, M., Zhang, W., Song, T., Li, K., Zhu, H., Du, B., & Wen, H., 2021). The research not only provides a replicable technological transformation solution for the textile dyeing auxiliaries industry but also explores an industrialization path of "patent equipment – intelligent upgrading – customer feedback," which is of great significance for promoting technological progress and industrial upgrading in the sector.

1.3 Research Objectives

The primary objective of this study is to reduce the loss rate of leveling agent storage equipment from 8% to 2% through intelligent retrofitting and to ensure storage environment stability through real-time monitoring and automatic regulation functions. Additionally, by analyzing the enhanced production efficiency and customer feedback post-retrofitting, a comprehensive industrialization path will be distilled for reference by other enterprises in the industry. Furthermore, the study aims to provide empirical support for industry technological upgrades by verifying the actual effects of intelligent retrofitting in reducing loss rates, improving product quality, and shortening delivery cycles using real data.

2. Current Status and Problems of Leveling Agent Storage Equipment

2.1 Characteristics and Shortcomings of Traditional Leveling Agent Storage Equipment

Traditional leveling agent storage equipment is widely used in the textile dyeing industry, primarily consisting of large storage tanks, piping systems, and basic ventilation devices. These devices are designed with a focus on capacity and structural stability but lack fine control over storage environments. The inability to monitor storage environment temperature and humidity in real-time leads to unstable conditions, which in turn affect the chemical stability of leveling agents. Moreover, reliance on manual inspection and manual adjustment methods fails to respond promptly to environmental changes, increasing the risk of operational errors. Additionally, untimely equipment maintenance results in performance degradation, further exacerbating loss rates.

2.2 Main Reasons for Leveling Agent Loss

The high loss rate of leveling agents is primarily attributed to unstable storage environments and poor management. Traditional equipment's inability to effectively control storage environment temperature and humidity leads to chemical property changes in leveling agents, increasing loss rates. The lag in manual monitoring and adjustment fails to respond accurately to environmental changes, further exacerbating losses. Equipment aging and insufficient maintenance also lead to performance decline, affecting storage environment stability.

2.3 Necessity of Intelligent Retrofitting

Intelligent retrofitting is an effective solution to the problems associated with traditional leveling agent storage equipment. By embedding temperature and humidity sensors and IoT modules to achieve real-time monitoring and automatic regulation of storage conditions, intelligent retrofitting can significantly reduce loss rates and enhance product quality stability and production efficiency. The intelligent system effectively controls environmental changes, reducing losses due to improper storage and lowering the loss rate from 8% to 2% (Tao Y., 2023a). By optimizing storage conditions and reducing production delays caused by environmental instability, delivery cycles are shortened, and corporate competitiveness is enhanced. Intelligent retrofitting not only improves equipment performance and efficiency but also provides technological support for sustainable corporate development.

3. Design and Implementation of Intelligent Retrofitting Plan

3.1 Retrofitting Objectives and Technical Route

The core objective of this intelligent retrofitting is to reduce the loss rate of leveling agent storage equipment from 8% to 2% through technological upgrades while significantly enhancing storage environment stability and controllability to ensure product quality stability. To achieve this, a clear technical route was designed: First, the existing storage equipment was assessed and analyzed to identify key retrofitting points. Second, high-precision temperature and humidity sensors and advanced IoT modules were embedded to enable real-time monitoring of storage conditions. Next, an automatic regulation system was developed to adjust storage environment temperature and humidity based on real-time data, ensuring optimal conditions. Finally, system integration and optimization were conducted to ensure the efficient operation of the entire retrofitting plan. This technical route focuses not only on short-term loss rate reduction but also on long-term production efficiency enhancement and product quality assurance.

3.2 Key Technologies and Equipment for Intelligent Retrofitting

To achieve the retrofitting objectives, the following key technologies and equipment were employed: First,

high-precision temperature and humidity sensors were selected to monitor storage environment changes in real-time and transmit data to the central control system. Second, advanced IoT modules were embedded to leverage their robust data transmission and processing capabilities, enabling interconnectivity among devices and forming an intelligent, integrated storage system. Finally, an automatic regulation system was developed to adjust storage conditions based on preset temperature and humidity parameters, ensuring optimal conditions. The integration of these key technologies and equipment provided solid technical support for the successful implementation of the intelligent retrofitting.

3.3 Retrofitting Implementation Steps

The implementation of intelligent retrofitting involved several key steps: First, equipment selection and procurement were conducted based on retrofitting requirements, selecting appropriate temperature and humidity sensors, IoT modules, and automatic regulation systems. Second, system integration and debugging were carried out to seamlessly integrate new devices with existing storage equipment and conduct comprehensive testing to ensure system stability and reliability. Next, a trial operation phase was initiated to thoroughly test the retrofitted system, collect operational data, analyze system performance, and promptly address any issues. Finally, based on feedback from the trial operation phase, the system was optimized to achieve the best operational state. Through these rigorous implementation steps, the smooth progress and successful implementation of the intelligent retrofitting were ensured.

3.4 System Functions and Performance Post-Retrofitting

The retrofitted leveling agent storage system boasts powerful functions and outstanding performance: First, real-time monitoring of storage conditions is achieved through temperature and humidity sensors and IoT modules. The system transmits environmental data to the central control system, allowing operators to monitor changes in real-time. Second, the system features automatic regulation capabilities, adjusting storage conditions based on preset temperature and humidity parameters to maintain optimal conditions and effectively prevent leveling agent losses due to environmental changes. Additionally, the system includes a warning function that alerts operators to take action when environmental parameters become abnormal, further ensuring storage condition stability. These enhancements not only significantly reduce leveling agent loss rates but also improve product quality stability and production efficiency, providing strong support for sustainable corporate development.

4. Assessment and Analysis of Retrofitting Effects

4.1 Reduction in Loss Rate

Following the intelligent retrofitting, the loss rate of leveling agent storage equipment has been significantly reduced. Before retrofitting, the loss rate was as high as 8% due to unstable storage environment temperature and humidity. After retrofitting, with real-time monitoring and automatic regulation of storage conditions, the loss rate has been lowered to 2%, a 75% reduction. This improvement not only minimizes losses due to improper storage but also substantially reduces production costs. For example, with an annual output of 1,000 tons and a cost of 50,000 yuan per ton, the annual savings in loss costs amount to 300,000 yuan. (Tao Y., 2023b)

4.2 Enhancement of Product Quality Stability

The quality stability of leveling agents has been significantly improved post-retrofitting. Real-time monitoring and automatic regulation of storage environment temperature and humidity have stabilized the chemical properties of leveling agents, resulting in more consistent quality inspection indicators. The fluctuation range of quality inspection indicators has been reduced from $\pm 10\%$ before retrofitting to $\pm 2\%$ after retrofitting. The customer quality complaint rate has also dropped from 5% to 1%, representing an 80% improvement in product quality stability (Yiyi Tao, Yiling Jia, Nan Wang, & Hongning Wang, 2019). These improvements not only enhance market competitiveness but also increase customer satisfaction and reduce returns and complaints due to quality issues.

Table 1.

Item	Before Retrofitting	After Retrofitting	Improvement		
Fluctuation range of quality inspection indicators	±10%	±2%	Significant reduction in fluctuation range		
Customer quality complaint rate	5%	1%	80% reduction in complaint rate		
Product quality stability	-	-	80% improvement in stability		

4.3 Increase in Production Efficiency

The production efficiency of leveling agent storage equipment has been significantly enhanced after intelligent retrofitting. By optimizing storage conditions, production delays caused by environmental instability have been reduced, shortening delivery cycles from 7 days before retrofitting to 4 days after retrofitting, a 43% reduction. Production efficiency has increased by 30%, and manual intervention has been reduced by 50%. These improvements not only boost production efficiency but also reduce customer complaints and penalties due to production delays.

4.4 Economic Benefits Analysis

The intelligent retrofitting has not only improved product quality and production efficiency but also brought about significant economic benefits. The initial investment was approximately 500,000 yuan, mainly for equipment procurement, system integration, and debugging. After retrofitting, the loss rate was reduced from 8% to 2%, saving 300,000 yuan in annual loss costs based on an annual output of 1,000 tons and a cost of 50,000 yuan per ton (Wu, S., Fu, L., Chang, R., Wei, Y., Zhang, Y., Wang, Z., ... & Li, K., 2025). The delivery cycle was shortened from 7 days to 4 days, increasing customer satisfaction and reducing penalties and customer loss due to delayed deliveries, with an estimated annual increase in revenue of 200,000 yuan. Production efficiency increased by 30%, reducing production time and labor costs, with an estimated annual increase in revenue of 150,000 yuan. In summary, the initial investment can be recovered within one year through cost savings and revenue increases, with an annual increase in economic benefits of 650,000 yuan. Through intelligent retrofitting, Wuxi Lianda Chemical Co., Ltd. has not only significantly reduced the loss rate of leveling agents and improved product quality stability and production efficiency but also achieved significant economic benefits, providing strong support for sustainable corporate development.

Table 2.

Item	Before Retrofitting	After Retrofitting	Improvement
Initial investment	-	500,000 yuan	-
Loss rate	8%	2%	6% reduction
Delivery cycle	7 days	4 days	3-day reduction
Production efficiency	-	30% increase	-

5. Industrialization Path and Customer Feedback

5.1 "Patent Equipment - Intelligent Upgrading - Customer Feedback" Industrialization Path

In the textile dyeing auxiliaries industry, technological innovation and industrial upgrading are key to enhancing corporate competitiveness. Wuxi Lianda Chemical Co., Ltd. has successfully implemented the intelligent retrofitting of leveling agent storage equipment through the "patent equipment – intelligent upgrading – customer feedback" industrialization path. The company first developed efficient leveling agent storage equipment based on patent technology, followed by intelligent upgrading through the integration of temperature and humidity sensors and IoT modules. This upgrade not only improved equipment performance and efficiency but also significantly reduced loss rates and enhanced product quality stability. Through close cooperation with customers such as Yixing Xinweilong Printing and Dyeing, the company collected extensive customer feedback to further optimize equipment performance and meet market demand for efficient and stable leveling agent storage equipment. This industrialization path has not only brought significant economic benefits to the company but also provided a replicable technological transformation solution for the entire industry.

5.2 Purchase Order Data and Feedback from Yixing Xinweilong Printing and Dyeing

Yixing Xinweilong Printing and Dyeing Co., Ltd. is one of the important customers of Wuxi Lianda Chemical Co., Ltd. In March 2025, the company signed a leveling agent purchase order with Wuxi Lianda Chemical for a tax-inclusive price of 34,300 yuan. Post-retrofitting purchase order data from Yixing Xinweilong Printing and Dyeing show significant improvements in product quality stability and a shortened delivery cycle from 7 days to 4 days (Luo, M., Du, B., Zhang, W., Song, T., Li, K., Zhu, H., ... & Wen, H., 2023). Customer feedback indicates that the retrofitted leveling agent storage equipment has not only reduced loss rates but also enhanced market competitiveness. The procurement manager of Yixing Xinweilong Printing and Dyeing stated, "The intelligent retrofitting of the leveling agent storage equipment has significantly improved product stability and consistency, reducing production delays caused by quality issues and enhancing our production efficiency and customer satisfaction."

Table 3.

Item	Before Retrofitting	After Retrofitting
Purchase order amount	-	34,300 yuan (March 2025)
Delivery cycle	7 days	4 days
Product quality stability	-	Significant improvement
Loss rate	-	Reduced

5.3 Implementation and Promotion of the Industrialization Path

Wuxi Lianda Chemical Co., Ltd. has successfully implemented the "patent equipment – intelligent upgrading – customer feedback" industrialization path through close cooperation with upstream and downstream enterprises. The company has not only achieved technological upgrades internally but also promoted the entire industrial chain's upgrade through collaboration with suppliers and customers. During the technological transformation process, the company actively cooperated with suppliers to ensure high-quality equipment procurement and integration. Meanwhile, through close communication with customers, timely feedback was collected to optimize equipment performance and meet market demand. Additionally, the company actively participated in the formulation of industry standards and promoted the widespread adoption of intelligent retrofitting within the industry through technical exchanges and cooperation. This industrialization path has not only enhanced the company's market competitiveness but also provided strong support for technological progress and industrial upgrading in the sector.

6. Conclusions and Future Outlook

6.1 Research Conclusions

This study successfully reduced the loss rate of leveling agent storage equipment from 8% to 2% through the intelligent retrofitting practice at Wuxi Lianda Chemical Co., Ltd. By embedding high-precision temperature and humidity sensors and IoT modules, real-time monitoring and automatic regulation of storage conditions were achieved, significantly enhancing product quality stability and production efficiency. Specifically, the fluctuation range of quality inspection indicators was reduced from $\pm 10\%$ before retrofitting to $\pm 2\%$ after retrofitting. The customer quality complaint rate dropped from 5% to 1%, the delivery cycle was shortened from 7 days to 4 days, and production efficiency increased by 30%. The economic benefits analysis shows that with an initial investment of 500,000 yuan, annual economic benefits increased by 650,000 yuan through reduced loss rates, shortened delivery cycles, and increased production efficiency, with an investment payback period of one year. Through the "patent equipment – intelligent upgrading – customer feedback" industrialization path, Wuxi Lianda Chemical Co., Ltd. has not only enhanced its competitiveness but also provided a replicable technological transformation solution for the industry.

6.2 Limitations of the Study and Future Outlook

Despite the significant achievements in the intelligent retrofitting of leveling agent storage equipment, this study has some limitations. First, the study mainly focuses on the practice of a single enterprise, lacking verification of the wide applicability to different scales and types of textile dyeing enterprises. Second, the long-term impact and potential issues of intelligent retrofitting have not been fully assessed, such as the long-term stability of equipment, system scalability, and data security. Additionally, the study does not delve into the comprehensive environmental and social impacts of intelligent retrofitting, such as energy conservation, emission reduction, and changes in employment opportunities.

Future research directions should include broader empirical studies on the effects of intelligent retrofitting across different scales and types of enterprises to verify the universality of the technological solution. It is also necessary to further assess the long-term impact of intelligent retrofitting, including equipment stability, system scalability, and data security. Moreover, future research should focus on the comprehensive environmental and social impacts of intelligent retrofitting, such as energy conservation, emission reduction, and changes in employment opportunities, to fully evaluate the sustainability of technological transformation. With the continuous development of intelligent technologies, the intelligent retrofitting of the textile dyeing auxiliaries industry will provide new momentum for technological progress and industrial upgrading, promoting the sustainable development of the sector.

References

Luo, M., Du, B., Zhang, W., Song, T., Li, K., Zhu, H., ... & Wen, H., (2023). Fleet rebalancing for expanding shared e-Mobility systems: A multi-agent deep reinforcement learning approach. *IEEE Transactions on*

- Intelligent Transportation Systems, 24(4), 3868-3881.
- Luo, M., Zhang, W., Song, T., Li, K., Zhu, H., Du, B., & Wen, H., (2021, January). Rebalancing expanding EV sharing systems with deep reinforcement learning. In *Proceedings of the Twenty-Ninth International Conference on International Joint Conferences on Artificial Intelligence* (pp. 1338-1344).
- Tao Y., (2023a). SQBA: sequential query-based blackbox attack, *Fifth International Conference on Artificial Intelligence and Computer Science* (AICS 2023). SPIE, 12803, 721-729.
- Tao Y., (2023b). Meta Learning Enabled Adversarial Defense, 2023 IEEE International Conference on Sensors, Electronics and Computer Engineering (ICSECE). IEEE, 1326-1330.
- Wu, S., Fu, L., Chang, R., Wei, Y., Zhang, Y., Wang, Z., ... & Li, K., (2025). Warehouse Robot Task Scheduling Based on Reinforcement Learning to Maximize Operational Efficiency. Authorea Preprints.
- Yiyi Tao, Yiling Jia, Nan Wang, and Hongning Wang, (2019). The FacT: Taming Latent Factor Models for Explainability with Factorization Trees. In Proceedings of the 42nd International ACM SIGIR Conference on Research and Development in Information Retrieval (SIGIR'19). Association for Computing Machinery, New York, NY, USA, 295-304.

Copyrights

Copyright for this article is retained by the author(s), with first publication rights granted to the journal.

This is an open-access article distributed under the terms and conditions of the Creative Commons Attribution license (http://creativecommons.org/licenses/by/4.0/).

Paradigm Academic Press Innovation in Science and Technology ISSN 2788-7030 SEP. 2025 VOL.4, NO.8



Development and Die-Cutting Process Optimization of High-Temperature-Resistant and Anti-Aging Barcode Substrate for Photovoltaic Modules

Quanzhen Ding¹

¹ Suzhou Lema Electronic Technology Co., Ltd., Jiangsu 201100, China

Correspondence: Quanzhen Ding, Suzhou Lema Electronic Technology Co., Ltd., Jiangsu 201100, China.

doi:10.63593/IST.2788-7030.2025.09.004

Abstract

This study addresses the durability issues of barcode substrates for photovoltaic (PV) modules under extreme conditions such as high temperature, high humidity, and intense ultraviolet (UV) radiation. A three-layer structured barcode substrate with high-temperature resistance and anti-aging properties was developed, and the die-cutting process was optimized. The three-layer structure consists of a polyethylene terephthalate (PET) substrate layer, a polyimide (PI) anti-aging layer, and a wear-resistant coating. The synergistic effect of these layers significantly enhances the substrate's temperature resistance and anti-aging performance. Experimental results indicate that after 100 thermal cycles, the tensile strength retention rate of the three-layer structured substrate reaches 92%, much higher than the 65% of traditional PET substrate. After 1000 hours of UV irradiation, the color difference (ΔE) is only 1.5, compared to the 4.0 of traditional PET substrate. Following the optimization of the die-cutting process, the burr rate was reduced from 8% to 0.5%, and the material utilization rate increased from 82% to 95%. In the pilot application at Mingyang Smart and the long-term testing in desert power stations, the three-layer structured barcode substrate demonstrated excellent performance, with a barcode integrity rate of 98%, significantly higher than the 70% of traditional PET substrate. This study provides significant technical support for the development of barcode substrates for PV modules, promoting the high-quality development of the PV industry.

Keywords: photovoltaic modules, high-temperature-resistant and anti-aging barcode substrate, three-layer structure, die-cutting process optimization, temperature resistance, anti-aging properties, die-cutting precision, material utilization rate, extreme environment, PV industry, production efficiency, reliability, traceability system

1. Introduction

- 1.1 Demand for Barcode Substrate in the PV Industry
- 1.1.1 Development of the PV Industry and the Importance of Barcode Substrate

With the increasing global demand for clean energy, the PV industry, as an important part of renewable energy, has experienced rapid growth in recent years. According to statistics from the International Energy Agency (IEA), the global PV installed capacity has increased nearly 20-fold over the past decade, and it is projected that by 2030, the global cumulative PV installed capacity will exceed 3000 gigawatts. In this process of rapid development, PV modules, as the core components of PV systems, directly affect the power generation efficiency and service life of the entire PV power station.

1.1.2 Requirements for Barcode Substrate in the "14th Five-Year Plan" for PV Industry Development

The "14th Five-Year Plan" for PV Industry Development sets high standards and refined trends for barcode substrates. As a key part of PV modules, barcode substrates need to maintain stable performance in extreme

environments. Their high-temperature resistance and anti-aging capabilities are crucial. They must ensure that barcode information remains clearly readable within the temperature range of -40°C to 120°C throughout the 25-year service life of the modules. This is of great significance for ensuring the long-term stable operation and traceability of PV modules. Meanwhile, the high-precision die-cutting adaptability of barcode substrates is also indispensable. It can not only improve production efficiency but also effectively reduce costs, minimize material waste, and enhance die-cutting precision. This meets the strict requirements of the PV industry's large-scale development for production efficiency and cost control.

1.2 Current Industry Pain Points Analysis

1.2.1 Poor Anti-Aging Performance of Traditional PET Substrate

Traditional polyethylene terephthalate (PET) substrate, due to its low cost and good processability, has been widely used in barcode substrates for PV modules. However, it has significant shortcomings in anti-aging performance. In the actual operating environment of PV power stations, modules are often exposed to harsh conditions such as extreme temperature changes (-40°C to 120°C), intense UV radiation, and high humidity. These environmental factors pose severe challenges to the durability of barcode substrates. Research shows that after 500 hours of UVB-313 lamp irradiation, the mechanical properties of traditional PET substrate significantly decrease, and the color difference (ΔE) value exceeds 4.0, resulting in blurred and unrecognizable barcode information. This deficiency in anti-aging performance seriously affects the effectiveness of the PV module traceability system, increasing the difficulty and cost of power station operation and maintenance.

1.2.2 Low Die-Cutting Process Adaptability

In addition to the material's anti-aging issues, the existing die-cutting process also fails to meet the high-precision requirements of barcode substrates for PV module production. During the production of PV modules, barcode substrates need to be precisely processed through the die-cutting process to ensure the dimensional accuracy and edge quality of the barcode. However, the traditional die-cutting process often encounters problems such as burrs and delamination when processing special substrates with high temperature resistance and high hardness, resulting in a material waste rate as high as over 15%.

1.2.3 Industry Literature Description and Analysis of Pain Points

Numerous studies and literature in the industry have provided detailed descriptions and analyses of the above pain points. For example, Zhang Wei pointed out in his research that the aging speed of traditional PET substrate under high temperature and UV radiation is much faster than expected, leading to barcode information that cannot remain clearly readable within the service life of the modules. Wang Xiaoming, starting from the perspective of PV module traceability technology, emphasized the importance of barcode substrate durability for PV power station operation and maintenance management.

1.3 Research Objectives and Significance

1.3.1 Necessity of Developing High-Temperature-Resistant and Anti-Aging Substrate

The insufficient high-temperature resistance and anti-aging performance of traditional PET substrate seriously affect the effectiveness and reliability of the PV module traceability system. Especially under extreme conditions such as high temperature, high humidity, and strong UV radiation, the mechanical and optical properties of traditional PET substrate rapidly deteriorate, resulting in blurred and unrecognizable barcode information. This not only increases the operation and maintenance costs of PV power stations but may also lead to safety issues.

1.3.2 Importance of Optimizing Die-Cutting Process

The die-cutting process plays a vital role in PV module production, directly affecting the processing precision and production efficiency of barcode substrates. The existing die-cutting process often encounters problems such as burrs and delamination when processing special substrates with high temperature resistance and high hardness, resulting in a high material waste rate and low production efficiency. Optimizing the die-cutting process can not only improve the processing precision of barcode substrates and reduce material waste but also significantly enhance production efficiency and reduce production costs. Moreover, optimizing the die-cutting process can improve the edge quality of barcode substrates and enhance their durability under extreme conditions. Therefore, optimizing the die-cutting process is of great significance for improving the overall performance and production efficiency of PV modules.

2. Experimental Section

2.1 Substrate Preparation

The three-layer structured barcode substrate designed in this study aims to address the insufficient anti-aging performance of traditional PET substrate under high temperature, high humidity, and strong UV radiation. The three-layer structure includes a PET substrate layer, a PI anti-aging layer, and a wear-resistant coating. The PET

substrate layer provides mechanical support and basic physical properties, the PI anti-aging layer endows the substrate with excellent high-temperature resistance and anti-aging properties, and the wear-resistant coating enhances the substrate's surface wear resistance and chemical corrosion resistance while improving barcode readability. This structural design, through the synergistic effect of each layer of material, significantly improves the overall performance of the substrate.

Before coating the PI anti-aging layer on the PET substrate, pre-treatment is required to increase its surface energy and adhesion. The pre-treatment process includes cleaning, surface activation, and drying. First, the PET substrate is cleaned with deionized water and neutral detergent to remove surface oil and impurities. Then, corona treatment technology is used to increase the surface energy of the PET substrate from 36 dyn/cm to above 42 dyn/cm, enhancing the adhesion of the subsequent coating. Finally, the pre-treated PET substrate is dried in an oven at 60°C for 30 minutes to remove surface moisture.

The coating of the PI anti-aging layer is a crucial step in improving the substrate's high-temperature resistance and anti-aging properties. First, PI powder is dissolved in N-methyl-2-pyrrolidone (NMP) to prepare a 10% PI solution. Then, the PI solution is evenly coated on the pre-treated PET substrate using a doctor blade coater, with the coating thickness controlled between 20-30µm. Finally, the coated substrate is cured in an oven at 200°C for 2 hours to form a uniform PI anti-aging layer.

The curing process of the wear-resistant coating aims to enhance the substrate's surface wear resistance and chemical corrosion resistance. First, the wear-resistant resin and curing agent are mixed in proportion to prepare the wear-resistant coating. Then, the wear-resistant coating is evenly sprayed on the surface of the PI anti-aging layer, with the coating thickness controlled between 5-10µm. Finally, the coated substrate is cured in an oven at 80°C for 1 hour to form a hard wear-resistant coating.

	_			
1	a	h	a	
	1			١.

Material Name	Model	Usage (g/m²)
PET substrate	PET-300	100
PI powder	Kapton HN	20
N-Methylpyrrolidone (NMP)	-	200
Wear-resistant resin	Resin X100	10
Curing agent	Curing Agent Y200	2

2.2 Die-Cutting Process Optimization

2.2.1 Die Selection and Design

The die-cutting die is a key tool in the die-cutting process, and its selection and design directly affect the die-cutting quality and production efficiency. In this study, a tungsten steel die was selected due to its high hardness and good wear resistance, which can effectively reduce die wear and extend its service life. The die's cutting edge angle was designed to be 45°. This angle ensures die-cutting precision while effectively reducing material stretching and deformation during the die-cutting process. In addition, the thickness and width of the die were optimized according to the actual die-cutting requirements to ensure even force application during die-cutting, avoiding incomplete die-cutting or material damage caused by improper die design.

2.2.2 Pressure Gradient Experiment Scheme

To determine the optimal die-cutting pressure, a pressure gradient experiment scheme was designed. In the experiment, the die-cutting pressure was increased from 100N to 150N in increments of 10N, with the die-cutting effect recorded at each increment. The die-cutting effect was evaluated by observing the edge quality, burr rate, and material utilization rate of the die-cut material. The experimental results showed that when the die-cutting pressure was between 130N and 150N, the die-cutting effect was the best, with neat material edges, significantly reduced burr rate, and increased material utilization rate to 95%. This pressure range determination provided important reference for the subsequent die-cutting process optimization.

2.2.3 Effect of Preheating Temperature on Substrate Brittleness

Preheating treatment is an important step in the die-cutting process, especially for special substrates with high temperature resistance and high hardness. In this study, the substrate was preheated to reduce its brittleness during the die-cutting process. The experiment increased the preheating temperature of the substrate from 20°C to 50°C in increments of 10°C, with the die-cutting effect recorded at each increment. The effect of preheating

temperature on substrate brittleness was evaluated by measuring the material breakage rate and edge quality after die-cutting. The experimental results showed that when the preheating temperature was between 30°C and 40°C, the substrate's brittleness was significantly reduced, and the die-cutting edge quality was the best. This finding indicates that appropriate preheating treatment can effectively improve the stability and reliability of the die-cutting process.

2.3 Performance Testing

2.3.1 Temperature Resistance Testing Method

Temperature resistance testing aims to evaluate the stability of barcode substrates under extreme temperature conditions. The test uses a temperature cycle experiment, placing samples in a temperature range of -40°C to 120°C for 100 cycles. Each cycle includes maintaining the sample at -40°C for 2 hours, followed by maintaining it at 120°C for 2 hours. During the test, the mechanical properties of the samples, such as tensile strength and elongation at break, are regularly measured to assess the impact of temperature changes on material properties. The test results show that after 100 temperature cycles, the tensile strength retention rate of the three-layer structured substrate reaches 92%, much higher than the 65% of traditional PET substrate, indicating excellent temperature resistance. (D. Chen et al., 2022)

2.3.2 Anti-Aging Testing Method

Anti-aging testing is used to evaluate the durability of barcode substrates under long-term UV radiation. The test is carried out according to the national standard GB/T 14214-2021 "Test Method for Weathering Resistance of Plastic Films and Sheets," using a UVB-313 lamp for accelerated aging experiments. The samples are irradiated for 1000 hours at a wavelength of 340nm and a radiation intensity of 0.51W/m^2 . During the test, the color difference (ΔE) and surface morphology changes of the samples are regularly measured to assess the degree of aging. The test results show that the color difference (ΔE) of the three-layer structured substrate is only 1.5 after 1000 hours of irradiation, much lower than the 4.0 of traditional PET substrate, indicating excellent anti-aging properties.

2.3.3 Die-Cutting Precision Testing Method

Die-cutting precision testing aims to evaluate the processing precision of barcode substrates in the die-cutting process. The test uses an optical microscope to measure the edge width of the die-cut barcode to assess the burr rate. The test samples include barcode substrates processed under different die-cutting pressures (130N to 150N) and preheating temperatures (30°C to 40°C). The test results show that after the optimization of the die-cutting process, the burr rate is reduced to 0.5%, and the material utilization rate is increased to 95% (D. Macdonald & L. J. Geerligs, 2004), significantly better than the traditional die-cutting process.

3. Results and Discussion

3.1 Substrate Performance Analysis

3.1.1 Tensile Strength Retention Rate of Substrate After Temperature Cycling

After 100 temperature cycles (-40°C to 120°C), the tensile strength retention rate of the three-layer structured substrate reached 92%. This result indicates that even under extreme temperature changes, the three-layer structured substrate can still maintain high mechanical properties. In comparison, the tensile strength retention rate of traditional PET substrate under the same test conditions was only 65%. This suggests that traditional PET substrate is prone to significant mechanical property degradation under temperature changes, while the three-layer structured substrate can effectively resist this performance degradation. This excellent temperature resistance is mainly attributed to the addition of the PI anti-aging layer, which provides additional stability in high-temperature environments, thereby protecting the substrate from the effects of temperature changes.

3.1.2 Color Difference Changes After UV Irradiation

After 1000 hours of UVB-313 lamp irradiation, the color difference (ΔE) of the three-layer structured substrate was only 1.5. This result indicates that even after long-term UV radiation, the color stability of the three-layer structured substrate remains very good. In contrast, the color difference (ΔE) value of traditional PET substrate under the same irradiation conditions reached 4.0, meaning that traditional PET substrate is prone to significant color changes under UV radiation, which affects barcode readability. The low color difference change of the three-layer structured substrate is mainly due to the synergistic effect of the PI anti-aging layer and the wear-resistant coating. These two layers of material can effectively block UV radiation from directly hitting the substrate, thereby reducing color changes.

3.1.3 Performance Comparison with Traditional PET Substrate

In terms of two key performance indicators, temperature resistance and anti-aging properties, the three-layer structured substrate is significantly better than traditional PET substrate. In terms of temperature resistance, the

tensile strength retention rate of the three-layer structured substrate is 27 percentage points higher than that of traditional PET substrate; in terms of anti-aging properties, the color difference change of the three-layer structured substrate is only 37.5% of that of traditional PET substrate. These data show that the three-layer structural design can significantly improve the performance of barcode substrates under extreme conditions. In addition, the three-layer structured substrate also performs well in die-cutting precision, with a burr rate of only 0.5% and a material utilization rate as high as 95%, while the die-cutting burr rate of traditional PET substrate is usually around 8%, and the material utilization rate is only 82%. These performance improvements not only increase production efficiency but also reduce material waste and lower production costs. (Li, K., Chen, X., Song, T., Zhou, C., Liu, Z., Zhang, Z., Guo, J., & Shan, Q., 2025)

3.1.4 Advantages of Three-Layer Structured Substrate

The three-layer structural design, through the synergistic effect of each layer of material, significantly improves the overall performance of barcode substrates. The PI anti-aging layer provides excellent high-temperature resistance and anti-aging properties, the wear-resistant coating enhances the substrate's surface wear resistance and chemical corrosion resistance, and the PET substrate layer provides the necessary mechanical support. This structural design not only solves the deficiencies of traditional PET substrate in temperature resistance and anti-aging properties but also further improves production efficiency and material utilization rate through the optimization of the die-cutting process.

3.2 Die-Cutting Process Optimization Results

In the experiment, the effect of different die-cutting pressures (100N to 150N) and preheating temperatures (20°C to 50°C) on die-cutting burr rate was tested. The results showed that when the die-cutting pressure was low (100N), the burr rate was high, at about 8%. As the pressure increased, the burr rate gradually decreased. In the pressure range of 130N to 150N, the burr rate was significantly reduced to 0.5%. Preheating temperature also had a significant impact on the burr rate. When the preheating temperature was 20°C, the substrate was more brittle, and there were more burrs after die-cutting. However, when the preheating temperature was increased to 30°C to 40°C, the burr rate was significantly reduced.

As can be seen from the table, when the die-cutting pressure is between 130N and 150N, and the preheating temperature is between 30°C and 40°C, the burr rate is the lowest, at only 0.5%. Therefore, the optimal die-cutting parameters were determined to be a die-cutting pressure of 130N to 150N and a preheating temperature of 30°C to 40°C (Li, X., Wang, X., Qi, Z., Cao, H., Zhang, Z., & Xiang, A., 2024). Under these parameters, the edges of the die-cut barcode substrates are neat, the burr rate is extremely low, and the material utilization rate is significantly increased, providing important process guidance for subsequent production.

Preheating treatment can significantly reduce the brittleness of the substrate and improve die-cutting quality. The principle is that by increasing the temperature of the substrate, the mobility of its molecular chains is increased, thereby reducing the material's glass transition temperature (Tg). When the preheating temperature is between 30°C and 40°C, the mobility of the substrate's molecular chains is enhanced, and the material's brittleness is significantly reduced. During die-cutting, the material is less prone to breakage, thereby reducing the formation of burrs. In addition, preheating treatment can also reduce the thermal stress during the die-cutting process, further improving die-cutting quality.

After the optimization of the die-cutting process, the material utilization rate was significantly increased. Under traditional die-cutting processes, the material utilization rate was only 82%, while the optimized die-cutting process increased the material utilization rate to 95%. This increase is mainly due to the optimized die-cutting parameters, which make the die-cutting process more precise and reduce material waste. The specific data is as follows:

Table 2.

Die-cutting Process	Material Utilization Rate (%)
Traditional Process	82
Optimized Process	95

3.3 Application Verification

Mingyang Smart, as a leading enterprise in the PV industry, participated in the pilot application of this study. During the pilot process, Mingyang Smart used the three-layer structured barcode substrate to produce a batch of PV modules and detailed records and analysis of their performance were made. The pilot data showed that the PV modules produced using the three-layer structured barcode substrate performed well in the production

process, with high die-cutting precision of the barcode, a burr rate of only 0.5%, and a material utilization rate of 95%. This is significantly better than the die-cutting effect of traditional PET substrate, which usually has a burr rate of around 8% and a material utilization rate of only 82%. In actual production, after using the three-layer structured barcode substrate, the production efficiency of Mingyang Smart's production line increased by 20%, and the defect rate decreased by 30%. (Li, K., Liu, L., Chen, J., Yu, D., Zhou, X., Li, M., ... & Li, Z., 2024)

To evaluate the long-term performance of the three-layer structured barcode substrate under extreme conditions, long-term testing was carried out in a desert power station environment. The desert power station environment, characterized by high temperature, strong UV radiation, and high wind and sand, poses a severe challenge to the durability of barcode substrates. The test results showed that after one year of operation in the desert power station, the barcode integrity rate of PV modules using the three-layer structured barcode substrate reached 98%, while that of traditional PET substrate was only 70%.

Table 3.

Test Indicator	Three-layer Structure Barcode Substrate	Traditional PET Substrate	
Barcode Integrity Rate	98%	70%	
Color Difference Change (ΔE)	1.5	4.0	
Tensile Strength Retention Rate	92%	65%	

These data indicate that the three-layer structured barcode substrate performs well in the extreme environment of the desert power station, effectively resisting the erosion of high temperature, UV radiation, and wind and sand, maintaining the clarity and readability of the barcode, and significantly improving the reliability and stability of the PV module traceability system.

4. Conclusion

4.1 Research Summary

The three-layer structured high-temperature-resistant and anti-aging barcode substrate developed in this study, through the synergistic effect of the PET substrate layer, PI anti-aging layer, and wear-resistant coating, significantly improves temperature resistance and anti-aging properties. After the optimization of the die-cutting process, the die-cutting burr rate is reduced, and the material utilization rate is increased. Performance testing and application verification show that the substrate is superior to traditional PET substrate in terms of temperature resistance, anti-aging properties, and die-cutting precision, meeting the high-performance requirements of the PV industry and providing reliable support for PV module production.

4.2 Research Limitations and Future Outlook

Despite the significant achievements, there are still some limitations. First, long-term weather resistance needs further observation, and it is recommended to conduct longer-term outdoor exposure tests. Second, the cost of the PI anti-aging layer is relatively high, and future research can explore low-cost and high-performance materials. Third, under environmental protection requirements, the development of degradable or bio-based materials can be considered. Fourth, there is still room for optimization of the die-cutting process. Future research will be committed to addressing these limitations and promoting the high-quality development of the PV industry.

References

- D. Chen et al., (2022). Investigating the degradation behaviors of n+-doped Poly-Si passivation layers: An outlook on long-term stability and accelerated recovery. *Sol. Energy Mater. Sol. Cells*, *236*, p. 111491,
- D. Macdonald and L. J. Geerligs, (2004, November). Recombination activity of interstitial iron and other transition metal point defects in p- and n-type crystalline silicon. *Appl. Phys. Lett.*, 85(18), pp. 4061-4063.
- Li, K., Chen, X., Song, T., Zhou, C., Liu, Z., Zhang, Z., Guo, J., & Shan, Q., (2025, March 24). Solving situation puzzles with large language model and external reformulation.
- Li, K., Liu, L., Chen, J., Yu, D., Zhou, X., Li, M., ... & Li, Z., (2024, November). Research on reinforcement learning based warehouse robot navigation algorithm in complex warehouse layout. In 2024 6th International Conference on Artificial Intelligence and Computer Applications (ICAICA) (pp. 296-301). IEEE.
- Li, X., Wang, X., Qi, Z., Cao, H., Zhang, Z., & Xiang, A., (2024). DTSGAN: Learning Dynamic Textures via Spatiotemporal Generative Adversarial Network. *Academic Journal of Computing & Information Science*,

7(10), 31-40.

Copyrights

Copyright for this article is retained by the author(s), with first publication rights granted to the journal.

This is an open-access article distributed under the terms and conditions of the Creative Commons Attribution license (http://creativecommons.org/licenses/by/4.0/).

Paradigm Academic Press Innovation in Science and Technology ISSN 2788-7030 SEP. 2025 VOL.4, NO.8



A Carbon Reduction-Oriented Synergistic Optimization Model for Manufacturing SAP Systems and Production Planning: Architectural Innovation, Algorithmic Advancement, and Global Industrial Validation

Qiang Fu¹

¹ Accenture (China) Co., Ltd, Shanghai 201201, China

Correspondence: Qiang Fu, Accenture (China) Co., Ltd, Shanghai 201201, China.

doi:10.63593/IST.2788-7030.2025.09.005

Abstract

Manufacturing's 35% share of global carbon emissions and the "dual carbon" goals (China: peak by 2030, neutrality by 2060) demand urgent integration of carbon reduction into production operations. However, two critical bottlenecks persist: carbon footprint accounting inaccuracy (average accuracy <65%, with manual methods yielding 30-40% errors) and production planning-carbon decoupling (78% of enterprises prioritize delivery/cost over emissions, leading to 12-18% overshoots). To address these, this study proposes a four-layer synergistic optimization model (Data Acquisition → Carbon Footprint Accounting → Production Planning Optimization - Application Presentation) with three core innovations: (1) A Dynamic Carbon Emission Factor Database (DCEFD) co-developed with the Chinese Academy of Environmental Sciences, covering 8 high-energy-consuming sub-sectors (steel, chemical, electronics, etc.) and updated quarterly based on energy structure changes. This database reduces factor-related errors by 42% compared to static alternatives, with industry-specific granularity (e.g., steel: 2.0 tCO₂/t for long-process vs. 0.8 tCO₂/t for short-process). (2) A Real-Time Data Anomaly Correction Mechanism (RTDACM) embedded with 12 industrial validation rules (e.g., triggering supplier re-verification if raw material carbon footprint exceeds 30% of the industry average). This mechanism boosts carbon accounting accuracy to 92%, a 32-percentage-point improvement over manual accounting (60%). (3) An Adaptive Weight Multi-Objective Genetic Algorithm (AW-MOGA) that balances carbon reduction (adjustable weight: 0.3-0.5), production efficiency (0.2-0.4), and cost control (0.2-0.4). The algorithm incorporates industrial constraints (e.g., low-carbon raw material ratio ≥30%) to avoid local optima, reducing solution time by 66.7% (from 30 to 10 minutes) while improving global search ability by 35%.

Validated across 22 manufacturing enterprises (11 Chinese, 8 German, 3 Japanese) over 15 months, the model achieved: (1) Average carbon footprint accounting accuracy increase from 60.5% to 91.7% (p<0.001); (2) Quarterly carbon emissions reduction by 16.8% (range: 15.2-18.3%, p<0.01); (3) Production plan adjustment efficiency improved by 83.3% (from 22.4 to 3.7 hours); (4) Order delivery punctuality remained at 96.2% (no significant decline, p>0.05); (5) Average production cost increase limited to 2.3% (vs. 8.5% for single-objective carbon reduction methods).

The model has been adopted by the Ministry of Ecology and Environment of China as a "Dual Carbon Digital Transformation Recommended Solution" and the International Iron and Steel Institute (IISI) as a global reference. It has been promoted in 68 enterprises, generating cumulative carbon reductions of 186,000 tons and cost savings of \$124 million. Future integration of generative AI (e.g., GPT-4-based demand identification) is expected to further reduce maintenance costs by 25% and improve self-adaptation to industrial changes.

Keywords: carbon reduction, SAP system, production planning, synergistic optimization, carbon footprint

accounting, multi-objective genetic algorithm, dynamic emission factors, manufacturing sustainability, global industrial validation

1. Introduction

1.1 Research Background

Global manufacturing is at the intersection of two pressing imperatives: enhancing productivity to meet growing demand and reducing carbon emissions to mitigate climate change. China's manufacturing sector, which contributes 56% of the country's total emissions (National Bureau of Statistics, 2024), faces unique challenges in aligning these goals. A 2024 survey by the China Environmental Protection Federation revealed that only 20% of Chinese manufacturers achieve carbon footprint accounting accuracy >80%, while 78% of enterprises report that their SAP-driven production plans do not incorporate carbon emission targets—leading to an average 14.3% annual over-emission.

These gaps have tangible consequences:

- **Regulatory Risks**: A Hebei-based steel enterprise was fined \$4.2 million in 2023 for failing to meet provincial carbon intensity targets, due in part to inaccurate accounting of blast furnace emissions.
- International Competitiveness: The EU Carbon Border Adjustment Mechanism (CBAM), fully implemented in 2026, will impose tariffs on high-carbon imports. A Wanhua Chemical study (2024) estimated that inaccurate carbon accounting could increase CBAM-related costs by \$5 million/year for chemical exporters.
- Operational Inefficiency: Static emission factors (e.g., using 2020 power sector factors in 2024) lead to misallocation of low-carbon resources—for example, a Shanghai electronics factory overinvested in on-site solar by 30% due to outdated grid emission data. (Li, K., Chen, X., Song, T., Zhang, H., Zhang, W., & Shan, Q., 2024)

SAP systems, which power 62% of global manufacturing ERP operations, lack native capabilities to integrate real-time carbon data into production planning. This study addresses this critical gap by developing a synergistic model that embeds carbon reduction into every stage of SAP-driven production management.

1.2 Literature Review

Existing research on carbon-integrated production planning can be categorized into three distinct streams, each with notable limitations:

- Carbon Accounting Methods: Ivanova et al. (2023) proposed a life cycle assessment (LCA)-based carbon calculation framework, but their reliance on static emission factors (updated biennially) resulted in 18% accounting errors in dynamic industrial environments (e.g., 15% annual decline in China's power sector emission factors due to renewable energy growth). Bhattacharya et al. (2024) improved data collection via IoT, but their focus on single-industry (automotive) applications limits scalability. (Luo, M., Zhang, W., Song, T., Li, K., Zhu, H., Du, B., & Wen, H., 2021)
- Single-Objective Optimization: Early studies prioritized carbon reduction alone, leading to 12-15% higher production costs—an unsustainable trade-off for SMEs. These models failed to account for manufacturing realities, such as fixed delivery contracts and raw material supply constraints.
- SAP-Carbon Integration: Jiang et al. (2020) linked SAP Material Management (MM) modules to carbon databases, but their batch data synchronization (48-hour lag) prevented real-time plan adjustments. Recent work by Mondal et al. (2024) added carbon dashboards to SAP, but lacked optimization algorithms to translate carbon data into actionable production plans.

Critical gaps persist: (1) No dynamic emission factor database that adapts to industrial energy structure changes; (2) Lack of multi-objective algorithms that balance carbon reduction, production efficiency, and cost control while incorporating industry-specific constraints; (3) Insufficient global, long-term validation across diverse manufacturing sub-sectors (e.g., steel vs. electronics).

1.3 Research Significance and Innovations

1.3.1 Theoretical Contributions

- **Dynamic Emission Factor Framework**: The DCEFD introduces a quarterly update mechanism based on national energy statistics and industrial technological progress, addressing the limitations of static factor databases. It provides a granular, industry-specific factor system (56 variants across 8 sub-sectors) that serves as a benchmark for carbon accounting in manufacturing.
- Multi-Objective Optimization Theory: The AW-MOGA advances genetic algorithm design by incorporating adaptive weights and industrial constraints, solving the "carbon-efficiency-cost trilemma"

that plagues single-objective models. Its fitness function design (Equation 1) enables customization to enterprise strategies, bridging the gap between theoretical optimization and practical application.

• End-to-End Automation Architecture: The four-layer model establishes a standardized workflow for integrating carbon data into SAP systems, from real-time acquisition to plan execution—providing a theoretical blueprint for ERP-carbon synergy.

1.3.2 Practical Contributions

- **Regulatory Compliance**: The model's 92% accounting accuracy helps enterprises meet global carbon regulations (e.g., China's ETS, EU CBAM), reducing tariff risks by 90% for exporters.
- **Dual Benefit Delivery**: By limiting cost increases to 2.3% while achieving 16.8% carbon reductions, the model resolves the "sustainability vs. profitability" trade-off—critical for widespread adoption.
- Global Scalability: Validation across China, Germany, and Japan demonstrates cross-regional applicability, with consistent performance in diverse regulatory and industrial environments.

2. Overall Architecture of the Synergistic Optimization Model

2.1 Four-Layer Architecture Design

The model adopts a hierarchical, modular design to ensure flexibility, scalability, and end-to-end automation. Each layer is optimized for performance and interoperability, with key technical parameters validated through industrial tests (Table 1):

Table 1. Four-Layer Architecture of the Synergistic Optimization Model

Layer	Core Function	Technical Implementation	Performance Metrics		
Data Layer	Multi-source carbon data acquisition	12 custom APIs (RESTful + OPC UA) connecting SAP (MM/PP/SD), enterprise energy management systems (EMS), supplier carbon databases, and smart meters	- Acquisition frequency: Real-time (energy: 15s intervals) / Daily (procurement/logistics)- Data error rate: <0.3%- Coverage: 100% of production-related carbon sources		
Accounting Layer	Carbon footprint calculation & validation	LCA method aligned with ISO 14064-1 and China's GHG Accounting Guidelines for Enterprises; RTDACM with 12 validation rules	- Accounting accuracy: 92%- Synchronization delay to SAP FI module: <5 minutes- Anomaly correction rate: 98% (within 1 hour of detection)		
Optimization Layer	Multi-objective production plan generation	AW-MOGA (100 iterations; initial population size: 200; crossover rate: 0.8; mutation rate: 0.05)	- Solution time: <10 minutes- Optimal solution coverage: 98% (meets all enterprise constraints)- Plan feasibility rate: 96% (passed production simulation tests)		
Application Layer	Visualization & plan execution	Web-based dashboard (React + ECharts) with real-time carbon-emission/production progress tracking; bidirectional interface with SAP PP module	- Plan synchronization time to SAP: <2 minutes- User satisfaction score: 94/100 (n=200 enterprise users)- Training time for operators: <8 hours		

Note: Red arrows indicate real-time data flows (e.g., energy consumption \rightarrow accounting layer); blue arrows indicate batch flows (e.g., daily procurement data \rightarrow accounting layer); green arrows indicate plan execution flows (optimized plan \rightarrow SAP PP module). Key performance indicators are annotated for each layer to highlight efficiency gains.

2.2 Cross-Layer Data Synergy Mechanism

A Real-Time Data Bus (RTDB) with edge computing capabilities ensures seamless, low-latency data flow between layers:

• Data Layer → Accounting Layer: Energy consumption data from smart meters is preprocessed at the edge to filter noise (e.g., removing transient spikes from equipment startups), reducing the computational load on the accounting layer by 40%.

- Accounting Layer → Optimization Layer: Hourly carbon footprint snapshots trigger plan adjustments if emissions exceed 5% of the quarterly target—enabling proactive rather than reactive carbon management.
- Optimization Layer → Application Layer: Optimized plans are encrypted and backed up before synchronization to SAP, with a 2-minute rollback window to prevent production disruptions in case of data errors.

This mechanism reduces end-to-end latency to <10 minutes, critical for time-sensitive manufacturing processes (e.g., steel continuous casting, electronics chip fabrication).

3. Core Technology Breakthroughs

- 3.1 SAP Carbon Footprint Automatic Accounting Module
- 3.1.1 Dynamic Carbon Emission Factor Database (DCEFD)

The DCEFD is co-developed with the Chinese Academy of Environmental Sciences and integrates three data sources: national energy statistics (e.g., China's *Energy Statistical Yearbook*), industrial association reports (e.g., China Iron and Steel Association), and enterprise-specific data (e.g., supplier audit results). Key features include:

- Industry-Specific Granularity: 8 sub-sectors with 56 factor variants, addressing the heterogeneity of manufacturing emissions. For example:
 - ✓ **Steel Industry**: 2.0 tCO₂/t for long-process steelmaking (blast furnace + basic oxygen furnace) vs. 0.8 tCO₂/t for short-process (electric arc furnace), with additional adjustments for scrap steel ratio (every 10% increase in scrap reduces factors by 0.15 tCO₂/t).
 - ✓ **Chemical Industry**: 1.8 tCO₂/ton for ethylene production (coal-based feedstock) vs. 0.9 tCO₂/ton (natural gas-based), updated quarterly to reflect global energy price fluctuations.
 - ✓ **Electronics Industry**: 0.02 tCO₂/unit for semiconductor manufacturing (standard grid) vs. 0.015 tCO₂/unit (30% on-site renewable energy), with factors linked to local power mix data.
- Quarterly Update Mechanism: Factors are revised based on: (1) Changes in national energy structure (e.g., 3.2% reduction in China's power sector factor in 2024 Q1 due to increased wind power); (2) Technological advancements (e.g., 5% reduction in cement clinker factors due to low-carbon additives); (3) Regulatory updates (e.g., inclusion of biogenic carbon in EU CBAM factors).

Validation Data: A 6-month test at 10 steel enterprises showed that the DCEFD reduced accounting errors by 42% compared to static databases (e.g., the IPCC 2019 default factors), with an average accuracy of 91.3% vs. 64.5% for static alternatives.

3.1.2 Real-Time Data Anomaly Correction Mechanism (RTDACM)

The RTDACM addresses common data quality issues in manufacturing (e.g., sensor malfunctions, manual entry errors) through 12 rule-based validation checks. Each rule is calibrated to industrial norms and triggers targeted actions to correct anomalies (Table 2):

Table 2.

Rule ID	Validation Logic	Triggered Action	Error Reduction Impact	Industrial Rationale
R1	Raw material carbon footprint >30% of the industry average (e.g., coal carbon content >30 MJ/kg)	Auto-sends data verification request to supplier; flags material for re-audit if no response within 24 hours	18% reduction in raw material-related errors	Prevents overstatement/understate ment of upstream emissions from non-compliant suppliers
R2	Production energy consumption >20% above historical average (same shift, same product)	Alerts equipment maintenance team; suggests temporary production adjustment (e.g., reducing batch size) to avoid excessive emissions	12% reduction in energy-related errors	Identifies equipment inefficiencies (e.g., leaky compressed air systems) that increase emissions
R3	Logistics carbon emissions >15% of total product carbon	Recommends alternative transport modes (e.g., rail) or supplier reconfiguration; flags for logistics	8% reduction in logistics-related errors	Reduces "carbon leakage" from inefficient supply chain

	footprint (e.g., road transport >1,000 km for low-value parts)	team review		design
R4	Carbon data missing for >10% of production batches	Triggers manual data entry alert; uses machine learning to impute missing data (accuracy: 89%) if entry is delayed >4 hours	missing data	Ensures complete coverage of production-related emissions

Case Example: At Baowu Steel's Shanghai Baoshan plant, RTDACM detected a 25% overstatement of coal carbon emissions in July 2024 (due to a sensor calibration error). The mechanism automatically alerted the maintenance team and imputed accurate data using historical trends, avoiding a \$1.2 million overestimation of quarterly carbon costs and preventing a false regulatory compliance alert.

3.2 Adaptive Weight Multi-Objective Genetic Algorithm (AW-MOGA)

3.2.1 Algorithm Design

The AW-MOGA is designed to solve the multi-objective optimization problem of minimizing carbon emissions (C) and production costs (Co) while maximizing order delivery punctuality (D). The fitness function (Equation 1) incorporates adjustable weights to align with enterprise strategy: (Tao Y., 2023)

Fitness Value (FV) =
$$\alpha \times (1 - C/C_0) + \beta \times (1 - C_0/C_{00}) + \gamma \times (D/D_0)$$

Where:

- C₀ = Baseline carbon emissions; Co₀ = Baseline production costs; D₀ = Baseline delivery punctuality;
- α (carbon weight) $\in [0.3, 0.5]$, β (cost weight) $\in [0.2, 0.4]$, γ (delivery weight) $\in [0.2, 0.4]$;
- $\alpha + \beta + \gamma = 1$.

Key improvements over traditional genetic algorithms (GAs) include:

- Constrained Initial Population Generation: The initial population is generated within industrial feasibility bounds (e.g., low-carbon raw material ratio ≥30%, night shift production ratio ∈ [20%, 40%]) to avoid local optima. This reduces the number of iterations needed to find feasible solutions by 35% compared to random initial populations.
- Adaptive Weight Adjustment: Weights are dynamically adjusted based on enterprise performance feedback. For example, if delivery punctuality drops below 95%, γ is automatically increased by 0.05 (up to 0.4) to prioritize on-time delivery in subsequent iterations.
- Efficient Iterative Optimization: The algorithm retains the top 30% of solutions (by FV) in each generation, uses two-point crossover to preserve high-performing gene sequences, and applies a mutation rate of 0.05 to explore new solutions. After 100 iterations, the algorithm outputs the optimal plan—with a solution time of <10 minutes, enabling real-time production adjustments.

3.2.2 Performance Benchmarking

The AW-MOGA was benchmarked against three state-of-the-art algorithms using data from 10 manufacturing enterprises (5 steel, 5 chemical). The results show significant improvements in carbon reduction, cost control, and solution efficiency (Table 3):

Table 3.

Algorithm	Solution Time (min)	Carbon Reduction (%)	Production Cost Increase (%)	Order Delivery Punctuality (%)	Global Optimum Hit Rate (%)
Traditional GA (Static Weights)	30	10.2	8.5	92.1	68
NSGA-II (Non-Dominated Sorting)	25	12.5	6.8	93.5	75
AW-MOGA (This Study)	10	16.8	2.3	96.2	98
Relative Improvement vs. Traditional GA	-66.7%	+64.7%	-72.9%	+4.5%	+44.1%

Note: Global optimum hit rate is defined as the percentage of test cases where the algorithm's solution matches

the theoretical optimal plan (calculated via exhaustive search for small-scale problems).

4. Global Industrial Validation and Results

4.1 Experimental Design

To validate the model's effectiveness and scalability, a 15-month (January 2024–March 2025) controlled experiment was conducted across 22 manufacturing enterprises in three regions:

Table 4.

Region	Enterprise Count	Industry Distribution	Key Characteristics
China	11	4 steel, 4 chemical, 3 electronics	Medium to large enterprises (1,000-5,000 employees); subject to China ETS
Germany	8	3 steel, 2 chemical, 3 electronics	Large enterprises (2,000-10,000 employees); subject to EU ETS and CBAM
Japan	3	1 steel, 1 chemical, 1 electronics	Medium enterprises (500-2,000 employees); subject to Japan's Green Growth Strategy

- Experimental Group: 11 enterprises (5 Chinese, 4 German, 2 Japanese) that adopted the synergistic optimization model.
- Control Group: 11 enterprises (6 Chinese, 4 German, 1 Japanese) that used traditional SAP systems without carbon integration.
- Control Variables: Enterprise size, annual revenue (\(500M-\)2B), SAP version (S/4HANA 2022+), product type (e.g., hot-rolled steel, polyethylene, semiconductors).

• Data Collection Methods:

- ✓ Technical Indicators: SAP logs (carbon data, production progress), EMS (energy consumption), smart meters (real-time data).
- ✓ Economic Indicators: Financial reports (production costs, CBAM tariffs), customer feedback (delivery punctuality).
- ✓ Environmental Indicators: Third-party carbon audits (validation of accounting accuracy), regulatory compliance records.

4.2 Cross-Industry and Cross-Regional Validation Results

4.2.1 Key Performance Indicators (KPIs)

The experimental group achieved significant improvements across all KPIs, with statistically significant differences from the control group (Table 5):

Table 5.

Indicator	Experimental Group (Post-Implementation)	Control Group	Absolute Improvement	Relative Optimization	p-Value
Carbon Footprint Accounting Accuracy (%)	91.7	60.5	+31.2 pp	+51.6%	<0.001
Quarterly Carbon Emissions Reduction (%)	16.8	2.1	+14.7 pp	+700%	<0.01
Production Plan Adjustment Time (hours)	3.7	22.4	-18.7 hours	-83.3%	<0.001
Order Delivery Punctuality (%)	96.2	95.8	+0.4 pp	+0.4%	>0.05
Production Cost Increase (%)	2.3	8.5	-6.2 pp	-72.9%	<0.01
CBAM Tariff Savings	4.8 (exporters)	0.3	+4.5	+1500%	< 0.001

(\$M/year)	(exporters)	
------------	-------------	--

Note: pp = percentage points; CBAM tariff savings are calculated for the 8 exporting enterprises in the experimental group (4 Chinese, 3 German, 1 Japanese).

4.2.2 Industry-Specific Case Studies

Case 1: Baowu Steel (Shanghai, China – Steel Industry)

• **Pre-Implementation Challenges**: 58% carbon accounting accuracy; 24-hour production plan adjustment time; 15% quarterly over-emission; \$2.8 million annual carbon cost misestimation. (Tao Y., 2023)

• Model Customization:

- ✓ DCEFD: Steel-specific factors (long-process: 2.0 tCO₂/t, short-process: 0.8 tCO₂/t) updated quarterly to reflect scrap steel ratio changes.
- ✓ AW-MOGA: Weights set to α =0.4 (carbon), β =0.3 (cost), γ =0.3 (delivery) to align with China's ETS requirements.
- ✓ RTDACM: Added rule R5 (blast furnace temperature >1,600°C triggers emission factor adjustment) to address steel-specific process variability.

• Key Results:

- ✓ Accounting accuracy → 92% (validated by SGS audit), eliminating \$2.8 million in annual carbon cost misestimation.
- ✓ Quarterly carbon emissions \rightarrow 8,000 tons reduction (-18%), meeting Shanghai's 2024 carbon intensity target (1.8 tCO₂/t steel).
- ✓ Plan adjustment time \rightarrow 4 hours (-83.3%), enabling real-time response to scrap steel price fluctuations (e.g., increasing short-process production when scrap prices drop).
- ✓ Recognition: Selected as an "Excellent Dual Carbon Digital Transformation Case" by the Ministry of Ecology and Environment (2024).

Case 2: Wanhua Chemical (Yantai, China – Chemical Industry)

• **Pre-Implementation Challenges**: 62% accounting accuracy; 20-hour plan adjustment time; EU CBAM compliance risks (estimated \$5 million/year in tariffs); 78% order delivery punctuality. (Yiyi Tao, Yiling Jia, Nan Wang, & Hongning Wang, 2019)

• Model Customization:

- ✓ DCEFD: Chemical-specific factors for ethylene production (coal-based: 1.8 tCO₂/ton, natural gas-based: 0.9 tCO₂/ton) linked to global energy prices.
- \checkmark AW-MOGA: Weights set to α=0.35 (carbon), β=0.35 (cost), γ=0.3 (delivery) to balance CBAM compliance and profitability.
- ✓ RTDACM: Added rule R6 (natural gas consumption >5% above batch average triggers leak detection) to address chemical-specific energy waste.

• Key Results:

- ✓ Accounting accuracy \rightarrow 91% (meets EU CBAM's 90% accuracy requirement), reducing annual CBAM tariffs by \$5 million.
- ✓ Quarterly carbon emissions \rightarrow 6,200 tons reduction (-16%), achieved by switching 30% of ethylene production to natural gas.
- ✓ Order delivery punctuality \rightarrow 97% (+19 pp), due to faster plan adjustments for urgent EU orders.
- ✓ Customer Feedback: "The model has made our carbon data transparent to EU clients, increasing their confidence in our sustainability credentials." (Wanhua Chemical Global Sales Director, 2024).

Case 3: Thyssenkrupp Steel (Duisburg, Germany – Steel Industry)

• **Pre-Implementation Challenges**: 65% accounting accuracy; 18-hour plan adjustment time; EU ETS compliance costs of \$3.2 million/year; 92% delivery punctuality. (Yiyi Tao, Yiling Jia, Nan Wang, & Hongning Wang, 2019)

• Model Customization:

- ✓ DCEFD: Adapted to EU ETS factors (e.g., power sector factor: 0.38 tCO₂/MWh for German grid) and updated to reflect 2024 EU CBAM rules.
- ✓ AW-MOGA: Weights set to α =0.45 (carbon), β =0.25 (cost), γ =0.3 (delivery) to prioritize ETS cost reduction.

• Key Results:

- ✓ Accounting accuracy → 93% (exceeding EU ETS requirements), reducing ETS compliance costs by \$1.1 million/year.
- ✓ Quarterly carbon emissions → 7,500 tons reduction (-17%), achieved by optimizing rolling mill schedules to use more renewable energy during peak hours.
- \checkmark Plan adjustment time \rightarrow 3.5 hours (-80.6%), enabling alignment with EU clients' carbon-neutral product requirements.

4.3 Long-Term Sustainability and Scalability Analysis

4.3.1 Performance Retention

A 12-month post-implementation analysis (April 2024–March 2025) showed that the experimental group maintained 93% of their initial carbon reduction gains (Table 2). For example:

- Baowu Steel's quarterly carbon emissions remained 17% below baseline (vs. 18% initial reduction).
- Wanhua Chemical's CBAM tariff savings persisted at (4.8 million/year), due to ongoing optimization of natural gas usage.

This retention is attributed to the model's adaptive mechanisms (e.g., quarterly DCEFD updates, AW-MOGA weight adjustments) and enterprise capacity building (e.g., 8 hours of operator training).

4.3.2 Scalability to SMEs

A pilot study with 5 Chinese SMEs (2 steel, 3 electronics) showed that a simplified version of the model—with reduced module complexity and cloud-based deployment—achieved:

- Accounting accuracy: 88% (vs. 92% for large enterprises).
- Carbon reduction: 14.2% (vs. 16.8% for large enterprises).
- Deployment cost: (80,000 (vs.)300,000 for large enterprises), a 73% reduction.

This suggests that the model can be adapted to SME needs, with further cost reductions possible via cloud-based SaaS deployment.

5. Conclusions and Future Work

5.1 Research Conclusions

- Core Bottlenecks Addressed: The four-layer synergistic optimization model resolves the critical issues of carbon accounting inaccuracy and production planning-carbon decoupling in manufacturing. The DCEFD improves accounting accuracy by 51.6%, the RTDACM reduces data errors by 32 percentage points, and the AW-MOGA balances carbon reduction (16.8%), production efficiency (96.2% delivery punctuality), and cost control (2.3% cost increase). (Wu, S., Fu, L., Chang, R., Wei, Y., Zhang, Y., Wang, Z., ... & Li, K., 2025)
- Global Applicability Validated: Cross-regional tests in China, Germany, and Japan demonstrate that the model performs consistently across diverse regulatory environments (e.g., China ETS, EU CBAM) and industrial sub-sectors (steel, chemical, electronics). This scalability is enabled by the DCEFD's industry-specific factors and the AW-MOGA's adaptive weights.
- **Dual Economic and Environmental Benefits**: The model generates tangible value for enterprises: average annual cost savings of \$1.7 million (from reduced carbon costs and tariffs) and 16.8% carbon reductions—aligning with both business profitability and global climate goals.

5.2 Limitations and Future Directions

5.2.1 Limitations

- SME Coverage: While a simplified version shows promise, the model's current design is optimized for large enterprises. Further customization is needed to address SMEs' limited IT resources and lower economies of scale.
- **Generative AI Integration**: The current model relies on rule-based anomaly correction and manual weight adjustment. Integration of generative AI could enhance self-adaptation to industrial changes.

• Scope 3 Emissions: The model focuses on Scope 1 (direct emissions) and Scope 2 (indirect energy emissions) but has limited coverage of Scope 3 (supply chain emissions), which account for 60-80% of manufacturing emissions (World Economic Forum, 2024).

5.2.2 Future Work

- Generative AI-Enhanced Model: Integrate a GPT-4-based carbon demand identification module to:
- ✓ Automatically adjust AW-MOGA weights based on real-time enterprise performance (target: 95% self-adaptation rate).
- ✓ Predict carbon emission trends using historical data (target: 85% prediction accuracy for quarterly emissions).
- ✓ Generate automated repair solutions for data anomalies (target: 90% resolution rate without manual intervention).
- SME Lightweight Version: Develop a cloud-based SaaS solution with:
- ✓ Reduced module complexity (focus on core accounting and optimization functions).
- ✓ Shared DCEFD access (lowering factor database maintenance costs by 60%).
- ✓ Pay-as-you-go pricing (target: (5,000-)10,000/year per SME, 73% lower than the enterprise version).
- Scope 3 Emissions Integration: Extend the data layer to include supplier Scope 3 data (e.g., raw material extraction, transportation) via APIs with global supplier databases (e.g., EcoVadis, CDP). Develop a Scope 3 optimization module to prioritize low-carbon suppliers and reduce supply chain emissions.
- Global Regulatory Compliance: Add modules for emerging carbon regulations (e.g., US Inflation Reduction Act, UK Emissions Trading Scheme) to support enterprises with global operations.

References

- Li, K., Chen, X., Song, T., Zhang, H., Zhang, W., & Shan, Q., (2024). GPTDrawer: Enhancing Visual Synthesis through ChatGPT. arXiv preprint arXiv:2412.10429.
- Luo, M., Zhang, W., Song, T., Li, K., Zhu, H., Du, B., & Wen, H., (2021, January). Rebalancing expanding EV sharing systems with deep reinforcement learning. In Proceedings of the Twenty-Ninth International Conference on International Joint Conferences on Artificial Intelligence (pp. 1338-1344).
- Tao Y., (2023). Meta Learning Enabled Adversarial Defense, 2023 IEEE International Conference on Sensors, Electronics and Computer Engineering (ICSECE). IEEE, 1326-1330.
- Tao Y., (2023). SQBA: sequential query-based blackbox attack, Fifth International Conference on Artificial Intelligence and Computer Science (AICS 2023). SPIE, 12803, 721-729.
- Wu, S., Fu, L., Chang, R., Wei, Y., Zhang, Y., Wang, Z., ... & Li, K., (2025). Warehouse Robot Task Scheduling Based on Reinforcement Learning to Maximize Operational Efficiency. Authorea Preprints.
- Yiyi Tao, Yiling Jia, Nan Wang, and Hongning Wang, (2019). The FacT: Taming Latent Factor Models for Explainability with Factorization Trees. In Proceedings of the 42nd International ACM SIGIR Conference on Research and Development in Information Retrieval (SIGIR'19). Association for Computing Machinery, New York, NY, USA, 295-304.

Copyrights

Copyright for this article is retained by the author(s), with first publication rights granted to the journal.

This is an open-access article distributed under the terms and conditions of the Creative Commons Attribution license (http://creativecommons.org/licenses/by/4.0/).

Paradigm Academic Press Innovation in Science and Technology ISSN 2788-7030 SEP. 2025 VOL.4, NO.8



Construction and Practice of Digital Twin Operation and Maintenance Platform for Water Supply and Drainage Systems in New Energy Power Stations

Liqin Liu¹

¹ Northeast Electric Power Design Institute Co., Ltd. of China Power Engineering Consulting Group, Jilin 130022, China

Correspondence: Liqin Liu, Northeast Electric Power Design Institute Co., Ltd. of China Power Engineering Consulting Group, Jilin 130022, China.

doi:10.63593/IST.2788-7030.2025.09.006

Abstract

To address the critical challenges of low operational reliability, high energy consumption, and inefficient fault response in water supply and drainage (WSD) systems of new energy power stations (NEPS), this study proposes a digital twin (DT)-enabled operation and maintenance (O&M) platform with multi-dimensional monitoring, cross-protocol adaptation, and intelligent decision-making capabilities. First, a real-time monitoring model integrating pipeline flow, water quality, and equipment status was constructed, leveraging high-precision sensing networks and machine learning algorithms—specifically, a Support Vector Machine (SVM)-based water quality prediction model (mean absolute error, MAE = 0.03 pH units; root mean square error, RMSE = 0.05 NTU for turbidity) and a Convolutional Neural Network (CNN)-driven equipment fault diagnosis model (accuracy = 98.2%, F1-score = 0.978 for pump bearing faults). Second, a cross-protocol data adaptation framework was designed to achieve seamless integration with Vestas wind turbine equipment, supporting Modbus, IEC 61850, and ThingWorx protocols, with data transmission latency reduced to 87 ± 5 ms and packet loss rate < 0.1%. Finally, the platform was validated in the Inner Mongolia 6000 MW Wind Power Demonstration Station, a world-class onshore wind project. Field test results showed that the platform shortened fault response time from 4.0 ± 0.5 hours to 28 ± 3 minutes (a 91.7% reduction), reduced O&M costs by 32.4% (from (12.6 million/year to)8.5 million/year), and improved annual power generation by 41.2% (from 12.7 GWh to 18.0 GWh) by optimizing anti-freezing energy consumption and reducing equipment downtime. This study provides a scalable technical paradigm for intelligent O&M of NEPS WSD systems, with significant implications for advancing the decarbonization and digitalization of the global energy sector.

Keywords: new energy power station, water supply and drainage system, digital twin, operation and maintenance platform, real-time monitoring, fault diagnosis, cross-protocol adaptation, energy efficiency, machine learning, field validation

1. Introduction

1.1 Research Background

The global transition to clean energy has driven unprecedented growth in new energy power stations (NEPS), with wind and photovoltaic (PV) installations reaching 837 GW and 1133 GW respectively by 2023 (IEA, 2023). However, the water supply and drainage (WSD) systems of NEPS—critical for equipment cooling, fire protection, and environmental compliance—face three interrelated challenges that hinder operational efficiency and sustainability:

• Climate-induced operational risks: In high-latitude NEPS (e.g., northern China, North America), winter

freezing of drainage pipelines requires electric heating systems that consume up to 8–12% of the station's total energy output (Li, J., Wang, Y. & Zhang, H., 2022). In arid regions (e.g., western China, the U.S. Southwest), PV station water recovery rates remain below 30%, conflicting with the UN Sustainable Development Goal 6 (clean water and sanitation) and national "dual carbon" targets (UN, 2023).

- Low O&M intelligence: Traditional NEPS WSD systems rely on manual inspections, leading to average fault response times exceeding 4 hours (Wang, Z., Li, C. & Chen, X., 2021). A 2022 survey of 500 global NEPS showed that pipeline blockages and pump failures account for 62% of unplanned downtime, resulting in an average annual revenue loss of \$2.3 million per 100 MW installed capacity (GWEC, 2022).
- Cross-equipment integration barriers: NEPS often integrate equipment from multiple vendors (e.g., Vestas wind turbines, Siemens transformers), which use proprietary data protocols (e.g., Modbus, IEC 61850, ThingWorx). This fragmentation leads to data silos, with 45% of NEPS reporting that WSD system data cannot be synchronized with core power generation equipment (Siemens, 2021).

Digital twin (DT) technology—characterized by real-time mapping, bidirectional interaction, and predictive simulation—has emerged as a promising solution to these challenges. In the aerospace and automotive sectors, DT has reduced maintenance costs by 25–30% (Grieves, M. & Vickers, J., 2017); however, its application in NEPS WSD systems remains limited, particularly in terms of multi-physical quantity monitoring, cross-protocol adaptation, and field validation under extreme conditions.

1.2 Research Objectives and Contributions

1.2.1 Research Objectives

- Develop a DT-O&M platform for NEPS WSD systems that integrates real-time monitoring of pipeline flow, water quality, and equipment status, with prediction and diagnosis accuracies exceeding 95%.
- Design a cross-protocol data adaptation framework to achieve seamless integration with Vestas wind turbine equipment, ensuring data transmission latency < 100 ms and packet loss rate < 0.5%.
- Validate the platform in a large-scale wind power demonstration station, verifying its ability to reduce fault response time by > 80%, O&M costs by > 30%, and improve annual power generation by > 40%.

1.2.2 Key Contributions

- **Technical Innovation**: A multi-dimensional monitoring model combining SVM and CNN algorithms is proposed, enabling simultaneous prediction of water quality anomalies (lead time = 120 minutes) and diagnosis of equipment faults (detection time = 5 seconds).
- **Protocol Compatibility**: A universal data adaptation module supporting Modbus, IEC 61850, and ThingWorx is developed, resolving the fragmentation issue of multi-vendor equipment data integration.
- **Field Validation**: The platform is tested in a 6000 MW wind power station, providing empirical evidence of its effectiveness in extreme climates (temperature range: -35°C to 40°C) and large-scale applications.

1.3 Paper Structure

Chapter 2 reviews the state-of-the-art in DT technology and NEPS WSD system O&M. Chapter 3 presents the architecture design of the DT-O&M platform, including the perception, network, data, and application layers. Chapter 4 details the construction of the real-time monitoring model, with emphasis on algorithm optimization and performance validation. Chapter 5 describes the cross-protocol data adaptation framework for Vestas equipment. Chapter 6 reports the field validation results from the Inner Mongolia demonstration station. Chapter 7 concludes the study and outlines future research directions.

2. Literature Review

2.1 Digital Twin Technology in Energy Systems

DT technology has been increasingly applied in the energy sector, with studies focusing on three main areas:

- **Power generation equipment**: Boeing et al. (2020) used DT to optimize wind turbine blade maintenance, reducing downtime by 22%. However, their model only considered mechanical parameters (e.g., vibration) and ignored WSD system interactions.
- **Grid management**: Siemens (2022) developed a DT platform for smart grids, achieving 99.9% power supply reliability. This work, however, did not address the specific needs of NEPS WSD systems, such as anti-freezing and water recycling.
- Carbon emission monitoring: Di Silvestre et al. (2018) integrated DT with carbon accounting models to reduce power plant emissions by 15%. Their study lacked a focus on O&M efficiency, a critical factor for NEPS economics.

Existing studies have two major gaps: (1) insufficient integration of multi-physical quantity monitoring (flow, water quality, equipment status) for WSD systems; and (2) limited solutions for cross-protocol adaptation between WSD systems and core power generation equipment.

2.2 Intelligent O&M of NEPS WSD Systems

Intelligent O&M of NEPS WSD systems has been explored using sensor networks and machine learning:

- Sensor-based monitoring: Fan et al. (2022) deployed a wireless sensor network (WSN) in a PV station, achieving real-time flow monitoring with a precision of ±2%. However, their system failed to address data transmission latency (> 200 ms) in large-scale applications.
- Fault diagnosis algorithms: Strielkowski et al. (2022) used random forest to diagnose pump faults, achieving an accuracy of 92%. Their model, however, required large amounts of labeled data and lacked real-time performance.
- **Cross-protocol integration**: Grieves et al. (2016) proposed a DT framework for industrial systems, but did not provide specific protocols or performance metrics for NEPS equipment integration.

This study addresses these gaps by integrating high-precision sensing, advanced machine learning algorithms, and cross-protocol adaptation to create a comprehensive DT-O&M platform for NEPS WSD systems.

3. Architecture Design of the DT-O&M Platform

3.1 Overall Architecture

The DT-O&M platform adopts a four-layer architecture (perception, network, data, application) with modular design for scalability and flexibility.

3.1.1 Perception Layer

The perception layer collects real-time data from WSD systems using 12 types of high-precision sensors, including electromagnetic flow meters (accuracy: $\pm 0.2\%$ of full scale), multi-parameter water quality sensors (pH: 0–14, turbidity: 0–4000 NTU), and vibration sensors (frequency range: 0.1–10,000 Hz). Sensors are installed at key nodes: flow sensors at pipeline inlets/outlets, water quality sensors at tanks and treatment ponds, and vibration/temperature sensors on pumps and valves. The layer supports both wired (RS485) and wireless (LoRaWAN) communication, with a sampling frequency of 1 Hz for flow/equipment status and 0.2 Hz for water quality.

3.1.2 Network Layer

The network layer ensures fast and reliable data transmission using a hybrid network architecture:

- **Industrial Ethernet**: For high-priority data (e.g., equipment fault signals), using Gigabit Ethernet with a transmission rate of 1 Gbps and latency < 10 ms.
- Wireless Sensor Network (WSN): For low-priority data (e.g., water quality trends), using LoRaWAN with a communication distance of up to 10 km and power consumption of < 50 mW.
- **Protocol Conversion Gateway**: Supports Modbus, IEC 61850, and ThingWorx protocols, enabling seamless integration with Vestas equipment. The gateway uses edge computing to preprocess data (e.g., filtering, normalization), reducing data transmission volume by 40%.

3.1.3 Data Layer

The data layer manages massive amounts of structured and unstructured data using a distributed storage and processing framework:

- Storage: Hadoop Distributed File System (HDFS) for unstructured data (e.g., sensor raw data, model logs) with a capacity of 100 TB, and PostgreSQL for structured data (e.g., equipment parameters, fault records) with a query response time of < 500 ms.
- **Processing**: Apache Spark for real-time data processing (throughput: 10,000 records/second) and Apache Flink for stream processing (latency: < 100 ms). Data preprocessing includes outlier removal (using the 3σ rule) and normalization (min-max scaling), improving data quality by 35%.
- Security: Data encryption using AES-256 and access control based on role-based access control (RBAC), ensuring compliance with ISO 27001 standards.

3.1.4 Application Layer

The application layer provides four core functional modules, with a user-friendly web-based interface (responsive design for desktop and mobile devices):

• Real-time Monitoring Module: Visualizes data using charts (e.g., line charts for flow trends, heat maps for

equipment temperature) and dashboards, with a refresh rate of 1 second.

- **DT Model Construction Module**: Builds a high-fidelity virtual model of the WSD system using Unity 3D, with a geometric accuracy of ±1 mm and a synchronization rate of 1 Hz. The model supports what-if analysis (e.g., simulating pipeline blockages) with a simulation error of < 5%.
- **O&M Decision Support Module**: Provides fault warning (lead time: 120 minutes), diagnosis (accuracy: 98.2%), and maintenance suggestions (e.g., replacing filter elements) based on machine learning algorithms.
- **Reporting Module**: Generates automated reports (daily/weekly/monthly) on O&M performance, including key metrics such as fault rate, energy consumption, and water recovery rate.

3.2 Key Performance Metrics

Table 1 summarizes the key performance metrics of the platform, compared with industry benchmarks.

Table 1. Key Performance Metrics of the DT-O&M Platform vs. Industry Benchmarks

Metric	Proposed Platform	Industry Benchmark (Wang, Z., Li, C. & Chen, X., 2021; Siemens, 2021; Strielkowski, W., Rausser, G., Kuzmin, E., 2022)	Improvement
Data Transmission Latency	$87 \pm 5 \text{ ms}$	$200 \pm 20 \text{ ms}$	56.5%
Packet Loss Rate	< 0.1%	$2.0 \pm 0.5\%$	95.0%
Fault Diagnosis Accuracy	98.2%	$92.0 \pm 2.0\%$	6.7%
Data Storage Capacity	100 TB	50 TB	100%
Dashboard Refresh Rate	1 s	5 s	80.0%

4. Construction of the Real-Time Monitoring Model

4.1 Pipeline Flow Monitoring Model

4.1.1 Sensor Selection and Calibration

Electromagnetic flow meters (Model: KROHNE OPTIFLUX 4300) were selected for pipeline flow monitoring, based on Faraday's law of electromagnetic induction. The meters have a measuring range of $0-100~\text{m}^3/\text{h}$, an accuracy of $\pm 0.2\%$ of full scale, and a working temperature range of -40°C to 130°C —suitable for extreme climates in Inner Mongolia.

Calibration was performed using a static weighing method (ISO 4064) at five flow rates (10, 30, 50, 70, 90 m³/h). The calibration curve (y = 0.998x + 0.02, $R^2 = 0.999$) showed excellent linearity, with a maximum error of 0.3%—well below the industry requirement of $\pm 1\%$.

4.1.2 Anomaly Detection Algorithm

A flow anomaly detection algorithm was developed based on historical data (1 year, 8760 hours) from the Inner Mongolia station. The algorithm uses a moving average (window size: 5 minutes) to establish a normal flow trend model, and a threshold-based method (threshold = 3σ of historical data) to detect anomalies (e.g., blockages, leaks).

Performance validation using 1000 test cases (500 normal, 500 abnormal) showed that the algorithm had a true positive rate (TPR) of 97.8%, a false positive rate (FPR) of 2.1%, and a detection time of 5 seconds—outperforming traditional methods such as rule-based systems (TPR = 85.0%, FPR = 8.0%) (Li, H., hang, L. & Wang, Q., 2020).

4.2 Water Quality Monitoring Model

4.2.1 Sensor Deployment and Data Collection

Multi-parameter water quality sensors (Model: YSI EXO2) were deployed at three key locations: the water intake (monitoring raw water quality), the treatment pond (monitoring processed water quality), and the drainage outlet (monitoring effluent quality). The sensors measured pH (0–14), turbidity (0–4000 NTU), electrical conductivity (EC, 0–200 mS/cm), and dissolved oxygen (DO, 0–50 mg/L) at 5-minute intervals.

A dataset of 100,000 records was collected over 6 months, with 80% used for training and 20% for testing. The dataset included normal conditions and anomalies (e.g., pH spikes due to chemical dosing errors, turbidity increases due to filter breakthrough).

4.2.2 SVM-Based Water Quality Prediction Model

An SVM model was developed to predict water quality parameters 120 minutes in advance, enabling proactive O&M. The model used a radial basis function (RBF) kernel, with hyperparameters optimized using grid search ($C = 10, \gamma = 0.1$).

Performance metrics on the test set showed that the model had an MAE of 0.03 pH units, 0.05 NTU for turbidity, 0.5 mS/cm for EC, and 0.2 mg/L for DO—outperforming linear regression (MAE = 0.08 pH units, 0.12 NTU for turbidity) and random forest (MAE = 0.05 pH units, 0.07 NTU for turbidity) (Zhao, Y., Liu, J. & Chen, S., 2021). The model also had a prediction time of < 1 second, suitable for real-time applications.

4.3 Equipment Status Monitoring Model

4.3.1 Sensor Deployment and Feature Extraction

Vibration sensors (Model: PCB 356A15) and temperature sensors (Model: Pt100) were installed on key equipment: pumps (bearing, motor), cooling towers (fan, gearbox), and valves (actuator). Vibration data was collected at 10-second intervals (sampling frequency: 10,000 Hz), and temperature data at 1-minute intervals.

Feature extraction was performed on the vibration data to capture fault-related information:

- Time-domain features: Mean, standard deviation, peak-to-peak value, skewness, kurtosis.
- **Frequency-domain features**: Peak frequency, root mean square (RMS) of the frequency spectrum, spectral centroid.

A total of 50 features were extracted, and principal component analysis (PCA) was used to reduce dimensionality to 10 features (explaining 92% of the variance), reducing model complexity and training time by 40%.

4.3.2 CNN-Based Equipment Fault Diagnosis Model

A CNN model was developed to diagnose equipment faults, with a structure of 3 convolutional layers (filters: 32, 64, 128), 2 max-pooling layers (pool size: 2×2), and 2 fully connected layers (units: 256, 10). The model was trained on a dataset of 50,000 samples (10 fault types: bearing wear, motor overload, fan imbalance, etc.) and tested on 10,000 samples.

Performance metrics showed that the model had an accuracy of 98.2%, a precision of 98.0%, a recall of 98.4%, and an F1-score of 0.978—outperforming traditional methods such as SVM (accuracy = 92.0%) and k-nearest neighbors (k-NN, accuracy = 88.0%) (Zhang, X., Li, D. & Wang, J., 2019). The model also had a diagnosis time of < 5 seconds, enabling real-time fault detection.

5. Cross-Protocol Data Adaptation for Vestas Equipment

5.1 Analysis of Vestas Equipment Data Protocols

Vestas wind turbines (Model: V162-6.2 MW) use three main protocols for data transmission:

- **Modbus**: A serial communication protocol used for monitoring turbine speed, power output, and temperature. The protocol has a baud rate of 9600–115200 bps, a parity bit of even, and a stop bit of 1.
- IEC 61850: An international standard for substation automation, used for high-voltage equipment (e.g., transformers) monitoring. The protocol supports sampled values (SV) and generic object-oriented substation event (GOOSE) messages, with a transmission rate of 1 Gbps.
- ThingWorx: A cloud-based platform used for remote monitoring and maintenance, providing pre-configured dashboards and analytics tools. The platform uses REST API for data access, with a response time of < 500 ms.

Key challenges in integrating these protocols with the DT-O&M platform include: (1) different data formats (Modbus uses binary, IEC 61850 uses XML, ThingWorx uses JSON); (2) varying transmission rates (Modbus: 9600 bps, IEC 61850: 1 Gbps); and (3) security requirements (ThingWorx requires OAuth 2.0 authentication).

5.2 Design of the Cross-Protocol Adaptation Framework

A three-stage adaptation framework was designed to address these challenges:

5.2.1 Data Acquisition Stage

A protocol-specific data acquisition module was developed for each Vestas protocol:

- **Modbus Module**: Uses a serial port (RS485) to connect to the turbine controller, with a data acquisition frequency of 1 Hz. The module supports Modbus RTU and ASCII modes, with a timeout period of 100 ms.
- **IEC 61850 Module**: Uses Ethernet to connect to the substation automation system, supporting SV and GOOSE messages. The module uses MMS (Manufacturing Message Specification) for data exchange, with

a transmission latency of < 10 ms.

• ThingWorx Module: Uses HTTPS to connect to the Vestas cloud platform, with OAuth 2.0 authentication. The module supports batch data retrieval (up to 1000 records per request) and real-time notifications (via WebSocket), with a data refresh rate of 5 seconds.

5.2.2 Data Format Conversion Stage

An ETL (Extract, Transform, Load) tool was developed to convert data from different formats to a unified JSON format:

- **Modbus Binary to JSON**: The module parses binary registers (e.g., 16-bit holding registers) into human-readable values (e.g., temperature in °C), using a register map provided by Vestas. The conversion accuracy is 100%, with no data loss.
- IEC 61850 XML to JSON: The module uses XSLT (Extensible Stylesheet Language Transformations) to convert XML elements to JSON key-value pairs (e.g., "Temperature": 35.2), with a conversion time of < 1 ms per record.
- ThingWorx JSON to Unified JSON: The module normalizes ThingWorx JSON data (e.g., "power_output_kw" to "PowerOutput") to align with the platform's data model, ensuring consistency across all protocols.

5.2.3 Data Synchronization Stage

A real-time data synchronization mechanism was implemented to ensure consistency between the platform and Vestas equipment:

- Time Synchronization: Uses Network Time Protocol (NTP) to synchronize clocks, with a time error of < 1 ms
- **Data Consistency Check**: Uses a hash-based method to verify data integrity, with a checksum calculated for each data packet. If a mismatch is detected, the platform requests retransmission.
- Conflict Resolution: In case of data conflicts (e.g., different values from Modbus and IEC 61850), the platform uses a priority-based rule (IEC 61850 > Modbus > ThingWorx) to select the most reliable data, based on the protocol's real-time performance.

5.3 Performance Validation of the Adaptation Framework

The adaptation framework was tested in a laboratory environment using a Vestas V162-6.2 MW turbine simulator. Key performance metrics were measured:

- **Data Transmission Latency**: The time from data generation in the turbine to reception by the platform was 87 ± 5 ms for Modbus, 9 ± 2 ms for IEC 61850, and 450 ± 20 ms for ThingWorx—all meeting the platform's requirements (< 100 ms for real-time data, < 500 ms for non-real-time data).
- Packet Loss Rate: The rate of lost data packets was < 0.1% for all protocols, due to the retransmission mechanism.
- **Data Accuracy**: The error between the platform's data and the turbine's actual data was < 0.5% for all parameters (e.g., power output, temperature), confirming the framework's reliability.

Table 2 summarizes the performance metrics of the adaptation framework.

Table 2. Performance Metrics of the Cross-Protocol Adaptation Framework

Protocol	Transmission Latency	Packet Loss Rate	Data Accuracy
Modbus	$87 \pm 5 \text{ ms}$	< 0.1%	< 0.5%
IEC 61850	$9 \pm 2 \text{ ms}$	< 0.1%	< 0.5%
ThingWorx	$450\pm20~ms$	< 0.1%	< 0.5%

6. Field Validation in the Inner Mongolia Wind Power Demonstration Station

6.1 Overview of the Demonstration Station

The Inner Mongolia 6000 MW Wind Power Demonstration Station is located in Siziwang Banner, Ulanqab City, Inner Mongolia, China—an area with abundant wind resources (annual average wind speed: 6.5 m/s) and extreme climate conditions (temperature range: -35° C to 40° C). The station consists of 968 Vestas V162-6.2 MW wind turbines, a 200 MW/800 MWh lithium-ion battery energy storage system, and a $\pm 800 \text{ kV}$ ultra-high

voltage (UHV) transmission line connecting to the Beijing-Tianjin-Hebei power grid.

The station's WSD system includes: (1) a water intake system (raw water from a nearby reservoir); (2) a treatment system (coagulation, sedimentation, filtration, disinfection); (3) a distribution system (pipes for cooling, fire protection, and domestic use); and (4) a drainage system (treated wastewater discharged to a nearby river, with a discharge standard of GB 18918-2002 Class A). The system has a total water consumption of 500,000 m³/year and an annual anti-freezing energy consumption of 12,000 MWh.

6.2 Platform Implementation Process

The platform was implemented in four phases over 6 months (January–June 2023):

- 6.2.1 Phase 1: Sensor Installation and Network Deployment (January-February 2023)
- **Sensor Installation**: 1200 sensors were installed, including 300 flow meters, 200 water quality sensors, 500 vibration/temperature sensors, and 200 pressure sensors. Sensors were calibrated on-site using portable calibration tools (e.g., a portable flow meter with an accuracy of ±0.1%).
- **Network Deployment**: 50 industrial Ethernet switches, 100 LoRaWAN gateways, and 20 protocol conversion gateways were deployed. The network was tested for coverage (100% coverage of the station) and reliability (99.9% uptime).
- 6.2.2 Phase 2: Data Layer and Application Layer Deployment (March–April 2023)
- **Data Layer**: HDFS and PostgreSQL were deployed on 10 servers (8-core CPU, 64 GB RAM, 10 TB HDD), with a distributed architecture for fault tolerance (no single point of failure). Spark and Flink were configured for real-time processing, with a throughput of 10,000 records/second.
- **Application Layer**: The four functional modules were deployed on a cloud server (AWS EC2), with a load balancer to distribute traffic. The web interface was tested for usability (user satisfaction score: 4.8/5) and responsiveness (page load time: < 2 seconds).
- 6.2.3 Phase 3: Cross-Protocol Adaptation and Integration (May 2023)
- The cross-protocol adaptation framework was integrated with the Vestas turbines, with 968 turbines successfully connected to the platform. Data synchronization was tested for 1 week, with no data loss or latency issues.
- The DT model was calibrated using actual data from the station, with a geometric accuracy of ± 1 mm and a simulation error of < 5%.
- 6.2.4 Phase 4: Trial Operation and Optimization (June 2023)
- The platform was operated in trial mode for 1 month, with O&M personnel trained on using the system. Feedback was collected and used to optimize the platform: (1) adding a mobile app for remote monitoring; (2) improving the fault diagnosis model's accuracy for low-speed bearing faults; (3) reducing the dashboard refresh rate to 1 second (from 2 seconds).
- 6.3 Field Test Results and Analysis

6.3.1 Fault Response Time Reduction

The platform's real-time monitoring and fault diagnosis functions significantly reduced fault response time. Before the platform was implemented, O&M personnel relied on manual inspections, with an average fault response time of 4.0 ± 0.5 hours. After implementation, the platform automatically detected faults and sent alerts to O&M personnel, with an average response time of 28 ± 3 minutes—a reduction of 91.7%.

Key faults detected by the platform included: (1) a pipeline blockage in the cooling system (detected in 5 seconds, resolved in 20 minutes); (2) a pump bearing fault (detected in 10 seconds, resolved in 35 minutes); (3) a water quality anomaly (pH spike, predicted 120 minutes in advance, resolved in 15 minutes).

6.3.2 O&M Cost Reduction

The platform reduced O&M costs in three ways: (1) reducing manual inspections (from 200 person-hours/week to 50 person-hours/week); (2) optimizing maintenance schedules (predictive maintenance instead of preventive maintenance); (3) reducing anti-freezing energy consumption (by 35%, from 12,000 MWh/year to 7,800 MWh/year).

Total O&M costs decreased from (12.6 million/year to)8.5 million/year—a reduction of 32.4%. Table 3 breaks down the cost reduction.

Table 3. O&M Cost Reduction Breakdown

Cost Category	Before Platform (\$ million/year)	After Platform (\$ million/year)	Reduction (%)
Labor	4.2	1.0	76.2
Maintenance	3.8	2.5	34.2
Energy (Anti-freezing)	2.4	1.6	33.3
Other (Materials, etc.)	2.2	3.4	-54.5*
Total	12.6	8.5	32.4

6.3.3 Power Generation Improvement

The platform improved annual power generation by optimizing equipment operation and reducing downtime:

- Anti-freezing Optimization: The platform's DT model simulated different anti-freezing strategies, selecting the optimal combination of electric heating and hot water circulation. This reduced anti-freezing energy consumption by 35%, freeing up energy for power generation.
- **Downtime Reduction**: The platform's fault diagnosis function reduced unplanned downtime by 90%, from 100 hours/year to 10 hours/year.
- Annual power generation increased from 12.7 GWh to 18.0 GWh—a 41.2% improvement. The increase in power generation translated to an additional annual revenue of (4.4 million (based on a power price of)0.08/kWh).

6.3.4 Environmental Impact Reduction

The platform also had positive environmental impacts:

- Water Conservation: The water quality prediction model optimized the treatment process, increasing water recovery rate from 28% to 45%—saving 85,000 m³/year of water.
- Carbon Emission Reduction: Reduced anti-freezing energy consumption (7,800 MWh/year) and increased power generation from renewable sources (18.0 GWh/year) led to a carbon emission reduction of 12,600 tons/year (based on a carbon intensity of 0.7 kg CO₂/kWh for grid electricity).

6.4 Comparison with Similar Studies

Table 4 compares the results of this study with similar studies on DT-O&M platforms for NEPS. The proposed platform outperforms existing studies in terms of fault response time reduction, O&M cost reduction, and power generation improvement—due to its multi-dimensional monitoring model, cross-protocol adaptation framework, and field validation in a large-scale station.

Table 4. Comparison with Similar Studies

Study	NEPS Type	Fault Response Time Reduction	O&M Cost Reduction	Power Generation Improvement
Boeing et al.	Wind	22%	15%	5%
Fan et al.	PV	50%	20%	10%
Strielkowski et al.	Wind	60%	25%	15%
This Study	Wind	91.7%	32.4%	41.2%

7. Conclusions

This study presents a comprehensive DT-O&M platform for water supply and drainage systems in new energy power stations, addressing the critical challenges of low reliability, high energy consumption, and inefficient fault response. Key conclusions are as follows:

- **Multi-dimensional Monitoring Model**: The integration of SVM and CNN algorithms enables accurate prediction of water quality anomalies (MAE = 0.03 pH units) and diagnosis of equipment faults (accuracy = 98.2%), providing a solid foundation for intelligent O&M.
- Cross-protocol Adaptation Framework: The framework supports Modbus, IEC 61850, and ThingWorx

- protocols, achieving seamless integration with Vestas equipment (transmission latency = 87 ± 5 ms, packet loss rate < 0.1%)—resolving the data silo issue.
- **Field Validation**: The platform was successfully tested in a 6000 MW wind power station, reducing fault response time by 91.7%, O&M costs by 32.4%, and improving annual power generation by 41.2%. These results confirm the platform's effectiveness and scalability.

The proposed platform provides a technical paradigm for advancing the digitalization and decarbonization of NEPS, with significant implications for the global energy sector.

References

- Boeing, B., Smith, J., Johnson, K., (2020). Digital Twin for Wind Turbine Blade Maintenance. *Renewable Energy*, 156, 1147-1158.
- Di Silvestre, M.L., Favuzza, S., Sanseverino, E.R., Zizzo, G., (2018). How Decarbonization, Digitalization and Decentralization are Changing Key Power Infrastructures. *Renewable and Sustainable Energy Reviews*, 93, 483-498.
- Fan, Z., Cao, J., Jamal, T., et al., (2022). The Role of 'Living Laboratories' in Accelerating the Energy System Decarbonisation. *Energy Reports*, *8*, 11858–11864.
- Global Wind Energy Council (GWEC), (2022). Global Wind Report 2022. Brussels: GWEC.
- Grieves, M., (2016). Digital Twin: The Industrial Internet of Things' Foundation Technology. *IEEE International Conference on Industrial Internet*, Seattle, WA, USA, pp. 1-6.
- Grieves, M., Vickers, J., (2017). Digital Twin: Mitigating Unpredictable, Undesirable Emergent Behavior in Complex Systems. In *Transdisciplinary Perspectives on Complex Systems*. Springer: Cham, Switzerland, pp. 85-113.
- International Energy Agency (IEA), (2023). Renewable Energy Market Update 2023. Paris: IEA.
- Li, H., Zhang, L., Wang, Q., (2020). Anomaly Detection for Pipeline Flow in Water Supply Systems Using Moving Average and Threshold Methods. *Water Resources Management*, *34*, 3879-3894.
- Li, J., Wang, Y., Zhang, H., (2022). Energy Consumption Analysis of Anti-freezing Systems in Northern Wind Power Stations. *Energy Conversion and Management*, 265, 115789.
- Siemens, (2021). Digital Twin for Smart Grids: A Technical White Paper. Munich: Siemens.
- Siemens, (2022). Smart Grid Digital Twin: Case Studies and Best Practices. Munich: Siemens.
- Strielkowski, W., Rausser, G., Kuzmin, E., (2022). Digital Revolution in the Energy Sector: Effects of Using Digital Twin Technology. In *Lecture Notes in Information Systems and Organization: Digital Transformation in Industry*. Springer: Cham, Switzerland, 55, pp. 43-45.
- United Nations (UN), (2023). Sustainable Development Goals Report 2023. New York: UN.
- Wang, Z., Li, C., Chen, X., (2021). Operational Challenges of Water Supply and Drainage Systems in New Energy Power Stations. *Journal of Cleaner Production*, 310, 127543.
- Zhang, X.; Li, D., Wang, J., (2019). Equipment Fault Diagnosis for Wind Turbines Using Convolutional Neural Network. *IEEE Transactions on Industrial Informatics*, 15, 2127-2135.
- Zhao, Y., Liu, J., Chen, S., (2021). Water Quality Prediction Using Machine Learning Algorithms: A Comparative Study. *Environmental Modelling & Software*, 140, 105085.

Copyrights

Copyright for this article is retained by the author(s), with first publication rights granted to the journal.

This is an open-access article distributed under the terms and conditions of the Creative Commons Attribution license (http://creativecommons.org/licenses/by/4.0/).

Paradigm Academic Press Innovation in Science and Technology ISSN 2788-7030 SEP. 2025 VOL.4, NO.8



Liver Transplantation: A Treatment Option for Survival in End-Stage Liver Disease

Haradhan Kumar Mohajan¹

¹ Associate Professor, Department of Mathematics, Premier University, Chittagong, Bangladesh Correspondence: Haradhan Kumar Mohajan, Associate Professor, Department of Mathematics, Premier University, Chittagong, Bangladesh.

doi:10.63593/IST.2788-7030.2025.09.007

Abstract

The liver is the largest internal organ in the body. A healthy liver is necessary for survival that can regenerate most of its own cells when these are damaged. It is an essential organ in digestion, and also undertakes several metabolic processes, such as bile production; bilirubin synthesis; and protein, lipid, fats, and carbohydrate metabolism. Liver transplantation (LT) is a surgery of liver that removes a whole liver or just part of a liver which no longer functions properly with therapies and medications, and replaces it with a healthy liver from a deceased donor or a portion of a healthy liver from a living donor. It is a well-recognized life-saving treatment option for people when liver cannot regenerate and the damage becomes about life-threatening due to liver cirrhosis, decompensated disease, liver cancer, acute liver failure, and hepatocellular carcinoma (HCC). The liver transplanted person needs a long-time follow up treatment with medications to prevent the body from rejecting of the new liver.

Keywords: liver transplantation, liver cirrhosis, donor, immunosuppression, rejection, MELD

1. Introduction

The liver is the largest internal organ of the body that is located within the peritoneal cavity, and is in the right upper quadrant of the abdomen. At present liver resection is practicing worldwide widely to minimize morbidity and reduce mortality (Sumadewi, 2023). Liver transplantation (LT) is a life-saving treatment option of a diseased liver through the replacement with a healthy liver from a deceased donor or a portion of a healthy liver from a living donor (Lucas, 2021). It is a treatment option for people who have significant complications due to end-stage chronic liver disease. It is a life-saving intervention for an increasing number of patients with end-stage liver disease when the liver no longer works as it should (Varma et al., 2011).

The LT can be orthotopic (same place) or heterotopic (other place), and can be performed in patients of all ages. At present orthotopic liver transplantation (OLT) is considered the gold standard treatment for end-stage liver disease, acute liver failure, and liver-based metabolic disorders. The first experimental attempt of hepatocyte liver transplantation (HLT) was developed in 1976 to treat the hyperbilirubinemic Gunn rat (Iansante et al., 2017). A healthy adult living-donor can donate a portion of his/her liver to someone with end-stage liver disease. Following the LT, the liver of the donor will regenerate within a few months (Freeman et al., 2005).

The surgical procedure of LT is very complex process. For a successful LT it is required a careful harvest of the donor organ and meticulous implantation into the recipient. The total procedures of LT must be done by highly trained transplant physicians and supporting medical team (Reddy et al., 2013). The LT offers live-saving therapy for patients with end-stage liver disease that is often caused by liver cirrhosis, such as liver cancer, liver failure; whose condition cannot be controlled with other treatments. It is the second most common solid organ transplantation after kidney transplantation worldwide (Mahillo et al., 2013).

The LT centers match donors with recipients based on compatible liver size and blood type. In 2011, more than 5,800 adult LTs were performed in the USA. It is estimated that in 2018 more than 32,000 LTs were conducted globally, and among them 8,200 were in the USA (Statistics Portal, 2018). More than 10,000 LTs are performed each year in Europe, and about 119,803 LTs took place across Europe between 1988 and 2015 (Blachier et al., 2013). In 2021, there were about 34,694 LTs performed globally that is an increase of 6.5% from 2020 and a 20% increase from 2015 (Terrault et al., 2023). In the USA, about 41,734 LTs were performed between 1992 and 2001 (Marcellin & Kutala, 2018). From 1988 to 2022, more than 200,000 LTs were performed in the USA, and only in 2022 there were 9,528, of which 526 were performed in patients under the age of 18 years (Lucey et al., 2023).

There are enormous improvements in surgical techniques, patient management, effective therapy, and immunosuppressive drugs in the last 60 years of LT (Maciel et al., 2021). After LT more than nine out of ten people are still alive after one year, around eight in every ten people live at least five years, with many people living for up to 20 years or more. However, donor organ shortage and lifelong need for immunosuppression are the main restrictions to LT (Adam et al., 2018).

2. Literature Review

The literature review section is an introductory unit of research, which exhibits the works of previous researchers in the same field within the existing knowledge (Polit & Hungler, 2013). Roberto Ferreira Meirelles Júnior and his coauthors have found that a major challenge in LT field is the insufficient number of donors compared with the growing demand of transplant candidates. They have emphasized that appropriated donor and receptor selection, allocation and organ preservation topics should contribute to improve the number and outcomes in LT (Meirelles et al., 2015). Astrid Marot and his coauthors have found that 14% of carefully selected patients with clinically severe alcoholic hepatitis (AH) not responding to medical therapy have alcohol relapse after LT (Marot et al., 2018).

Emrah Otan and his coworkers have aimed to evaluate the outcomes of living donor liver transplantation (LDLT) patients in whom neurological complications developed early during postoperative follow-up in the intensive care unit (ICU). They have observed that over the last two decades, postoperative management and new immunosuppressive regimens have been developed. The survival of orthotopic liver transplantation (OLT) recipients has improved (Otan et al., 2015). Altan Alim and his coauthors have wanted to identify the indications, survival, and complications of LT in congenital metabolic diseases. They have also described demographic information of patients, liver graft types, and donor information (Alim et al., 2022).

Nadim Mahmud has reviewed the general indications and contraindication to LT, and has provided an overview of the transplant evaluation process. He believes that LT may be life-saving for patients with acute liver failure or end-stage liver disease. It is therefore critical for healthcare providers caring for patients with liver disease to be familiar with the general indications for transplantation and to know when it is appropriate or inappropriate to refer for transplant evaluation (Mahmud, 2020). Norah A. Terrault and her coworkers have shown that LT offers live-saving therapy for patients with complications of cirrhosis and stage T2 hepatocellular carcinoma. They have also presented a status report on the most pressing topics in LT and future challenges (Terrault et al., 2023).

Nicole Bianchin Maciel and her coworkers have shown that immunosuppressive drugs have important role in transplant of solid grafts to avoid episodes of acute and chronic rejection and to improve graft survival and patient survival (Maciel et al., 2021). Rosana Guerrero-Domínguez and her coauthors have found that renal failure is one of the most common and major complications among 17-95% LT recipients that is associated with prolonged hospital stay in the intensive care unit, the need for postoperative dialysis, infectious complications, acute rejection, and increased mortality (Guerrero-Domínguez et al., 2014).

3. Research Methodology of the Study

To rationalize the selection of a research methodology, a researcher must understand its philosophical origins and unique characteristics (Rieger, 2019). Methodology is a guideline for the accomplishment of a good research (Kothari, 2008). Therefore, research methodology is the specific procedures that are used to identify, select, process, and analyze materials related to the topics (Somekh & Lewin, 2005). To prepare this paper, I have used the secondary data sources that are related to liver transplantation (Mohajan, 2017, 2018, 2020). I have consulted the published journal articles, books and handbooks of famous authors, websites, etc. to complete the paper (Mohajan, 2024a-q).

4. Objective of the Study

Main objective of this article is to discuss the pre- and post- complications of liver transplantation. At present acute and chronic liver diseases are increasing due to virus infection, pharmacological drug consumption, poor diet and lifestyle, alcoholism, cancer metastasis, and some other factors (LeCluyse et al., 2012). Liver transplantation (LT) is the only therapeutic option for patients with life-limiting liver disease in the form of acute

liver failure and end-stage chronic liver disease (Mahmud, 2020). Other minor objectives of the study are as follows:

- to show the overview and basic physiology of liver,
- to focus on historical background of LT, and
- to show the liver transplantation complications and success.

5. Overview of Liver

The liver is the largest and the most complex internal organ of the body. It is located within the peritoneal cavity, and is in the right upper quadrant of the abdomen. It is a wedge or cone shaped with the base on the right and the apex to the left (Ramachandran & Kumar, 2019). It is dark pinkish-brown peritoneal organ, in an average adult human weighs 1.5 to 2kg, which is roughly 2-3% of the total body weight. An average liver volume in healthy adult people is 1,225cm³ (±217) (Juza & Pauli, 2014). The liver consists of two lobes: i) the right lobe (larger), ii) the left lobe (smaller) that are divided by the plane of middle hepatic vein (Bismuth, 1982).

6. Basic Physiology of Liver

The liver is the largest internal organ in the body that accomplishes many complex functions. It is the powerhouse of the body for metabolism and a center for numerous physiological processes (Mohajan, 2024a,b). It performs a group of essential functions of the body, such as vascular, immunological, metabolic, and secretory and excretory functions (Alamri, 2018). The functions of liver in brief are blood detoxification and purification; synthesis of plasma proteins; storage of glycogen, vitamins (e.g., A, D, E, C), minerals (e.g., iron and copper); production and excretion of bile and urea; detoxification of drugs and toxins; the metabolism of carbohydrates, fats and proteins; filtration of bacteria, degradation of endotoxins and lactate metabolism, etc. (Jastrow, 1908). The liver is the only organ that has the extraordinary property of self-regeneration (Ozougwu, 2014).

The liver has a dual blood supply: the portal vein provides 75% and the hepatic artery provides 25% of the blood supply. Each vessel provides 50% of oxygen delivery. After LT sufficient blood flow through the hepatic artery is essential for the viability of a new liver graft. In every minute about 1500ml of blood flows through the liver that is about 25% of the cardiac output, which is more than any other organ (Abbasoglu et al., 1998).

7. Historical Background of LT

In 1955, Stuart Welch performed a heterotopic LT in the canine species. In 1956, Jack Cannon is credited with the first animal orthotopic LT although the species was not disclosed. The first attempts at LT were performed on dogs in 1954 by Italian professor of surgery Vittorio Staudacher (1913-2005) (Busuttil et al., 2012). The first attempted human LT was performed in 1st March 1963 in the world by American physician, researcher, and expert on organ transplants Thomas Earl Starzl (1926-2017) who has often been referred to as "the father of modern transplantation." The patient was a three years old boy with biliary atresia who underwent LT, but he died due to coagulation disorder and uncontrolled bleeding (Starzl et al., 1963). In 1967, he transplanted liver of a 19 months old girl with hepatoblastoma who was able to survive for over one year before dying of metastatic disease. In the first five LTs no patient survived more than 23 days (Zarrinpar & Busuttil, 2013). In 1979, survival after liver transplantation improved significantly to a 1-year survival rate of over 70% due to the development of cyclosporine (Starzl et al., 1989). Since the first successful human LT reported by Thomas Starzl in 1963, the LT has evolved rapidly and more than 100,000 procedures performed to date, and survival rates have improved significantly up to 71% at 10 years after LT (Adam et al., 2012).

8. Total LT Activities

The major indications for LT are irreversible hepatic failure irrespective of the etiology of the liver disease. Not all the patients who face irreversible liver failure ultimately will undergo for a LT. It is necessary to the explanation of the indicators of liver failure, the timing of transplant evaluation, pre- and post- transplant management, and the potential benefit of LT (O'Leary et al., 2008).

8.1 Sign and Causes of LT

If the patients have evidence of fulminant hepatic failure, life-threatening systemic complications, cirrhosis with complications, such as hepatic encephalopathy, ascites, hepatocellular carcinoma, cryptogenic cirrhosis, hepatorenal syndrome, and bleeding caused by portal hypertension, are considered for LT (O'Leary et al., 2008). The symptoms of liver failure are jaundice, a condition that causes yellowing of the skin and the whites of the eyes, fatigue, weakness, loss of appetite, nausea, weight loss, muscle loss, itching, bruising, or bleeding easily because blood does not clot, bleeding in the stomach, vomiting blood, passing black stools ascites, the buildup of fluid in the abdomen, forgetfulness, confusion (Khan et al., 2006).

People with either acute or chronic liver failure may need a LT for survival. The most common reasons for LT are chronic viral hepatitis by any virus (mainly hepatitis B virus (HBV) and hepatitis C virus (HCV)),

autoimmune hepatitis, primary biliary cholangitis (PBC), primary sclerosing cholangitis (PSC), secondary biliary cirrhosis (SBC), alcoholic liver disease, non-alcoholic fatty liver disease, hepatocellular carcinoma (HCC), liver cancer, and liver failure. One of the most common reasons is cirrhosis caused by long-term alcohol abuse. In children, biliary atresia is the most common cause for LT (Starzl et al., 1989).

8.2 Liver Donor

The LT is a life-saving surgery of the patients with acute and chronic liver diseases, where the donors play important roles. The donor will be a family member or non-family member with blood matching who can provide support before, during, and after surgery (Hashikura et al., 1994). The voluntary and benevolent donor must be 18-60 years. S/he must be in excellent physical and emotional health, cannot have any history of cancer with normal liver function (Otan et al., 2015). First successful living donor liver transplant (LDLT) was performed on a child in 1990 in Australia, and the LDLT was his mother (Strong et al., 1990). Most of the time, a liver is donated from someone who has died that is now known as a deceased donor. When an organ donor dies, the liver is removed by a surgeon and replace to the transplant recipient as quickly as possible. Livers for transplant must be matched for body size and blood type (Amara et al., 2022). The children need a small portion of the left lobe of liver of the adult donor. On the other hand, adult to adult living donor transplantation is achieved by using the entire right lobe of liver of the donor (Broelsch et al., 1991).

The liver donation operation is a major surgery that requires a 5-10-day hospitalization and 2-3-month period of recovery (Llovet et al., 2018). The donor surgery has a very low risk of death, the liver of donor regenerates to its original size within a few months. Both livers of donor and receiver will grow back to normal size within a few weeks after surgery (Kim & Testa, 2016). Not all candidates are suited for liver donation. The blood vessels to the liver and bile ducts in the liver of the donor must be suitable for transplantation. The LT centers match donors with recipients based on compatible liver size and blood type. Usually, older patients with cardiac or respiratory complications are not allowed for liver donation (Wiesner et al., 2003). The demand for organs is increasing day by day, in parallel the usable deceased and live donors are also expanding gradually (Terrault et al., 2023). In 2020, more than 90% of LT deceased donors, and only 4.3% of living donors were in the Western world. But, in many Asian countries most transplants are from living donors LT (Kwong et al., 2022).

8.3 LT Assessment

A LT is a complex process that requires hundreds of steps before, during and after LT. The LT evaluation are reviewed in details by a patient selection committee consists of transplant surgeons, hepatologists, house-staffs (junior physicians), anesthesiologists, psychologists, transplant coordinators, advanced practice nurses, social workers, dietitians, pharmacists, research coordinators, pastoral counselors, and a finance office representative (O'Leary et al., 2008). Some people wait a long-time for their LT, while others need an urgent LT. The LT donors are scarce worldwide; liver allocation prioritizes patients, who likely will die soonest without transplantation (Goudsmit et al., 2023). The patient needs many tests before the surgery to decrease the potential risks of heart attack, stroke, and death (Schlegel et al., 2023). Many people have positive emotions, such as hope, joy, and gratitude, and some have difficult emotions, such as fear, sadness, anxiety, irritability, anger, and grief, fear of dying during the transplant journey (Levenson & Olbrisch, 1993).

A LT is considered when a person might die from liver disease within the next 1-3 years. The three scoring systems are used for urgent LT: i) the Model for End-stage Liver Disease (MELD) scoring system when the patient's age is 12 and older, ii) The Child-Turcotte-Pugh (CTP) classification has been used to assess surgical risk in LT (Pugh et al., 1973), and iii) the Pediatric End-stage Liver Disease (PELD) scoring system when the patient's age is less than 12. These scores have been validated to predict the survival time in most patients with chronic liver disease (Wiesner et al., 2003). The MELD/PELD scores are numerical scales based on the patient's risk of dying while waiting for LT. Both of them are dependent on bilirubin, international normalized ratio (INR) albumin, creatinine, growth failure, and age listed (Freeman et al., 2005). The MELD-Na orders transplant candidates from less ill (MELD 6) to extremely ill (MELD 40). Usually, the LT may be approved the patients with decompensated cirrhosis or MELD≥15 (Martin et al., 2014).

The LT is a major surgery that lasts 6-8 hours, and has major risks. After surgery, a patient is taken to the intensive care unit (ICU) where s/he is placed on a mechanical ventilator that supports breathing for average two days, and then transfer to the medical floor (Lucey et al., 2023). Frequent tests are conducted to assess the functioning of the new liver. After 10 to 14 days the patient can leave the hospital, and needs follow up treatment as outpatient for continued monitoring of the new liver. Nutrition recommendations will be different for each individual according to the dietitian (Adam et al., 2018).

Some complications from liver surgery are infection, bleeding, clotting of the artery to the liver, blocked blood vessels to the new liver, leakage of bile or blocked in bile ducts, inactiveness in immune system, poor function of the new liver, inactivity of new liver for a short-time right after surgery, and post-transplant lymphoproliferative

disease (PTLD) (Hernandez et al., 1998). Renal dysfunction is common after LT.

8.4 Post LT Situation

Most of the LT persons are able to return to a normal and healthy lifestyle, and can enjoy an improved quality of life. They are able to start normal exercise after their recuperation, and women are able to conceive and have normal post-transplant pregnancies and deliveries. Proper nutrition maintenance is necessary after LT to control the changes in the body (Lewis & Howdle, 2003). If autoantibodies develop after LT then various complications arise, such as chronic hepatitis, severe graft dysfunction, chronic rejection, loss of graft, and death (Dubel et al., 1998). The LT patients need multiple visits to the hospital for evaluation rest of life. Some LT patients may experience feelings of stress, anxiety, guilt, confusion, irritability, trouble in sleeping, and depression. Sometimes there is an increased risk for developing certain types of cancers, such as post-transplant lymphoma (Rothenhäusler et al., 2002).

After LT the patient must take antirejection or immunosuppressive medicines that weaken the immune system response for the rest of life (Thuluvath et al., 2007). Calcineurin-inhibiting immunosuppressive medications are the mainstay of post-transplant immunosuppression. Medicines prednisone, tacrolimus, azathioprine, mycophenolate mofetil, cyclosporine, and sirolimus are used to prevent organ rejection after LT that help to prevent rejection of the new liver. The side-effects of immunosuppressive medications can be very hard on the body (DiMartini et al., 2008). These medications can increase blood pressure, cholesterol, blood sugar, kidney problems, and weight gain that have a chance of developing heart disease, stroke, and diabetes. Heart disease is the leading cause of death with post-transplant patients after the first three months (Berlakovich et al., 2000). Some of the more annoying side-effects after LT are hair loss, insomnia, diarrhea, nausea, headaches, swelling, and neuropathy (Paugam et al., 2009). Recurrence of fatty liver disease and obesity after LT is a problem because it leads to metabolic syndrome with higher risk for stroke and heart attacks (Rothenhäusler et al., 2002).

The LT has several disadvantages, such as the risks of complications related to surgery, the high cost of the procedure, and the need for lifelong immunosuppression (Iansante et al., 2017). The immune-mediated rejection is determined through the lab findings, such as elevated aspartate aminotransferase (AST), alanine aminotransferase (ALT), gamma-glutamyl transpeptidase (GGT), etc. Sometimes abnormal liver function values, such as prothrombin time, ammonia level, bilirubin level, albumin concentration, and abnormal blood glucose can increase (Jain et al., 2000). Immune system helps the people to fight against infections that are done by recognizing from non-self. Anything it sees as non-self is attacked by the immune system and destroyed. The new liver naturally is recognized as non-self and is attacked by the immune system, and this process is called rejection (Lucey et al., 2023). Some patients are not allowed for LT, those who have severe cardiopulmonary disease, uncontrolled sepsis, active extrahepatic malignancy, acquired immune deficiency syndrome (AIDS), and who are in brain death (Osorio et al., 1994).

9. Conclusions

In this study, I have found that liver is an essential organ of human to sustain life. It is the only organ in the body that can regenerate itself. It plays an important role in metabolism through the preservation and regulation of the levels of lipid and glucose in the body as well as energy metabolism. No artificial device is available to support or replace a damage live. Therefore, LT is an effective and established life-saving procedure for the patients with end-stage liver disease. Recently, despite a significant progress has been made in the area of LT, organ scarcity remains a significant constraint, and also the recipients continue to face long-term immunosuppression complications. I have observed that LT is a comparatively safe and successful life-saving treatment option that can be applied in patients with acute and chronic liver disease.

References

- Abbasoglu, O., et al., (1998). Does Intraoperative Hepatic Artery Flow Predict Arterial Complications after Liver Transplantation? *Transplantation*, 66(5), 598-601.
- Adam, R., et al., (2012). Evolution of Indications and Results of Liver Transplantation in Europea. A Report from the European Liver Transplant Registry (ELTR). *Journal of Hepatology*, *57*(3), 675-688.
- Adam, R., et al., (2018). Annual Report of the European Liver Transplant Registry (ELTR): 50-Year Evolution of Liver Transplantation. *Transplant International*, *31*(12), 1293-1317.
- Alamri, Z. Z., (2018). The Role of Liver in Metabolism: An Updated Review with Physiological Emphasis. *International Journal of Basic & Clinical Pharmacology*, 7(11), 2271-2276.
- Alim, A., et al., (2022). Liver Transplantation for Congenital Metabolic Disorders. *Cerrahpaşa Medical Journal*, 46(1), 21-25.
- Amara, D., et al., (2022). Surgical Complications after Living and Deceased Donor Liver Transplant: The NSQIP Transplant Experience. *Clinical Transplantation*, 36(6), e14610.

- Berlakovich, G. A., et al., (2000). General Compliance after Liver Transplantation for Alcoholic Cirrhosis. *Transplant International*, 13(2), 129-135.
- Bismuth, H., (1982). Surgical Atnaomy and Anatomical Surgery of the Liver. World Journal of Surgery, 6(1), 3-9.
- Blachier, M., et al., (2013). The Burden of Liver Disease in Europe: A Review of Available Epidemiological Data. *Journal of Hepatology*, 58(3), 593-608.
- Broelsch, C. E., et al., (1991). Liver Transplantation in Children from Living Related Donors. Surgical Techniques and Results. *Annals of Surgery*, 214(4), 428-437.
- Busuttil, R. W., et al., (2012). The First Report of Orthotopic Liver Transplantation in the Western World. *American Journal of Transplantation*, 12(6), 1385-1387.
- DiMartini, A., et al., (2008). Age, MELD Score, and Organ Functioning Predict Post Transplant Tacrolimus Neurotoxicity. *Liver Transplantation*, 14(6), 815-822.
- Dubel, L., et al., (1998). High Incidence of Antitissue Antibodies in Patients Experiencing Chronic Liver Allograft Rejection. *Transplantation*, 65(8), 1072-1075.
- Freeman, R. B., et al., (2005). Excellent Liver Transplant Survival Rates under the MELD/PELD System. *Transplantation Proceedings*, *37*(2), 585-583.
- Goudsmit, B. F. J., et al., (2023). Survival Benefit from Liver Transplantation for Patients with and without Hepatocellular Carcinoma. *JHEP Reports*, 5(12), 100907.
- Guerrero-Domínguez, R., et al., (2014). Perioperative Renal Protection Strategies in Liver Transplantation. *Nefrologia*, 34(3), 276-284.
- Hashikura, Y., et al., (1994). Successful Living-Related Partial Liver Transplantation to an Adult Patient. *Lancet*, 343(8907), 1233-1234.
- Hernandez, D., et al., (1998). Risk Factors of Graft Loss in Orthotopic Liver Transplantation. *Transplantation Proceedings*, 30(7), 3241-3242.
- Iansante, V., et al., (2017). Human Hepatocyte Transplantation for Liver Disease: Current Status and Future Perspectives. *Hepatocyte Transplantation*, 83(1), 232-240.
- Jain, A., et al., (2000). Long-Term Follow-Up after Liver Transplantation for Alcoholic Liver Disease under Tacrolimus. *Transplantation*, 70(9), 1335-1342.
- Jastrow, M., (1908). The Liver in Antiquity and the Beginnings of Anatomy. *Transactions & Studies of the College of Physicians of Philadelphia*, 20(11), 117-139.
- Juza, R. M., & Pauli, E. M., (2014). Clinical and Surgical Anatomy of the Liver: A Review for Clinicians. *Clinical Anatomy*, 27(5), 764-769.
- Khan, S. A., et al., (2006). Acute Liver Failure: A Review. Clinical Liver Disease, 10(2), 239-258.
- Kim, P. T., & Testa, G., (2016). Living Donor Liver Transplantation in the USA. *HepatoBiliary Surgery and Nutrition*, 5(2), 133-140.
- Kothari, C. R., (2008). *Research Methodology: Methods and Techniques* (2nd Ed.). New Delhi: New Age International (P) Ltd.
- Kwong, A. J., et al., (2022). OPTN/SRTR 2020 Annual Data Report: Liver. *American Journal of Transplantation*, 22(Suppl 2), 204-309.
- LeCluyse, E. L., et al., (2012). Organotypic Liver Culture Models: Meeting Current Challenges in Toxicity Testing. *Critical Reviews in Toxicology*, 42(6), 501-548.
- Levenson, J. L., & Olbrisch, M. E., (1993). Psychosocial Evaluation of Organ Transplant Candidates: A Comparative Survey of Process, Criteria, and Outcomes in Heart, Liver, and Kidney Transplantation. *Psychosomatics*, 34(4), 314-323.
- Lewis, M. B., & Howdle, P. D., (2003). Neurologic Complications of Liver Transplantation in Adults. *Neurology*, *61*(9), 1174-1178.
- Llovet, J. M., et al., (2018). Pilot Study of Living Donor Liver Transplantation for Patients with Hepatocellular Carcinoma Exceeding Milan Criteria (Barcelona Clinic Liver Cancer Extended Criteria). *Liver Transplantation*, 24(3), 369-379.
- Lucas, A. R., (2021). Liver Transplantation. Journal of Transplantation Technologies & Research, 11(3), e104.
- Lucey, M. R., et al., (2023). Liver Transplantation. The New England Journal of Medicine, 389(20), 1888-1900.

- Maciel, N. B., et al., (2021). Liver Transplantation: Tacrolimus Blood Levels Variation and Survival, Rejection and Death Outcomes. *Archives of Gastroenterology*, 58(3), 370-376.
- Mahillo, B., et al., (2013). Global Database on Donation and Transplantation: goals, Methods and Critical Issues. *Transplantation Reviews*, 27(2), 57-60.
- Mahmud, N., (2020). Selection for Liver Transplantation: Indications and Evaluation. *Current Hepatology Reports*, 19(3), 203-212.
- Marcellin, P., & Kutala, B. K., (2018). Liver Diseases: A Major, Neglected Global Public Health Problem Requiring Urgent Actions and Large-Scale Screening. *Liver International*, 38(Suppl. 1), 2-6.
- Marot, A., et al., (2018). Liver Transplantation for Alcoholic Hepatitis: A Systematic Review with Metaanalysis. *PLoS ONE*, *13*(1), e0190823.
- Martin, P., et al., (2014). Evaluation for Liver Transplantation in Adults: 2013 Practice Guideline by the American Association for the Study of Liver Diseases and the American Society of Transplantation. *Hepatology*, 59(3), 1144-1165.
- Meirelles, R. F. Jr., et al., (2015). Liver Transplantation: History, Outcomes and Perspectives. *Einstein*, 13(1), 149-152.
- Mohajan, H. K., (2017). Two Criteria for Good Measurements in Research: Validity and Reliability. *Annals of Spiru Haret University Economic Series*, 17(3), 58-82.
- Mohajan, H. K., (2018). Aspects of Mathematical Economics, Social Choice and Game Theory. PhD Dissertation, Jamal Nazrul Islam Research Centre for Mathematical and Physical Sciences (JNIRCMPS), University of Chittagong, Chittagong, Bangladesh.
- Mohajan, H. K., (2020). Quantitative Research: A Successful Investigation in Natural and Social Sciences. *Journal of Economic Development, Environment and People*, 9(4), 50-79.
- Mohajan, H. K., (2024a). Alcoholic Liver Disease: Diagnosis and Treatment Strategies. Unpublished Manuscript.
- Mohajan, H. K., (2024b). Anatomy of Human Liver: A Theoretical Study. Unpublished Manuscript.
- Mohajan, H. K., (2024c). Liver Diseases: Epidemiology, Prevention, and Management Strategy. Unpublished Manuscript.
- Mohajan, H. K., (2024d). Management Strategies of Fatal Liver Infection Due to Hepatitis C Virus (HCV). Unpublished Manuscript.
- Mohajan, H. K., (2024e). Transmission, Diagnosis, and Treatment of Acute and Chronic Hepatitis E. Unpublished Manuscript.
- Mohajan, H. K., (2024f). Management of Acute and Chronic Hepatitis B and C Viral Infections. Unpublished Manuscript.
- Mohajan, H. K., (2024g). Epidemiological Investigation of Hepatitis F Viruses (HFV). Unpublished Manuscript.
- Mohajan, H. K., (2024h). Hepatitis A and Hepatitis E Viruses can Develop Acute Viral Hepatitis: Prevention is the Best Policy. Unpublished Manuscript.
- Mohajan, H. K., (2024i). Alcoholic Hepatitis: Diagnosis and Management Procedures. Unpublished Manuscript.
- Mohajan, H. K., (2024j). A Study on Functions of Liver to Sustain a Healthy Liver. Unpublished Manuscript.
- Mohajan, H. K., (2024k). Hepatitis A Virus (HAV) Infection: A Prevention Strategy through Hygienic Maintenance and Vaccination. Unpublished Manuscript.
- Mohajan, H. K., (2024l). Prevention of Hepatitis B Virus (HBV) is Essential to Avoid Chronic Liver Disease. Unpublished Manuscript.
- Mohajan, H. K., (2024m). Clinical Practice, and Diagnosis and Treatment Strategies of Chronic Hepatitis D Virus (HDV). Unpublished Manuscript.
- Mohajan, H. K., (2024n). Hepatitis G Viruses (HGV): A Study on Prevalence, Transmission, and Co-Infection. Unpublished Manuscript.
- Mohajan, H. K., (2024o). Prevention and Treatment Strategies of Viral Hepatitis. Unpublished Manuscript.
- Mohajan, H. K., (2024p). Hepatitis D and E Viruses Cause Liver Damage: Management and Prevention are the Best Policies of Elimination These. Unpublished Manuscript.
- Mohajan, H. K., (2024q). Alcoholic Liver Cirrhosis: A Chronic Liver Failure Due to Alcohol Abuse.

- Unpublished Manuscript.
- O'Leary, J. G., et al., (2008). Indications for Liver Transplantation. Gastroenterology, 134(6), 1764-1776.
- Osorio, R. W., et al., (1994). Predicting Recidivism after Orthotopic Liver Transplantation for Alcoholic Liver Disease. *Hepatology*, 20(1), 105-110.
- Otan, E., et al., (2015). Evaluation of Early Postoperative Neurological Complications Following Living Donor Liver Transplantation. *Archives of Neuropsychiatry*, *52*(1), 15-18.
- Ozougwu, J. C., (2014). Hepatoprotective Effects of Allium Cepa Extracts on Paracetamol-Induced Liver Damage in Rat. *African Journal of Biotechnology*, 13(26), 2679-2688.
- Paugam, B. C., et al., (2009). Postreperfusion Syndrome during Liver Transplantation for Cirrhosis: Outcome and Predictors. *Liver Transplantation*, 15(5), 522-529.
- Polit, D. F., & Hungler, B. P., (2013). *Essentials of Nursing Research: Methods, Appraisal, and Utilization* (8th Ed.). Philadelphia: Wolters Kluwer/Lippincott Williams and Wilkins.
- Pugh, R. N. et al., (1973). Transection of the Oesophagus for Bleeding Oesophageal Varices. *British Journal of Surgery*, 60(8), 646-649.
- Ramachandran, K., & Kumar, R. D., (2019). A Study on the morphological Variations of the Liver and Its Clinical Significance. *Indian Journal of Anatomy and Surgery of Head, Neck and Brain*, 5(4), 110-113.
- Reddy, M. S., et al., (2013). Matching Donor to Recipient in Liver Transplantation: Relevance in Clinical Practice. *World Journal of Hepatology*, 5(11), 603-611.
- Rieger, K. L., (2019). Discriminating among Grounded Theory Approaches. Nursing Inquiry, 26(1), e12261.
- Rothenhäusler, H. B., et al., (2002). Psychiatric and Psychosocial Outcome of Orthotopic Liver Transplantation. *Psychotherapy and Psychosomatics*, 71(5), 285-297.
- Schlegel, A., et al., (2023). A Multicenter Randomized-Controlled Trial of Hypothermic Oxygenated Perfusion (HOPE) for Human Liver Grafts before Transplantation. *Journal of Hepatology*, 78(4), 783-793.
- Somekh, B., & Lewin, C., (2005). Research Methods in the Social Sciences. Sage Publications.
- Starzl, T. E., et al., (1963). Homotransplantation of the Liver in Humans. *Surgery, Gynecology and Obstetrics*, 117, 659-676.
- Starzl, T. E., et al., (1989). Liver Transplantation. New England Journal of Medicine, 321(16), 1014-1022.
- Statistics Portal, (2018). Estimated Number of Worldwide Liver Transplants in 2018, by Region. http://www.statista.com/statistics/398685/livertransplants-by-world-region/
- Strong, R. W., et al., (1990). Successful Liver Transplantation from a Living Donor to Her Son. *New England Journal of Medicine*, 322(21), 1505-1507.
- Sumadewi, K. T., (2023). Embryology, Anatomy and Physiology of the Liver: Review. *Indian Journal of Clinical Anatomy and Physiology*, 10(4), 138-144.
- Terrault, N. A., et al., (2023). Liver Transplantation 2023: Status Report, Current and Future Challenges. *Clinical Gastroenterology and Hepatology*, 21(8), 2150-2166.
- Thuluvath, P. J., et al., (2007). Trends in Post-Liver Transplant Survival in Patients with Hepatitis C between 1991 and 2001 in the United States. *Liver Transplantation*, 13(5), 719-724.
- Varma, V., et al., (2011). Indications and Contraindications for Liver Transplantation. *International Journal of Hepatology*, 2011(2090-3448), 121862.
- Wiesner, R., et al., (2003). Model for End-Stage Liver Disease (MELD) and Allocation of Donor Livers. *Gastroenterology*, 124(1), 91-96.
- Zarrinpar, A., & Busuttil, R. W., (2013). Liver Transplantation: Past, Present and Future. *Nature Reviews Gastroenterology & Hepatology*, 10(7), 434-440.

Copyrights

Copyright for this article is retained by the author(s), with first publication rights granted to the journal.

This is an open-access article distributed under the terms and conditions of the Creative Commons Attribution license (http://creativecommons.org/licenses/by/4.0/).

Paradigm Academic Press Innovation in Science and Technology ISSN 2788-7030 SEP. 2025 VOL.4, NO.8



Design and Engineering Practice of a Visual-Voice Multimodal Collaborative Perception System for Community Security

Yang Zhong¹

¹ Kingdee Software (China) Co., Ltd., Shenzhen, Guangdong 518025, China

Correspondence: Yang Zhong, Kingdee Software (China) Co., Ltd., Shenzhen, Guangdong 518025, China.

doi:10.63593/IST.2788-7030.2025.09.008

Abstract

Aiming at the inherent limitations of single-modal perception in community security scenarios—visual detection is susceptible to low-light conditions and occlusions, while voice recognition often suffers from misjudgments due to environmental noise—this study designs and implements a deep learning-based visual-voice multimodal collaborative perception system. Centered on the core of "heterogeneous modal complementary enhancement", the system adopts a modular technical architecture through feature-level fusion and dynamic decision-making collaborative strategies: (1) The visual module employs an improved YOLOv12s algorithm, integrating adaptive Retinex contrast enhancement and dynamic Gaussian Mixture Model (GMM) background modeling to enhance the robustness of object detection under complex lighting; (2) The voice module is built on a CRNN (CNN+BiLSTM) architecture, combining multi-channel beamforming and SpecAugment data augmentation to strengthen abnormal sound recognition in noisy environments; (3) The multimodal collaboration module innovatively introduces an attention-based feature alignment mechanism and scene-adaptive threshold decision-making to achieve efficient fusion of cross-modal information.

Validated on the self-constructed CommunityGuard V1.0 community security dataset (covering 50 hours of multi-scenario synchronized audio-visual data, including day/night, sunny/rainy, and noisy/quiet sub-scenarios), the multimodal collaborative detection achieves F1-Scores that are 5.8% and 13.6% higher than those of visual single-modal and voice single-modal detection, respectively. Particularly in night-noisy scenarios (illumination < 20lux, noise ≥ 65dB), the F1-Score reaches 85.6%, representing a maximum improvement of 17.4% over single-modal detection. The end-to-end inference latency is stably maintained at 5ms(+- 1)ms (on Tesla T4 GPU TensorRT10) (Redmon, J., & Farhadi, A., 2018), meeting real-time requirements for community security. Meanwhile, the system is lightweight and deployable on edge devices.

Keywords: community security, multimodal collaborative perception, feature-level fusion, YOLOv12s Improvement, CRNN, attention mechanism, real-time detection, edge deployment, abnormal sound recognition, dynamic decision-making

1. Introduction

1.1 Research Background: From Engineering Pain Points

Urbanization has expanded community scales and increased population density, shifting security demands from "post-incident forensics" to "pre-incident early warning". However, traditional solutions face significant engineering implementation bottlenecks:

• Over-reliance on single visual modality: In low-light conditions (<20lux) at night, the missed detection rate of mainstream video surveillance exceeds 30%. Dynamic interferences such as occlusions from community green belts and temporary parking result in false alarm rates as high as 15%-20%, wasting security resources. Field surveys show that a medium-sized community (1,500 households)

records 30-40 invalid dispatches monthly due to false alarms, accounting for over 60% of total dispatches.

- Isolated limitations of voice perception: Existing voice alarm devices rely on fixed thresholds to identify abnormal sounds (e.g., glass breaking, distress calls). In complex noisy environments—such as community traffic noise (60-70dB) and crowd chatter (55-65dB)—recognition accuracy drops by 20%-30%, and there is no linkage with visual information for verification. For instance, a community once triggered a voice alarm due to wind-induced trash can collisions; without visual evidence, security personnel spent 20 minutes confirming no threat. (Wang, C. Y., Bochkovskiy, A., & Liao, H. Y. M., 2023)
- Lack of multimodal adaptation: Current multimodal security research focuses on intelligent transportation and smart homes, with few customized solutions for communities' "open scenarios + dynamic crowds + resource-constrained hardware". Especially, robustness optimization for challenging scenarios (low light, noise) is insufficient. While existing multimodal systems achieve over 95% accuracy in ideal laboratory environments, performance typically declines by 15%-25% in real complex community settings.

The core value of multimodal collaboration lies in complementary advantages: the visual modality excels at "spatial localization and object shape recognition" (e.g., confirming climbing behaviors), while the voice modality offers "non-line-of-sight perception and event-driven capabilities" (e.g., identifying glass breaking when visuals are unavailable). Their fusion forms a 3D perception loop of "space-time-semantics", addressing blind spots of single modalities.

1.2 Research Objectives: Defining Engineering Goals

Guided by "solving community security engineering pain points", the core objectives are:

- Technical level: Overcome perception robustness bottlenecks in low-light and noisy scenarios, design a deployable visual-voice collaboration mechanism, ensuring multimodal detection achieves F1-Score ≥85% in all sub-scenarios and false alarm rate ≤5%. Prioritize algorithm optimization for night-noisy scenarios to eliminate missed detections of critical events (e.g., trespassing, distress calls).
- System level: Construct a modular, scalable architecture supporting synchronized access of cameras (1080p@15fps) and 4-channel microphone arrays (16kHz). Ensure end-to-end latency ≤50ms and compatibility with common community edge hardware (e.g., NVIDIA Jetson Xavier NX), optimizing hardware resource utilization to avoid high deployment costs.
- Application level: Realize "accurate abnormal event recognition + hierarchical alarming", distinguishing 12 types of visual anomalies (e.g., climbing, crowd gathering, falling) and 8 types of voice anomalies (e.g., distress calls, glass breaking). Output structured alarm information (time, location, event type, confidence) to support security decision-making, improving residents' sense of safety and advancing smart community development. Ensure security personnel verify and respond to alarms within 3 minutes.

2. Related Work

2.1 Visual Detection Technology: From Algorithm Optimization to Scene Adaptation

The core demands of visual detection for community security are "real-time performance + low-light robustness". Traditional methods (e.g., background subtraction, inter-frame motion detection) achieve over 85% accuracy in simple static scenarios (e.g., empty parking lots) but exceed 25% false detection rate under dynamic community interferences (e.g., wind-blown branches, pet movements) (Popoola et al., 2012). Deep learning enables automatic feature extraction:

- Evolution of object detection algorithms: Faster R-CNN achieves end-to-end detection with over 90% accuracy via Region Proposal Network (RPN) but only 5-10fps inference speed, insufficient for real-time community monitoring (Redmon et al., 2018). The YOLO series balances accuracy and speed through "single-stage regression"; YOLOv12s achieves 30fps at 1080p resolution, with 4.3% higher accuracy than YOLOv4, becoming the mainstream for community scenarios (Wang et al., 2023). However, its accuracy for small objects (e.g., climbing tools) remains below 75% in low light. (Gong, Y., Chung, Y. A., & Glass, J. R., 2021)
- Low-light optimization status: Techniques like Retinex-Net and LLNet enhance image brightness by 3-5 times but introduce noise and increase false detections when directly applied to detection models. Some studies optimize robustness via "enhancement-detection joint training" but incur high costs (over 48 hours per model) and lack adaptation to dynamic community backgrounds (Gong et al., 2021).

The current research gap is the absence of lightweight visual solutions for "dynamic background + low light" in communities and the lack of collaborative verification with voice perception to compensate for visual limitations.

2.2 Voice Detection Technology: From Noise Suppression to Event Association

Key challenges for community voice detection are "noise robustness + event semantic matching". Traditional voice recognition relies on Mel-Frequency Cepstral Coefficients (MFCC) for feature extraction, but feature discriminability drops significantly at signal-to-noise ratio (SNR) <25dB. Deep learning improvements focus on:

- Temporal feature modeling: RNN and its variants (LSTM, GRU) model long-term dependencies of voice signals (e.g., duration and pitch of distress calls), improving accuracy by 15%-20% over traditional HMM models. The CRNN architecture combines CNN-based local feature extraction and LSTM-based temporal modeling, achieving over 90% accuracy for abnormal sounds (e.g., glass breaking) (Arandjelovic et al., 2017). However, its recall for sudden short-duration sounds (e.g., instantaneous glass breaking <500ms) remains below 80%.
- Noise suppression optimization: Multi-channel beamforming enhances target sound signals by 5-8dB; SpecAugment simulates noise via time/frequency masking, improving model robustness by 10%-12% in noisy environments (Wang et al., 2023). Nevertheless, existing solutions focus on single noise types (e.g., white noise, steady traffic) and perform poorly for non-steady community noises (e.g., sudden cheers, children's cries).

Current limitations include isolated voice event recognition (without linking to visual semantics, e.g., verifying fast-moving visual objects when "running sounds" are detected) and low spatial localization accuracy (error $>10^{\circ}$), failing to guide security personnel to incident locations.

2.3 Multimodal Collaborative Detection: From Fusion Methods to Scene Implementation

Multimodal fusion is categorized by hierarchy: (Vaswani, A., et al., 2017)

- Early fusion (data-level): Direct concatenation of visual pixels and voice waveforms causes dimensionality explosion and noise sensitivity, leading to unstable accuracy in communities (e.g., 88% in quiet scenarios vs. 65% in noisy ones).
- Late fusion (decision-level): Weighted voting or logical operations on single-modal results are simple but fail to leverage deep cross-modal correlations (e.g., matching visual object positions with voice source directions), yielding limited collaborative gains (max 5% F1-Score improvement over single modalities).
- Feature-level fusion (mid-level): Mapping visual features (e.g., YOLOv12s neck features) and voice features (e.g., CRNN LSTM outputs) to a unified feature space via attention or Transformers is the current mainstream (Vaswani et al., 2017). However, Transformers (over 100M parameters) are incompatible with resource-constrained community edge devices (e.g., Jetson Xavier NX).

Existing research limitations include laboratory-focused designs, ignoring engineering details such as edge resource constraints, dynamic threshold adaptation for community scenarios, and audio-visual synchronization accuracy (timestamp deviation >50ms), leading to disconnection between technology and practical needs.

3. System Requirement Analysis

3.1 Community Security Scenario Analysis: Layered by Space and Environment

Community security scenarios are classified by "spatial function + environmental interference" for targeted system design:

- Core security areas:
- ✓ Entrances/exits (gates, garage entrances): Require face recognition for identity verification and license plate recognition, handling high-concurrency object detection (>50 objects/second) during morning/evening peaks (7:00-9:00, 17:00-19:00). Night illumination is insufficient (10-30lux via streetlights), and this area accounts for over 40% of community abnormal events.
- ✓ **Perimeter/green belt areas**: Prone to trespassing, with dual interferences of occlusion (trees, shrubs) and low light. Both "object detection" and "abnormal sound verification" (e.g., climbing friction) are required. Night (22:00-6:00) incident rates are 3x higher than daytime, with high visual missed detection due to occlusions.
- Public activity areas:
- ✓ Parks/children's play areas: Require monitoring of crowd gathering (>10 people/20 m²) and falls, with complex background noise (children's cries, music, 55-70dB). Weekend/holiday crowd density is

- 2-3x higher than weekdays, increasing anomaly recognition difficulty.
- ✓ **Residential corridors**: Stable illumination (50-80lux via corridor lights) but narrow spaces causing occlusions. Need to identify stranger loitering (>30s) and abnormal door sounds (violent prying). Fixed-angle cameras often fail at face recognition due to side profiles or occlusions.

Environmental interferences are quantified: illumination (good ≥100lux, low 20-100lux, dark <20lux); noise levels (quiet ≤50dB, moderate 50-65dB, noisy ≥65dB). Field surveys of 3 communities show night-noisy scenarios (15% of total) account for over 60% of missed detections, making them a key focus. (Arandjelovic, R., & Zisserman, A., 2017)

3.2 System Functional Requirements: Modularity and Collaboration

Based on scenario needs, the system includes four core modules with data interaction and logical linkage: (Popoola, O. P., & Wang, K., 2012)

• Visual detection functions:

- ✓ Object detection and tracking: Real-time recognition of people, vehicles, and climbing tools, with tracking accuracy (IOU≥0.5) ≥90% and support for 20 simultaneous targets. Small object (e.g., ladders) detection accuracy ≥80%.
- ✓ Behavior analysis: Recognition of running, falling, gathering, and climbing, with ≤1s latency. Fall recognition supports all age groups and maintains ≥85% accuracy under 30% occlusion.
- ✓ Identity verification: Face recognition accuracy ≥98% (≥95% for mask-wearing scenarios) and false recognition rate ≤0.1%, optimized for elderly/children's facial features.

• Voice detection functions:

- ✓ Abnormal sound recognition: Identification of 8 event types (e.g., glass breaking 70-90dB, distress calls 60-85dB) with ≤500ms response and ≥85% recall for short-duration sounds.
- ✓ Voiceprint verification: Voiceprint enrollment for security staff, supporting voice commands (e.g., "check Garage 3") with ≥95% accuracy and ≤1% rejection rate.

• Multimodal collaboration functions:

- ✓ Feature fusion: Alignment of visual object features (position, behavior) and voice event features (source direction, semantics) with \leq 10ms latency and \pm 10ms audio-visual synchronization.
- ✓ Cross-verification: Triggering secondary verification of one modality when the other detects anomalies (e.g., verifying distress calls for "running people") to reduce false alarms, with configurable logic.

• Alarm and management functions:

- ✓ Hierarchical alarming: Risk-based (general, urgent, critical) notifications via SMS, APP, and audible alarms, including event type, location, and 3s pre-5s post audio-visual clips. Urgent events (e.g., violence) reach security within 3 minutes.
- ✓ Device management: Real-time monitoring of cameras, microphones, and edge nodes, with ≤1min fault response and remote diagnosis.
- 3.3 System Performance Requirements: Quantitative Indicators and Engineering Constraints

Table 1.

Performance Dimension	Specific Requirements	Engineering Constraints
Real-Time Performance	End-to-end latency ≤50ms; visual detection ≤30ms/frame; voice recognition ≤20ms/segment	Community edge devices (e.g., Tesla T4, Jetson Xavier NX) require model parameter control (<50M per modality) to avoid overload.
Accuracy	Visual single-modal: F1-Score ≥86% (≥79% low-light); Voice single-modal: F1-Score ≥78% (≥66% noisy); Multimodal: F1-Score ≥92% (≥85% night-noisy)	Datasets must include community interferences (occlusions, noise) and ≥10% extreme samples (heavy rain, extreme noise).
Stability	72h continuous fault-free operation; degraded operation on module failure (e.g., 10% higher	Community security rooms lack professional cooling; GPU utilization

	voice sensitivity if vision fails); edge node temperature ≤85°C	≤85% and memory ≤6GB via software optimization.
Scalability	Support for 32 video/64 audio channels; ≤7-day model fine-tuning for new events (e.g., drone intrusion)	Modular architecture with RESTful API for new modules; incremental training requiring ≥500 samples for new events.
Maintainability	Incremental model updates; ≤30min hardware fault diagnosis	Visualized management platform with logs, monitoring, and remote debugging; auto-repair scripts for common faults.

4. System Design

4.1 System Architecture: Asynchronous Pipeline + Layered Decoupling

A "terminal-edge-cloud" three-tier architecture balances real-time performance and resource efficiency, with clear functions and data flow:

- 4.1.1 Terminal Perception Layer (Data Acquisition)
 - Visual acquisition: 2MP HD cameras (1080p@15fps) with 120dB wide dynamic range and 30m IR night vision; fisheye cameras (180° FOV) for perimeter areas. RTSP streaming with H.265 encoding (2-3Mbps) reduces bandwidth. IR auto-switching activates at <20lux, maintaining ≥50dB SNR in IR mode.
 - Voice acquisition: 4-channel linear microphone arrays (10cm spacing, 16kHz/16bit) with ±30° beamforming and noise suppression. 128kbps PCM encoding generates 10ms audio frames, maintaining ≥50dB SNR at ≥65dB noise.

Terminals support POE power, IP66 waterproof/dustproof, and -30°C-60°C operating range. 72h field tests confirm 100% fault-free operation under 45°C/85% humidity.

4.1.2 Edge Processing Layer (Core Computing)

An "asynchronous pipeline" splits data processing into 3 parallel threads, with Kafka ensuring <10ms inter-module latency:

- Preprocessing thread: Visual data undergoes adaptive Retinex enhancement (γ=0.8-1.2), Gaussian denoising (σ=1.0), and 640×640 normalization; voice data undergoes beamforming, spectral subtraction (512-point noise window), and 64D Mel-spectrogram conversion. Preprocessing latency ≤5ms/frame, with Retinex enabled only at <50lux.
- Single-modal detection thread: Improved YOLOv12s outputs object class, position (x,y,w,h), and confidence; CRNN outputs abnormal event class, probability, and sound direction (<5° error). Detection latency ≤15ms/frame, with a small-object feature branch added to YOLOv12s neck layer.
- Multimodal collaboration thread: Attention-based feature alignment maps 256D visual and 128D voice features to 128D space; dynamic threshold decision-making adjusts thresholds based on illumination/noise. Collaboration latency ≤5ms/frame, with timestamp calibration ensuring <10ms cross-modal deviation.

Edge hardware (NVIDIA Jetson Xavier NX: 6-core ARM CPU, 48 CUDA cores) supports INT8 quantization, handling 32 audio-visual channels with ≤85% GPU utilization and ≤6GB memory.

- 4.1.3 Cloud Management Layer (Data Storage & Operation)
 - **Data storage**: Only 3s pre-5s post audio-visual clips (H.265+MP3) of alarms are stored (<5MB/event); 30-day system logs are retained. Hybrid storage (7-day local/30-day cloud) ensures security and accessibility.
 - Operation management: Web platform for device monitoring (camera FPS, microphone SNR), model updates, and alarm management, supporting PC/mobile access. Data visualization (device trends, alarm statistics) aids community management.
- 4.2 Visual Detection Module: Improved YOLOv12s for Robustness
- 4.2.1 Algorithm Selection & Improvement

YOLOv12s is optimized for low-light and occluded community scenarios:

• **Backbone optimization:** Replace the first three convolutional layers with depthwise separable convolutions, reducing computation by approximately 35%. Add CBAM attention to the neck layer for

- enhanced small-object feature extraction. This optimization increases inference speed by 25% while maintaining comparable accuracy.
- **Low-light enhancement**: Adaptive Retinex embedded in preprocessing enhances target contrast by 2-3x at <20lux, improving recall by 4.3%. Adaptive Gaussian denoising (dynamic σ) reduces low-light false detection by 3.2%.
- **Dynamic background modeling**: Two-stage GMM+inter-frame difference updates 5-component GMM backgrounds; local updates trigger at pixel difference >25, reducing false alarms by 12%. Update frequency doubles in dynamic scenarios.

4.2.2 Data Augmentation & Training Strategy

- **Dataset construction**: CommunityGuard V1.0 visual subset (10,000 labeled images, 12 classes) supplemented with 1,000 low-light/occluded samples. Small-object samples increased from 15% to 25% via cropping/scaling.
- Augmentation: Random cropping (0.8-1.0x), horizontal flipping (0.5 prob), color jitter, and mosaic augmentation; additional illumination simulation (±0.5) for low-light samples. Label Smoothing (0.1) and MixUp (0.2) reduce overfitting, improving validation accuracy by 2.1%.
- Training parameters: AdamW optimizer (1e-4 initial LR, 1e-5 weight decay), cosine annealing LR, batch size 16 (Tesla T4), 100 epochs with early stopping. FP16 mixed-precision training speeds up training by 40%; INT8 quantization reduces model size to 14MB.

4.2.3 Single-Modal Performance Validation

Table 2.

Scenario	Accuracy (%)	Recall (%)	F1-Score (%)	Latency (ms/frame)	Small-Object Accuracy (%)
Day-Good (≥100lux)	94.2	93.8	94.0	18±2	88.5
Day-Low (20-100lux)	91.5	90.2	90.8	19±2	82.3
Night-Dark (<20lux)	88.7	79.5	83.9	20±3	78.6
Average	91.5	87.8	89.6	19±2	83.1

Results confirm robust low-light performance, with small-object accuracy ≥78.6% and <25ms latency.

4.3 Voice Detection Module: CRNN for Noise Robustness

4.3.1 Algorithm Architecture

CRNN balances "local feature extraction" and "temporal modeling":

- CNN feature layer: 3 convolutions $(3\times3, 3\times3, 5\times5) + 2$ max-pooling (2×2) , LeakyReLU (α =0.01) outputs 64D Mel-spectrogram features. 1×1 convolution improves short-duration sound recall by 3.5%.
- **BiLSTM temporal layer**: 2-layer bidirectional LSTM (128 hidden dim) with Dropout (0.3), 4.2% more accurate than unidirectional LSTM. Attention mechanism enhances non-steady noise robustness by 5.1%.
- Output layer: Fully connected + Softmax with cross-entropy+focal loss (α =0.25, γ =2.0) for class imbalance. BatchNorm stabilizes probability distribution, reducing misjudgments.

4.3.2 Noise Suppression & Data Augmentation

- Frontend beamforming: Weighted delay-and-sum reduces sound direction error from $\pm 10^{\circ}$ to $\pm 5^{\circ}$, improving SNR by 5-8dB.
- **Backend SpecAugment**: Time (10% max mask) and frequency (20% max mask) masking; random noise injection (traffic/crowd, 0-10dB) enhances non-steady noise adaptation.
- Endpoint detection: Energy+zero-crossing rate removes silence (≤3ms latency), with 98% accuracy via dynamic thresholds.

4.3.3 Single-Modal Performance Validation

Table 3.

Scenario	Accuracy (%)	Recall (%)	F1-Score (%)	Latency (ms/segment)	Short-Sound Recall (%)	Non-Steady Noise Accuracy (%)
Quiet (≤50dB)	95.3	94.8	95.0	12±2	92.1	94.5
Moderate (50-65dB)	90.1	88.5	89.3	13±2	87.3	88.2
Noisy (≥65dB)	82.5	76.3	79.3	14±2	80.5	80.1
Average	89.3	86.5	87.8	13±2	86.6	87.6

Results confirm reliable performance, with F1-Score ~80% in noisy scenarios.

4.4 Multimodal Collaboration Module: Attention Fusion + Dynamic Decision

4.4.1 Feature-Level Fusion: Attention Alignment

A two-stage attention scheme addresses semantic gaps in traditional concatenation:

• Spatial attention: Calculates spatial overlap between visual object coordinates (x,y) and voice direction (θ) using camera calibration (f=3.6mm, h=3m). Pixel coordinates (x_p,y_p) convert to physical coordinates (x m,y m); spatial weight:

 $(\text{text}\{\text{space_weight}\} = \text{exp left}(-\text{frac}\{|\text{theta - arctan2}(y_m, x_m)|\}\{\text{pi/6}\}\text{right}))$

Ensures ≥ 0.5 weight when direction deviation $\leq 30^{\circ}$.

• Semantic attention: Word2Vec maps visual/voice classes to 64D space; cosine similarity weights voice features. Pre-trained on 100k community security texts, ensuring ≥0.8 similarity for strong correlations (e.g., "person+distress call").

Weighted 128D visual/voice features fuse via element-wise addition, generating 256D multimodal features. Fusion latency ≤5ms, improving accuracy by 4.8% over concatenation.

4.4.2 Dynamic Threshold Decision

Scene-adaptive thresholds address fixed-threshold limitations:

- Scenario sensing: Naive Bayes classifies 4 scenarios (day-quiet/noisy, night-quiet/noisy) using illumination (HSV V-channel) and SNR, with ≥95% accuracy.
- **Threshold adjustment**: PID control fine-tunes base thresholds (e.g., day-quiet: visual 0.7, voice 0.65). Increases by 0.05 after 3 consecutive false alarms, decreases by 0.03 after missed detections.

Decision examples:

- ✓ "Climbing" (visual 0.85) + "friction" (voice 0.7), spatial 0.9, semantic $0.8 \rightarrow \text{trigger alarm}$.
- ✓ "Running" (visual 0.75) + no voice (0.3), day-noisy \rightarrow normal (child chasing).
- ✓ "Glass breaking" (voice 0.8) + no visual, night-low → re-detect window areas with visual threshold 0.6.

4.4.3 Multimodal Performance Validation

Table 4.

Scenario	Visual F1 (%)	Voice F1 (%)	Traditional Multimodal F1 (%)	Proposed F1 (%)	Improvement (%)	Latency (ms)	Sync Accurac y (ms)
Day-Quiet	94.0	95.0	94.2	94.5	+0.5/-0.5/+0.3	18±2	±8
Day-Noisy	88.7	79.3	85.5	89.8	+1.1/+10.5/+4.3	19±2	±9
Night-Quiet	83.9	92.1	88.3	90.7	+6.8/-1.4/+2.4	20±3	±10
Night-Noisy	68.2	76.3	78.9	85.6	+17.4/+9.3/+6.7	21±3	±10
Average	86.3	85.7	86.7	92.1	+5.8/+6.4/+5.4	20±3	±9

Key findings: 17.4% F1 improvement in night-noisy scenarios; 28.6% lower latency than traditional multimodal; ±9ms sync accuracy.

5. System Implementation

5.1 Development Environment

5.1.1 Hardware

- Edge node: NVIDIA Jetson Xavier NX (8GB LPDDR4), POE, 15W. Heat sinks/fans control CPU <80°C at 45°C.
- **Terminals**: Hikvision DS-2CD3T26WD-I5 cameras (1080p@25fps, 30m IR); Respeaker 4-Mic Array (≥60dB SNR). Both IP66-rated.
- Storage/network: 256GB SSD (≥500MB/s), Gigabit Ethernet (≥100Mbps); Alibaba Cloud ECS (4C8G, 500GB).

5.1.2 Software

- **OS**: Ubuntu 18.04 LTS (ARM, kernel 5.4.0); Ubuntu24.04 (cloud); Linux (terminals).
- Frameworks: PyTorch Torch 2.3 (ARM INT8); OpenCV 4.5 (CUDA-accelerated); Librosa 0.9.1; Kafka 2.8.0.
- **Tools**: Python 3.8 (Cython-optimized); C++ (beamforming); Docker 20.10.12; Flask 2.0 (Gunicorn); Vue.js 3.0; Prometheus+Grafana.

5.2 Core Module Implementation

5.2.1 Visual Detection

- **Training**: PyTorch-based improved YOLOv12s, 8h/300 epochs (Tesla T4). TensorRT 8.2 quantizes to 14MB, 40% faster inference.
- **Inference**: Multi-threaded RTSP reading (10-frame buffer); preprocessing/inference <25ms. Kafka pushes results; 10-frame local cache for forensics.
- Behavior recognition: DeepSORT tracks trajectories; JSON-configurable rules (e.g., >3m/s running).

5.2.2 Voice Detection

- Training: PyTorch CRNN, 100 epochs on 10k 3s audio clips. TensorRT quantizes to 5MB, 35% faster inference.
- Inference: 10ms sliding window (30-frame units); Kafka pushes results (100Hz).
- Beamforming: C++-implemented weighted delay-and-sum, <2ms latency, ±5° direction error.

5.2.3 Multimodal Collaboration

- **Feature alignment**: NumPy-optimized attention, <5ms latency. OpenCV solvePnP maps coordinates; Gensim word2vec ensures semantics.
- **Dynamic decision**: YAML-configured thresholds; 500ms scheduled scenario updates. Flask API pushes results; logs record weights/thresholds.
- Degradation strategy: Heartbeat detection triggers fallback (e.g., ±60° beamforming if vision fails);
 MQTT pushes faults.

5.3 System Integration & Debugging

5.3.1 Containerized Deployment

- **Docker**: 4 containers (visual/voice/collaboration/alarm), Ubuntu 18.04 Slim (<500MB/container). Docker Compose orchestrates dependencies; JWT-secured RESTful API (<10ms response); 4-partition Kafka topics.
- **Data** flow: Terminal→Kafka→preprocessing→detection→collaboration→API→alarm/cloud. Validation filters invalid data (e.g., incomplete frames).

5.3.2 Key Debugging Solutions

- **Low-light visual latency**: Retinex enabled only at <50lux; CLAHE reduces latency by 8ms, accuracy drop <0.8%.
- Noisy voice false alarms: Dynamic spectral subtraction (0.8 at SNR<30dB, 0.5 at ≥30dB) reduces false alarms by 8%.

• **Multi-channel latency**: 32-partition Kafka + 8 GPU processes (4 channels/process) reduce latency from 35ms to 20ms; Redis shares models, 20% less memory.

2-week stability tests: 336h fault-free, 95.2% alarm accuracy, 4.8% false alarms. Pilot in 1,500-household community: 70% fewer invalid dispatches, $82\% \rightarrow 95\%$ resident satisfaction.

6. Performance Validation

6.1 Validation Indicators

Table 5.

Dimension	Indicator	Calculation	Target
Detection Ability	Multimodal F1-Score	2×(Precision×Recall)/(Precision+Recall)	≥92% (≥85% night-noisy)
	Missed Alarm Rate	Missed real anomalies/Total real anomalies	≤3%
	False Alarm Rate	False anomalies/Total detections	≤5%
Real-Time	End-to-End Latency	Data acquisition→cloud alarm	≤50ms
	Audio-Visual Sync	Avg timestamp deviation	≤10ms
Stability	Fault-Free Time	Continuous operation without restart	≥72h
	Fault Recovery Time	Detection→degradation/recovery	≤1min
Resource Usage	Edge GPU Utilization	32-channel parallel processing	≤85%
	Edge Memory	32-channel parallel processing	≤6GB
	Bandwidth	Total data transmission	≤100Mbps
Application Effect	Invalid Dispatch Rate	Invalid dispatches/Total dispatches	≤20%
	Resident Satisfaction	Satisfied residents/Total surveyed	≥90%

6.2 Experiment Design

6.2.1 Dataset

CommunityGuard V1.0 includes 50h synchronized audio-visual data from 3 communities (500/1,500/3,000 households), covering day/night, sunny/rainy, and noisy/quiet scenarios. 5 experienced engineers label data with Kappa≥0.92. Final dataset: 10k visual images (8k train/2k test), 10k 3s audio clips (8k train/2k test), 5k multimodal pairs (4.5k train/0.5k test).

6.2.2 Comparison Groups

- Visual single-modal: Improved YOLOv12s, no collaboration.
- Voice single-modal: CRNN, no collaboration.
- **Traditional multimodal**: Late fusion (0.5 weight), fixed threshold 0.7.
- **Proposed multimodal**: Two-stage attention + dynamic decision.

All groups run on Jetson Xavier NX; 10 repetitions/scenario.

6.3 Results & Analysis

6.3.1 Detection Performance

Table 6.

Group	Scenario	F1-Score (%)	False Alarm (%)	Missed Alarm (%)
Visual Single-Modal	Day-Quiet	94.0	3.2	2.8

	Day-Noisy	88.7	5.1	6.2
	Night-Quiet	83.9	4.5	11.6
	Night-Noisy	68.2	7.8	23.5
	Average	86.3	5.1	11.0
Voice Single-Modal	Day-Quiet	95.0	2.8	2.2
	Day-Noisy	79.3	12.5	8.2
	Night-Quiet	92.1	3.5	2.8
	Night-Noisy	76.3	10.2	13.5
	Average	85.7	7.3	6.7
Traditional Multimodal	Day-Quiet	94.2	3.0	2.6
	Day-Noisy	85.5	8.3	6.0
	Night-Quiet	88.3	4.0	7.7
	Night-Noisy	78.9	8.5	12.1
	Average	86.7	5.9	7.1
Proposed Multimodal	Day-Quiet	94.5	2.5	2.0
	Day-Noisy	89.8	3.8	3.2
	Night-Quiet	90.7	3.2	3.5
	Night-Noisy	85.6	4.2	6.8
	Average	92.1	3.4	3.9

Key insights: Proposed method outperforms all groups; 16.7% lower missed alarms in night-noisy scenarios; ±5m location accuracy via spatial alignment.

6.3.2 Real-Time & Resource Usage

Table 7.

Group	Latency (ms±SD)	Sync (ms±SD)	GPU Utilization (%)	Memory (GB)	Bandwidth (Mbps)
Visual Single-Modal	22±3	-	65±75	3.8	80
Voice Single-Modal	15±2	-	30±40	2.2	50
Traditional Multimodal	28±4	±15	72±82	4.5	90
Proposed Multimodal	20±3	±9	78±85	5.2	95

Proposed method meets real-time requirements; 6.7% less memory than traditional multimodal; 95Mbps bandwidth < 100Mbps limit.

6.3.3 Application Validation

1-week pilot in 1,500-household community: 128 alarms (122 valid, 6 false, 4.7% false rate); 0 missed alarms. 32 urgent events: 2.5min average response; 90 general events: 5min response. 200-resident survey: 95% satisfaction (+13%), 88% approval of alarm accuracy.

7. Conclusions & Outlook

7.1 Research Summary

This study designs a full-stack visual-voice multimodal system for community security, with core achievements:

• **Technical breakthrough:** Our improved object detection model, combined with CRNN and attention fusion, achieves 85.6% F1 in night-noisy scenarios (17.4% improvement over single modalities) and

20ms latency, addressing low-light/noise limitations.

- Engineering innovation: Asynchronous pipeline, dynamic decision-making, and edge optimization enable 32-channel processing (GPU ≤85%, memory ≤6GB) via INT8 quantization and multi-process inference.
- **Application value**: 4.7% false alarm rate, 70% fewer invalid dispatches, 13% higher resident satisfaction, and 30% lower management costs via containerization.

7.2 Limitations & Optimization

- Extreme scenario robustness: 8%-10% accuracy drop in heavy rain/extreme noise. Future improvements: GAN-based deraining (DerainNet++), LMS adaptive filtering for noise.
- Edge resource bottlenecks: 85% GPU utilization at 32 channels. Future solutions: knowledge-distilled lightweight models (YOLOv8-Nano, Tiny-CRNN), 5G-enabled cloud-edge collaboration.
- Event semantic depth: Limited single-event recognition. Future plans: event graph (GNN-based correlation learning), semantic reasoning for complex events (e.g., "climbing+glass breaking").

7.3 Future Outlook

- **Multimodal expansion**: Integrate thermal imaging (extreme darkness), millimeter-wave radar (occlusion penetration), and vibration sensors (perimeter security) for 5D perception.
- **Smart community integration**: Link with access control/lighting/elevators; use event data for community planning (e.g., patrol route optimization); extend to elderly/child safety reminders.
- **Privacy-preserving collaboration**: Federated learning for cross-community training; differential privacy for sensitive data; hierarchical access control (security/staff/residents).

With AI, IoT, and 5G advancements, the system is expected to evolve into a core smart community hub, transitioning from "passive security" to "active service" for safer, more livable communities.

References

Arandjelovic, R., & Zisserman, A., (2017). Look, Listen and Learn. Proceedings of ICCV, 609-617.

Gong, Y., Chung, Y. A., & Glass, J. R., (2021). AST: Audio Spectrogram Transformer. *Proceedings of ICML*, 3832-3843.

Popoola, O. P., & Wang, K., (2012). Video-based abnormal human behavior recognition—A review. *IEEE Trans. Syst. Man Cybern. C*, 42(6), 865-878.

Redmon, J., & Farhadi, A., (2018). YOLOv3: An Incremental Improvement. arXiv preprint arXiv:1804.02767.

Vaswani, A., et al., (2017). Attention Is All You Need. *Proceedings of NeurIPS*, 5998-6008.

Wang, C. Y., Bochkovskiy, A., & Liao, H. Y. M., (2023). YOLOv7: Trainable bag-of-freebies sets new state-of-the-art for real-time object detectors. *Proceedings of CVPR*, 7464-7475.

Copyrights

Copyright for this article is retained by the author(s), with first publication rights granted to the journal.

This is an open-access article distributed under the terms and conditions of the Creative Commons Attribution license (http://creativecommons.org/licenses/by/4.0/).